UNIVERSITÀ DEGLI STUDI DI GENOVA

SCUOLA POLITECNICA

DICCA

Dipartimento di Ingegneria Civile, Chimica e Ambientale

MASTER'S THESIS IN CHEMICAL AND PROCESS ENGINEERING

Experimental study on a proton exchange membrane electrochemical reactor

Supervisors: Prof. Paola Costamagna
Dr. Peter Holtappels

Co-supervisors: Dr. Jinju Zhang
Dipl.-Ing. Anke Urban

Student:

Jessica Domaoa

4979603

Table of Contents

Acknowledgements

I would first like to express my sincere gratitude to my supervisor, Professor Costamagna, who has been a precious guide to me not only academically and professionally, but also on a personal level. A highly dedicated and supportive professor, you were always present, available and ready to calmly face any unexpected challenge along the journey. You taught me that, even if the Nobel Prize may go to someone else, the value of one's work remains meaningful in itself. I also owe you the opportunity to take part in the Erasmus programme, which has profoundly enriched my personal and academic path.

A special thank you goes to my other supervisor, Peter, who guided me throughout the six months of research at KIT. Thank you for your patience, and for the countless presentations and meetings, although confusing at first, eventually turned into invaluable moments of growth. I am also grateful for having been encouraged not to be overly harsh on myself.

I would also like to thank my co-supervisors, Jinju Zhang and Anke Urban, for their invaluable help, from equipment that stubbornly refused to work to long days of spray coating. I would also like to thank Neha, who made my days at IMVT lighter with shared lunches (my delicious ready to eat meals!) and our improbable searches through the department's storage rooms.

My warmest thanks also go to my university classmates. From C1 room on the first floor to B13 room after four flights of stairs, you made lectures more enjoyable and exams more manageable. Thank you for the laughter, the lunches in the conservatory gardens and in the perpetually crowded study room, the table football matches in the vicoli, the strictly non alcoholic aperitivi (at least for me) and the bowling nights which somehow seemed to bend the laws of physics. Thank you to Giulia, Giulio, Jacopo, Seba, Rebecca, Teo, and everyone I met on this journey.

I would also like to thank another person I met in the classroom, right in the middle of an exam: Lorenzo. Thank you for teaching me that it is possible, and sometimes necessary, to make room for fun, even the night before an exam. Thank you for bearing with me in my hungry and nervous moment, for smiling at my "sleep-deprivation hangovers" and for always being there, as a partner but above all as a friend.

My thoughts also go to the friends I have not been able to see often in recent years. Thank you for the few but intense moments together, for the long catch-up conversations, for the nostalgia for what we have been through and the excitement about what is still to come. Thanks to Giorgia, Seb, Riccardo.

Last but not least, I would like to thank my family. I am deeply grateful to my parents for all the sacrifices they have made, which allowed me not only to graduate once, but to pursue a second degree as well. Through this experience in Germany, I had just a first taste of what it means to be a foreigner in another country, and I will never stop being grateful for all the hard work you have done for me. Also, thanks to my sister, Julia, for the years we spent living together

in Genoa, just you and me and, from time to time, two little dogs jumping around and filling the house with joy and chaos.

Abstract

This master's thesis work was carried out at the Karlsruhe Institute of Technology (KIT), Germany, within the Institute for Micro Process Engineering (IMVT), through the Erasmus+ Traineeship program.

In the initial phase, a comprehensive revamping of an existing but long unused experimental setup was performed. This involved verifying the proper functioning of all instruments and mechanical components, as well as replacing damaged parts where necessary.

Several electrochemical cells were fabricated and tested. The electrodes were prepared using a carbon paper gas diffusion layer (Sigracet 39BB, Fuel Cell Store) while optimizing the catalyst ink formulation through the selection of suitable solvents and preparation parameters. The catalytic inks were deposited by ultrasonic spray coating. The tested cells consisted of one symmetric configuration with platinum electrodes on both sides and two asymmetric configurations with copper on the cathode and platinum on the anode. In all cases, the Celtec®-P membrane was employed.

Experimental tests were conducted by feeding hydrogen to the anode, while the cathode was alternately supplied with nitrogen (inert atmosphere) or carbon dioxide to investigate its electrochemical reduction. The effects of temperature and pressure were analysed, especially under elevated conditions representative of a Low Temperature Fischer-Tropsch environment inside a proton exchange membrane electrochemical reactor. Pressure showed little influence, whereas temperature strongly affected the membrane state. Moreover, the membrane was also influenced by humidity, which was found to play a significant role in the system behaviour, contrary to the initial expectations. Electrochemical measurements demonstrated current densities up to 830 mA/cm^2 at a cell voltage of 0.54 V, indicating promising cell performance.

Overall, the results confirmed that the Celtec®-P membrane can operate effectively under elevated temperatures and pressures conditions, highlighting the potential of this approach for developing electrochemical processes integrate into e-fuels production.

1. Introduction

1.1. CO_2 electrochemical reduction and relevance to carbon recycling

Since the Industrial Revolution, the global economy has relied heavily on fossil based energy sources, leading to a sharp increase in CO_2 emissions and severe environmental problems such as global warming and ocean acidification. In response to this crisis, there is a growing need to reduce dependence on fossil fuels to achieve net zero carbon emissions, in line with the targets set by the Paris Agreement.

A promising technology in this direction is electrocatalytic CO_2 reduction (ECO_2RR), which converts carbon dioxide into e-fuels and chemical products using electricity from renewable sources. This process not only enables CO_2 reutilization and energy storage but can also support a zero emission electricity based energy system.

A variety of compounds can be produced from CO_2, including CO, CH_4, methanol, formic acid, ethylene, ethanol and propanol. However, the formation of more complex molecules requires higher energy input and involves longer reaction pathways. Looking ahead, this technology could become a key driver of the energy transition, making a decisive contribution to limiting the increase in global temperature to 1.5°C.[1]

1.2. Syngas Production and Fischer-Tropsch Synthesis

In parallel with direct ECO_2RR routes to fuels and chemicals, increasing attention is being given to power to fuels pathways in which CO_2 is first converted to syngas and subsequently upgraded to synthetic hydrocarbons via Fischer-Tropsch synthesis. In these integrated concepts, renewable electricity is used to produce green hydrogen and to operate high temperature electrochemical or thermochemical processes, enabling the generation of e-fuels suitable for hard-to-decarbonise sectors.

Captured $CO2_2$ should not be regarded only as a waste stream, but rather as a valuable feedstock for the production of synthetic fuels. In addition to the well established CO_2 utilization technologies, such as the Sabatier reaction and conventional Fischer-Tropsch synthesis, innovative approaches based on electrocatalytic Fischer-Tropsch processes have been recently emerged. In these systems, renewable energy is employed to convert CO_2 into e-fuels which can act both as chemical carriers for the storage of intermittent renewable energy and nearly carbon neutral fuels for hard to decarbonise sectors, including heavy transportation and energy intensive industrial processes [2].

A key intermediate in these conversion pathways is syngas, a mixture of carbon monoxide and hydrogen used as a feedstock in Fischer-Tropsch syhthesis and in other fuel and chemical production processes. Traditionally, syngas has been generated from fossil based resources through methane and hydrocarbon reforming routes such as steam reforming, dry reforming, partial oxidation and gasification reforming, all of which operate at high temperature and require substantial external heat input. In addition to these conventional approaches, alternative technologies for syngas production are being developed to reduce the carbon footprint of the process through electrification. Among these, high temperature electrolysis, plasma assisted processes and intensified microchannel reactors have shown great promise as they can be directly integrated with renewable energy systems [3] [4] [5].

Electrolysis plays a central role in power to fuels pathways. Green hydrogen produced via water electrolysis can be combined with CO_2 through reverse water gas shift (RWGS) reaction to obtained syngas with adjustable H_2/CO ratios, depending on the downstream Fischer-Tropsch requirements. An even more integrated alternative is the co-electrolysis of CO_2 and H_2O, enabling the direct production of syngas using only renewable electricity and captured CO2 as main inputs. The syngas produced in this way can be further converted through Fischer-Tropsch synthesis [6].

Two main Fischer-Tropsc configurations are typically distinguished. High temperature Fischer-Tropsch (HTFT) operates at 300-330°C and pressure up to 30 bar using iron catalyst, producing mainly low-octane gasoline (40%, 65 RON), oxygenates and light olefins. Low temperature Fischer-Tropsch (LTFT) operates at lower temperatures, 200-230°C with cobalt catalyst producing predominantly long chain waxes (>50%) and a high quality diesel fraction (15%, >75 CN), together with gaseous hydrocarbons [7].

Going beyond conventional HTFT and LTFT, highly integrated concepts have been proposed in which CO2 and H2 are directly fed to a single electrochemical unit operated at temperatures and pressures compatible with Fischer-Tropsch synthesis. Within such configuration, syngas generation and subsequent hydrocarbon formation are expected to occur within a single unit that combines electrochemical syngas generation and catalytic Fischer-Tropsch conversion in a common reaction environment, thereby simplifying the process layout and enhancing system compactness. At the same time, this level of electrochemical integration introduces significant challenges related to thermal management, electrode, membrane and catalyst stability under prolonged and dynamic operating conditions and the maintenance of high conversion efficiencies during load transients, which remain key research topics for scalable deployment of electrocatalytic Fischer-Tropsch technology [8]

1.3. Electrolyser types and membrane-based cell configuration

The design of electrochemical reactors has a fundamental impact on the electrochemical reduction of carbon dioxide, as it defines crucial aspects of performance, including current density, Faradaic efficiency, product selectivity and overall stability. Beginning with Hori's pioneering work in the 1980s, different cell configurations have been proposed, with reactor configuration shown to influence not only the achievable current density but also the onset potential and product selectivity, parameters that are often related to the intrinsic properties of the electrocatalyst [9].

Among these configurations, H-type cells, named after their characteristic shape, represent the most widely adopted setup for lab scale ECO_2RR experiments. In this design, a diaphragm separates the cell into two distinct compartments: the cathodic compartment, which contains the working and reference electrodes and the anodic compartment, which houses the counter electrode. The separator ensures proper ionic conductivity while preventing the crossover of reaction products to the anode, where oxidation processes could occur. H-type cells are favoured for their simplicity, low cost and suitability for the rapid testing of new electrocatalysts and electrolytes. However, they are poorly suited for handling large volumes of gaseous CO_2, as the mass transfer toward the electrode surface remains limited even under vigorous catholyte stirring [9].

To overcome these limitations and meet the demands of industrial scale CO_2 conversion, which requires higher production rates, flow cells have been developed. In these systems, gaseous CO_2 is continuously fed to the catalyst through gas diffusion electrodes (GDEs) with high porosity, typically fabricated from carbon based materials incorporating polytetrafluoroethylene (PTFE) to enhance hydrophobicity and mechanical stability. The catalytic layer is deposited onto the GDE via techniques such as spray coating or screen printing. The key difference between the flow cell and the H-type cell is the establishment of a three-phase interface composed of the gaseous CO_2, the liquid electrolyte and the solid catalytic layer: one side of the GDE faces the gas stream and the opposite side contacts the electrolyte. This architecture effectively overcomes the solubility limitation of CO_2in aqueous media. Additional advantages come from the use of strongly alkaline electrolytes, which suppress the hydrogen evolution reaction (HER), enhance CO_2RR kinetics and improve selectivity toward specific reduction products [10].

Despite these improvements, flow cells still face several performance and durability challenges. The presence of two separate compartments introduces significant ohmic resistance, while operational issues such as GDE flooding, carbonate precipitation and species cross over between compartments often hinder stability. Moreover, the large electrolyte volumes required, compromise cost-effectiveness and raise concerns regarding process scalability[10].

A further development in CO_2 electrolysis cell design is the membrane electrode assembly. (MEA) configuration. In this architecture, the anode and cathode are pressed directly against opposite sides of an io-exchange membrane, forming a sandwiched structure without separate liquid compartments. This arrangement minimises the distance between the electrodes and reduces the ohmic losses. Gaseous CO_2 is continuously supplied to the cathode while the anode is typically operated with electrolytes such as $KHCO_3$, KOH, CsOh or even pure water to drive the oxygen evolution reaction. Ionic transport occurs exclusively through the ionomer phases and the membrane, eliminating the liquid catholyte and its associated resistance. The MEA configuration can reduce the overall cell resistance, thereby decrease the energy consumption and simplifying the structure of the electrolytic cell. Nevertheless, MEA system share some of the drawbacks observed in flow cell configuration, including GDE flooding, carbonate salt formation and crossover, all of which limit long term operational stability [10].

In **Figure 1** the cell configurations discussed in this section are shown.

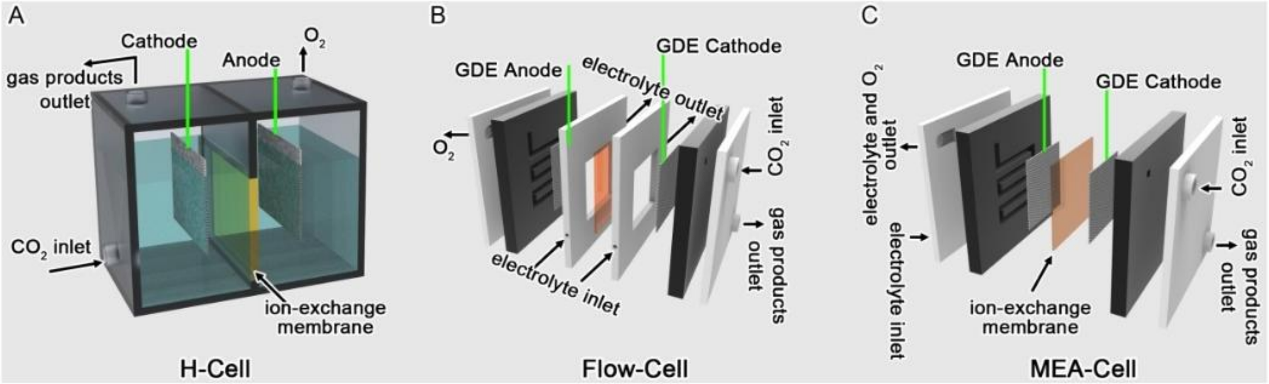

Figure 1 a) H Cell; b) Flow Cell; c) MEA Cell [10]

1.4. Electrochemical characterization techniques

Electrochemical techniques play a significant role in modern analytical chemistry and in the investigation of redox processes in electroactive systems. In this section, the basic concepts of linear sweep voltammetry (LSV), chronoamperometry (CA), chronopotentiometry (CP) and electrochemical impedance spectroscopy in potentiostatic (PEIS) and galvanostatic (GEIS) configurations are presented. Together, these techniques provide the basis for the experimental approaches discussed later in this thesis.

Linear sweep voltammetry (LSV) measures the current at a working electrode while the potential, applied with respect to a reference electrode, increases linearly over time, with scan rates ranging from a few millivolts per second to as high as 1000000V/s. the set up typically involves a potentiostat and a three electrode configuration: the working electrode, where the oxidation or the reduction reaction of interest occurs, the counter electrode, which completes the circuit, and the reference electrode, which maintains a stable potential. The measured current reflects the electron transfer processes at the electrode-electrolyte interface: reacting species are consumed at the surface, replaced by new ones via diffusion. When diffusion becomes rate limiting, the current reaches a plateau or exhibits a characteristic peak [11].

Chronoamperometry (CA) is a potential controlled electrochemical technique in which the potential of the working electrode is rapidly stepped to a defined value and then kept constant. The resulting current is monitored as a function of time [12].

Chronopotentiometry (CP) is a galvanostatic technique in which the current at the working electrode is held at a constant value for a defined period of time. Typically, the current is imposed between the working and counter electrode, while the potential is measured with respect to a reference electrode [13].

Potentiostatic electrochemical impedance spectroscopy (PEIS) is an impedance spectroscopy technique performed under potentiostatic control. The potential of the working electrode is kept at a constant DC value and a small sinusoidal potential perturbation (AC) is superimposed.

Galvanostatic electrochemical impedance spectroscopy (GEIS) is the analogous impedance technique conducted under galvanostatic control. In this case, a constant DC current is imposed and a small sinusoidal current perturbation (AC) is applied, while the corresponding potential variation is recorded [14].

2. Previous work and thesis aim

Prior to this work, several experiments had been conducted. This section provides a very brief and preliminary summary of the tests previously performed, in order to give an essential overview of the experimental path that preceded the present study.

A cell consists of platinised titanium felt anode with IrO_2 as catalyst, a carbon paper cathode loaded with Ag and an anion exchange membrane (AEM, Sustainion® X37-50 Grade RT) assembled as a membrane electrode assembly (MEA) was tested. In all experiments, gaseous CO_2 was continuously supplied to the cathode side. The cell was operated at 1 bar and 25, 50 and 80°C, using 1 M KOH as anolyte (temperature was kept below 90°C to prevent a reduction in proton mobility within the membrane). Gas product analysis revealed only CO and H_2, with Faradaic Efficiency (FE) for CO of 93% at 50°C, and additionally, the formation of carbonate species was observed. The system was then tested at 3 and 5 bar, pressure variation did not show any significant influence on the product distribution, which remained limited to CO and H_2, with an overall FE close to 100%. Further tests were performed using 0.1 M $KHCO_3$ anolyte. In this case as well, only CO and H_2 were detected and the carbonate formation issues were again observed, however compared to the 1 M KOH anolyte, a partial suppression of the hydrogen evolution (HER) was observed [15].

A further cell configuration employed the same pair of electrodes (a platinised titanium felt anode with IRO_2 and carbon paper cathode with Ag), in this case coupled with a cation exchange membrane (CEM, Nafion® 212) in an MEA configuration. A 1 M $KHCO_3$ solution was used as anolyte. Experiments carried out at 25, 50, 75°C and, subsequently, at 3 and 5 bar (at 25°C) showed exclusive formation of CO and H_2, with the CO FE being only weakly affected but changes in temperature and pressure, while carbonate deposition phenomena were again observed [16].

In an additional series of experiments, a cell was tested using the same anode, but a carbon paper cathode coated with Cu and, subsequently, with a tandem AgCu and CuAg catalysts (distinguished by the order of metal deposition), combined with an AEM (Sustainion® X27-50 Grade RT) in an MEA configuration. With 0.1 M $KHCO_3$ as the anolyte, under ambient conditions using Cu as the only catalyst, ethylene was produced (FE 15.1%), in addition to CO and H_2. When 1 M KOH was employed as the anolyte and the cell was operated at 25, 50 and 80°C, ethylene was again formed, although with a lower yield than in 0.1 M $KHCO_3$ anolyte. Propylene was also detected, with FE values below 5%. In tests with tandem AgCu and CuAg catalysts, using either 1M KOH or 1 M $KHCO_3$ as the anolyte, ethylene was obtained in both cases, with a maximum FE of 6.5%. for 1M KOH as the anolyte, the effect of pressure was also investigated by increasing it to 10, 15, 20 bar (at 25°C), under these conditions, ethylene was formed with FE not exceeding 4% and propylene with FE below 2% [17].

Finally, a configuration consisting of the same anode, a carbon paper cathode with Ag and a high temperature cation exchange membrane (BASF Celtec®-P) was evaluated. Tests carried out at 120, 150 and 1801°C showed the exclusive formation of CO and H_2, with an increase in the HER as the temperature raised. When the cathodic catalyst was replaced with Cu and the same temperatures were applied, an almost exclusive production of hydrogen was instead observed [18].

In this study, the BASF Celtec®-P membrane was selected because, according to the manufacturer, its operation is independent of humidification and it can be employed at temperatures up to 180°C. Conventional polymer electrolyte membranes, by contrast, require proper hydration to maintain adequate proton conductivity. Above 100°C water tends to vaporize, promoting membrane dehydration. In addition, in high temperature systems, fouling phenomena associated with electrolyte leaching from the membrane have been reported, which can be mitigated by using hydrogen as the proton source. For this reason, platinum was chosen as the anodic catalyst, while copper was selected as the cathodic catalyst based on the results obtained in the previous experiments. In this context, the present work aims to explore the overall concept of an electrochemical cell capable of operating under low Fischer-Tropsch conditions, at 180°C and 20 bar.

3. Methods and Materials

This chapter describes the materials, operational procedures and instruments used in this study, which was conducted at the Karlsruhe Institute of Technology (KIT).

3.1. System Overview

An initial phase of the study was dedicated on analysis and understanding the test rig already available at the IMVT Department. For this purpose, a Process Flow Diagram was developed, as shown in **Figure 3**, which illustrates the overall configuration of the se-tup, its main components and the measurement and control devices.

The system includes a nitrogen feed line, shown in grey, employed as a buffer gas to regulate the reactor pressure. Pressure regulation is achieved using back pressure regulators (BPR1 and BPR2). Nitrogen is also employed to ensure an inert atmosphere on the cathode side during reference measurements.

In addition, a carbon dioxide feed line, identified in orange, is humidified with deionized water inside the tank TK 1-1 before being introduced into the cathodic side of the electrolysis cell ECCO2-1. The products generated at the cathode are directed to the collection tank TK 1-2, where liquid products, if present, are accumulated, while the gaseous products pass through the adsorption column ADS 1-1, which removes residual water vapour. Afterwards, a three-way valve allows the user to select the destination, directing the stream either to the analytical system via gas chromatography or to the exhaust line connected to the ventilation system. In this work, the gas chromatograph was not employed due to technical malfunction that could not be repaired in time.

The first water line, marked in purple, is used to fill the tank TK 1-1 by means of an ISMATEC Reglo ICC peristaltic pump, **Figure 2**.

A hydrogen feed line, represented in blue, is also present. The Hydrogen is humidified in the tank TK 2-1, filled with deionized water supplied via a second water line, also shown in purple, using the same peristaltic pump mentioned above. The outlet products from the anode side are collected in the TK 2-2 tank, where the liquid phase accumulates, whereas the gaseous and unreacted components are vented to the exhaust system.

The gas flow rates supplied to the reactor are controlled by Brooks Instrument mass flow controllers, previously calibrated and indicated as FIC 1-1, FIC 1-2 and FIC 1-3, corresponding respectively to the nitrogen, carbon dioxide and hydrogen lines.

As previously mentioned, two back pressure valves are present, one located at the outlet of the cathode side (BPR1) and the other at the outlet of the anode side (BPR2). This setup ensures the same pressure is maintained on both sides of the membrane. The pressure set point is regulated via ALICAT-FlowVision 2.0 software.

Pressure indicators are installed at the inlet and outlet of the cathode, labelled as PI 1-1 and PI 1-2, respectively, and at the inlet and outlet of the anode, labelled as PI 2-1 and PI 2-2, respectively. Additionally, pressure indicators are present at the inlet of each gas supply line, PI 1-3 for the nitrogen line, PI 1-4 for the CO2 line and PI 2-3 for the hydrogen line. A final pressure indicator, PI 1-5, is located on the outlet line of the cathode, just before the gases enter the gas chromatograph.

Regarding the cell temperature, it is regulated using dedicated temperature indicators and controllers, TIC 1-1 for the cathode side and TIC 2-1 for the anode side. Heating is provided by four heating rods inserted inside the cell. Additionally, another temperature indicator and controller, TIC 1-2, can be used to heat tank TK-1 via heating cables. The temperature set point is adjusted through the dedicated control panel located on the test rig. Temperature indicators are installed at the cathode inlet and outlet, labelled as TI 1-1 and TI 1-2 respectively, and at the anode inlet and outlet, TI 2-1 and TI 2-2 respectively.

Figure 2 Ismatec Reglo ICC Digital Peristaltic Pump

In the **Table 1** a list of the equipment and instrument is shown.

Instrument & Equipment List			
TAG	**NUMBER**	**DESCRIPTION**	**Manufacturer**
PI	1-1	Pressure Indicator	West 8010
PI	1-2	Pressure Indicator	West 8010
PI	1-3	Pressure Indicator	West 8010
PI	1-4	Pressure Indicator	West 8010
PI	1-5	Pressure Indicator	West 8010
PI	2-1	Pressure Indicator	West 8010
PI	2-2	Pressure Indicator	West 8010
PI	2-3	Pressure Indicator	West 8010
TI	1-1	Temperature Indicator	Eurotherm
TI	1-2	Temperature Indicator	Eurotherm
TI	2-1	Temperature Indicator	Eurotherm
TI	2-2	Temperature Indicator	Eurotherm
LI	1-1	Level Indicator	Kobold
FIC	1-1	Flow indicator controller	Brooks Instrument
FIC	1-2	Flow indicator controller	Brooks Instrument
FIC	1-3	Flow indicator controller	Brooks Instrument
TIC	1-1	Temperature Indicator Controller	Eurotherm
TIC	2-1	Temperature Indicator Controller	Eurotherm
TIC	1-2	Temperature Indicator Controller	Eurotherm
LI	2-1	Level Indicator	Kobold
ECCO2	1	CO2 Electrolyzer cell	Parr Instrument
TK	1-1	Heated Humidifier Tank	Swagelok
TK	1-2	Storage Tank	Swagelok
TK	2-1	Humidifier Tank	Swagelok
TK	2-2	Storage Tank	Swagelok
ADS	1-1	Humidity Adsorber Column	Duran

Table 1 Instrument and equipment list of the test rig

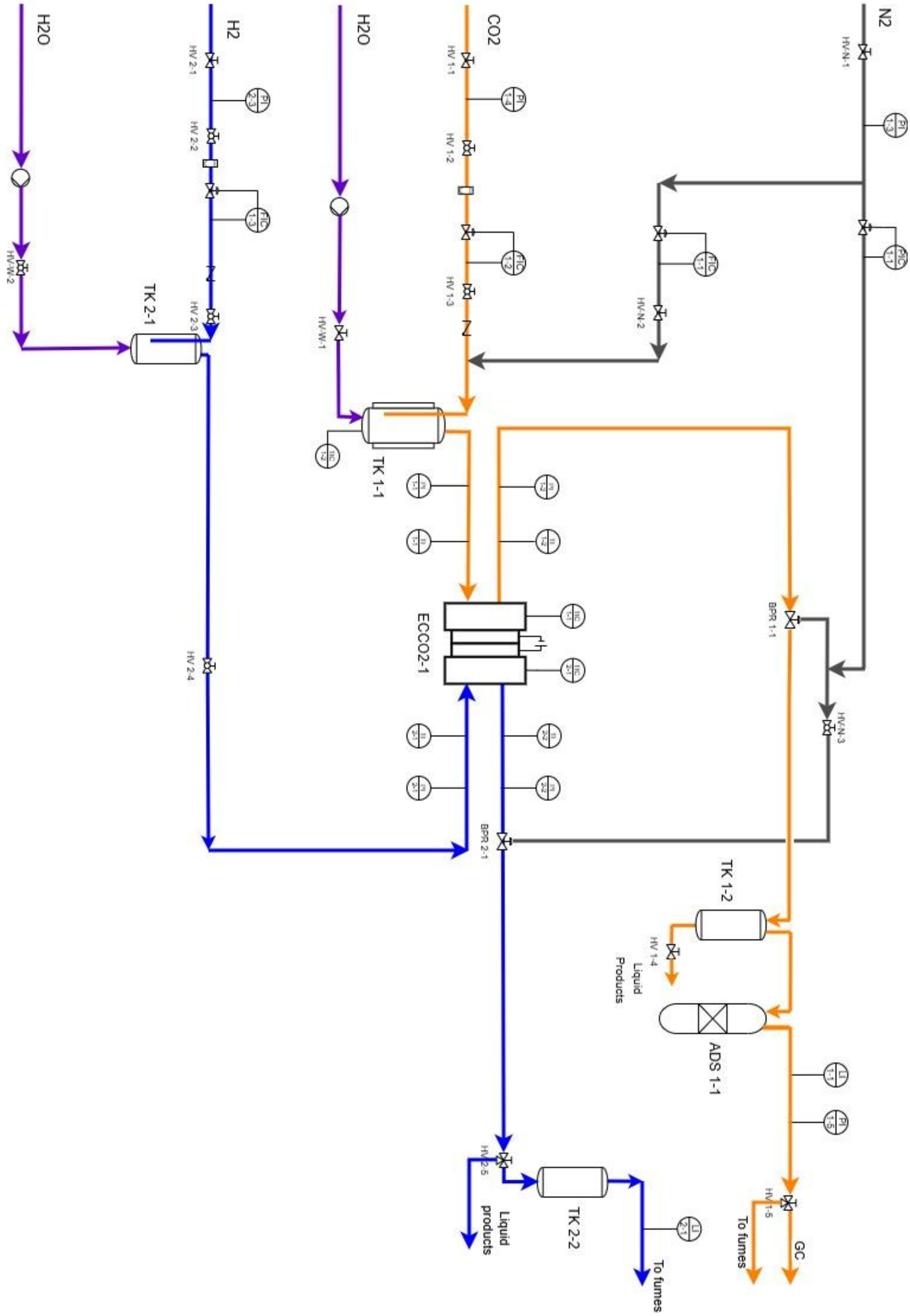
N2
CO2
H2O
H2
H2O
HV-N-1
PI 1-3
PIC 1-1
FIC 1-1
HV-N-2
HV 1-1
PI 1-4
HV 1-2
FIC 1-2
HV 1-3
HV-W-1
TK 1-1
TIC 1-2
HV 2-1
PI 2-3
HV 2-2
FIC 1-3
HV 2-3
TK 2-1
HV-W-2
ECCO2-1
TIC 1-1
TIC 2-1
BPR 1-1
HV-N-3
BPR 2-1
HV 2-4
TK 1-2
HV 1-4
Liquid Products
ADS 1-1
LI 1-1
PI 1-5
HV 1-5
To fumes
GC
TK 2-2
HV 2-5
Liquid products
LI 2-1
To fumes

Figure 3 PFD

The system used is shown in the **Figure 4**.

In the upper section, the reaction area is shown in red while the lower section represents the humidification and collection zone, outlined in green. On the right side, the control station is marked in blue.

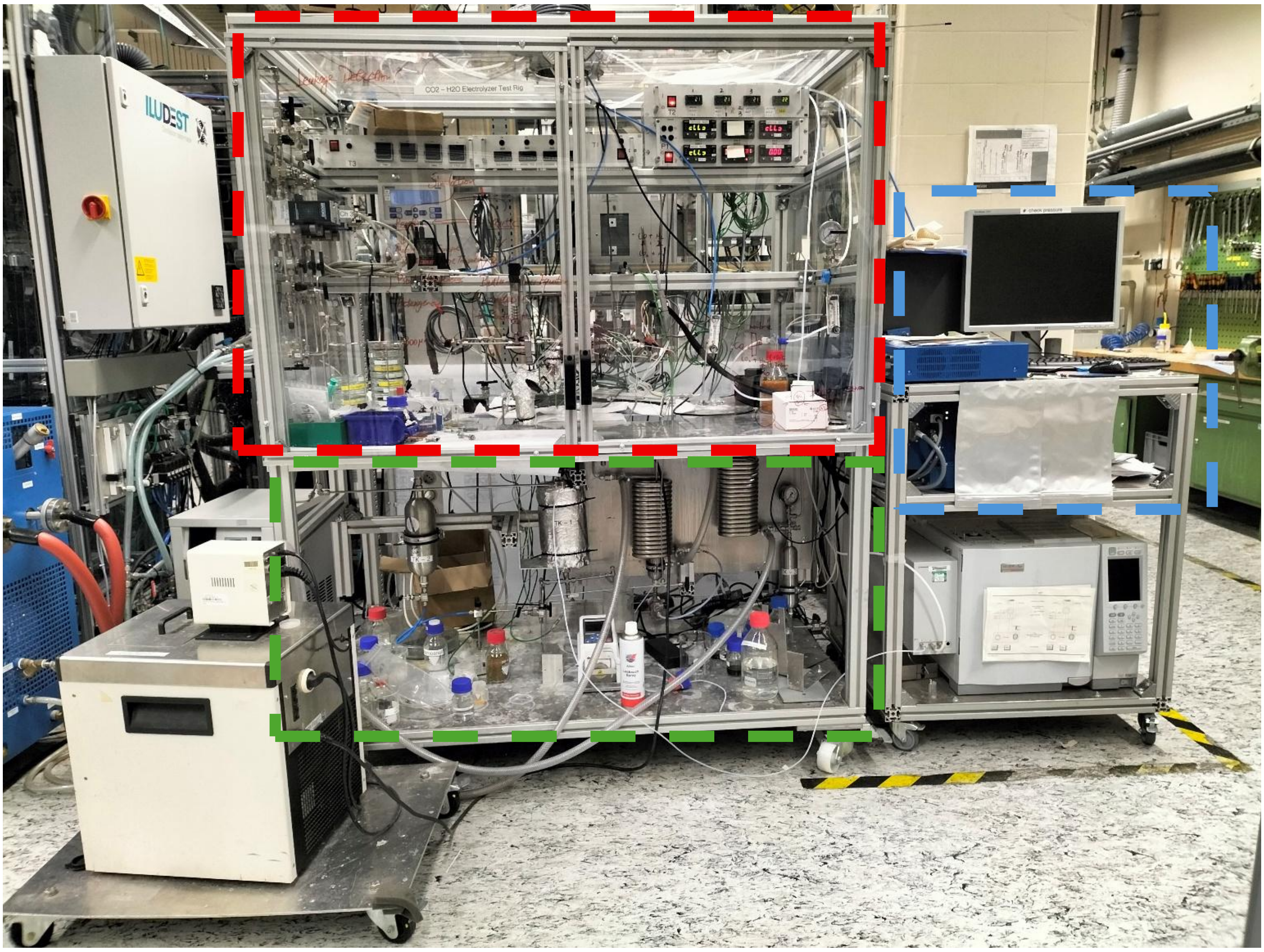

Figure 4 Photo of the system: reaction area (red), humidification and collection area (green) and control station (blue)

3.2. System validation and leakage testing

Before operating the test rig with experimental samples, the correct functionality of the system and the absence of gas leaks had to be verified. The system validation phase included a series of preliminary tests aimed at ensuring the gas-tightness of the set-up, the reliability of the sensors, and the proper functioning of the auxiliary equipment.

A first test was carried out by feeding the system with nitrogen in order to detect any potential leaks along joints and fittings. The inspection was performed using a leak detector spray (Alltec), **Figure 5**. In the next step, a second test was performed under hydrogen flow, using a Peaker® s sensor (UST) for gas leak detection, **Figure 6**. All fittings that showed signs of wear or leakage were replaced with new Swagelok components.

The temperature and pressure controllers and indicators were also checked to verify their operational reliability. For the pressure regulation devices, the system was pressurised by placing a Teflon disk (0.5 mm thick, 56 mm diameter) inside the housing. During this procedure, a faulty pressure sensor was detected, which displayed a reading of 1.23 bar even in the absence of applied pressure. The sensor was therefore replaced with a Wika S20 model equipped with a cooled section.

The condition of the silica gel adsorbent was also evaluated. A small amount of the material was immersed in distilled water, showing a colour change from orange to dark green, indicative of partial water saturation. The adsorbent beads were placed in an oven at 120°C for one hour, recovering their original colour, thus confirming that the adsorbent material in the system was not fully saturated with water.

The glass tank located upstream of the adsorber was removed because of a gas leak in the sealing that could not be repaired. Therefore, it was permanently excluded from the configuration, as an existing stainless-steel reservoir was already installed in the system.

The performance of the Shimadzu 2010-Plus gas chromatograph (GC) was also tested. The initial analysis, performed by feeding only CO2, showed consistent chromatographic peaks, however in the following tests the instrument stopped providing reliable results. Despite several repair attempts, due to the long delivery time of spare parts (as the instrument is manufactured in the UK) and limited technician availability, it was not possible to restore the GC to working condition in time for this study.

Finally, the operation of the Knauer K-1800 HPLC pump was verified. The pump was unable to draw water from reservoir and for this reason an ISMATEC Reglo ICC peristaltic pump, previously mentioned, was employed as an alternative to supply water to the tanks.

Figure 5 Alltec leak detector spray

Figure 6 Peaker® s sensor from UST

3.3. Electrochemical Cell Components

The experiments were conducted using a zero-gap MEA-type electrochemical cell. The external structure of the cell is made of stainless steel on both the cathode and anode sides, and it can be heated by inserting heat cartridges.

Inside there are two titanium flow field plates featuring spiral channels that allow for uniform gas flow on the cathode side and electrolyte or gas flow on the anode side. Each plate is equipped with a titanium bolt serving as a current collector.

O-rings, made of Viton, are used as seals to ensure proper sealing, while two alignment pins guarantee precise alignment of the parts. The cell is closed with eight socket head cap screws.

The external housings were supplied by Parr Instrument Company, while the flow field plates were manufactured by the department IMVT using milling techniques.

The hardware mentioned above is shown in **Figure 7**.

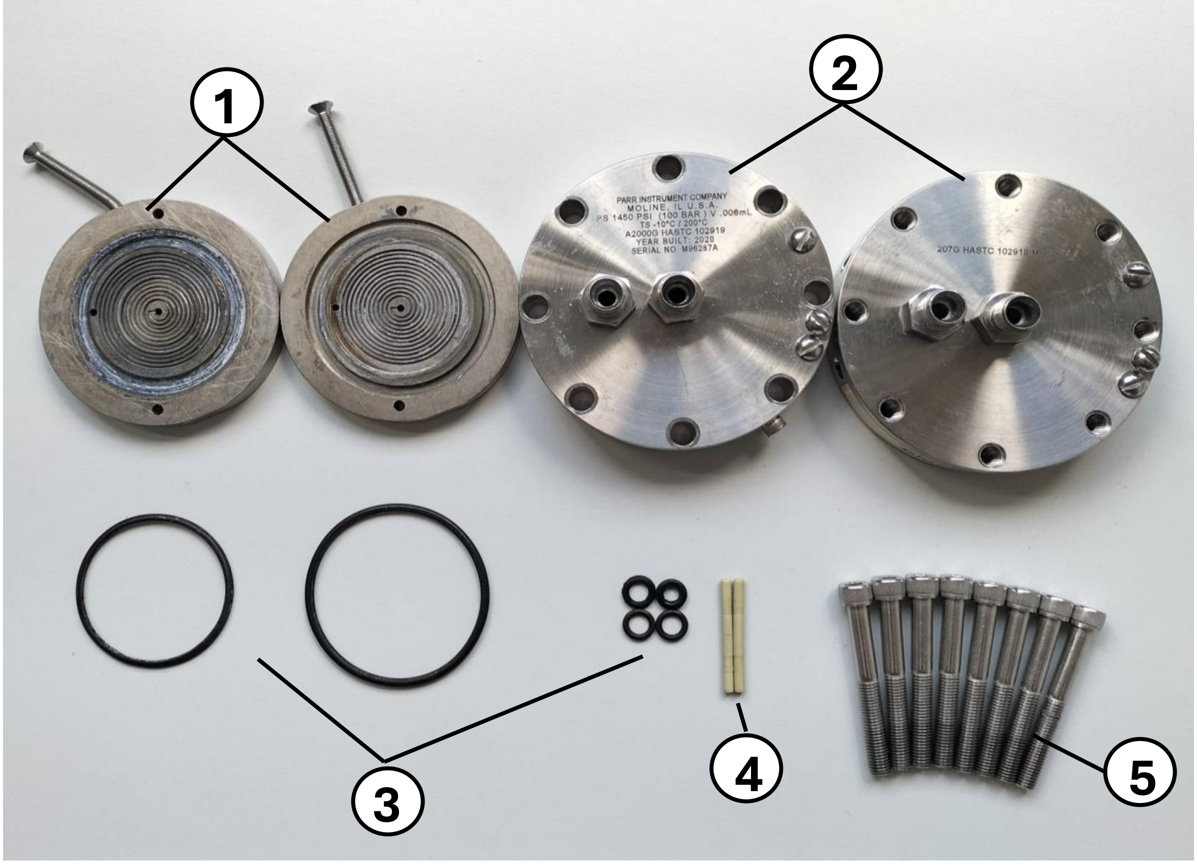

Figure 7 1) Titanium flow field plates, 2) External housings, 3) O-rings, 4) Alignment pins, 5) Socket head cap screws

DuPont™ Kapton® sheets were used as electrical insulators in the tested electrochemical cell configurations, **Figure 8**. This high-performance polymer offers excellent thermal resistance up to 400°C. The foils were precisely cut using punching tools specific to the Parr Instrument cell shown in **Figure 9**.

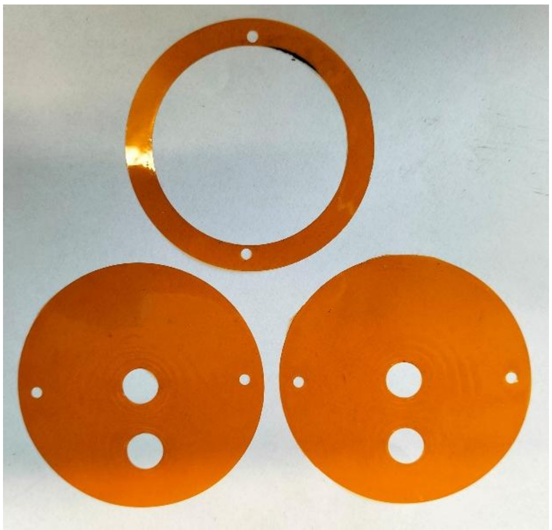

Figure 8 Kapton® foils used

Figure 9 Punching tools and hammer used for Kapton® foils

Figure 10 illustrates an exploded image of the cell setup. This schematic representation shows the individual components and their positions within the assembly.

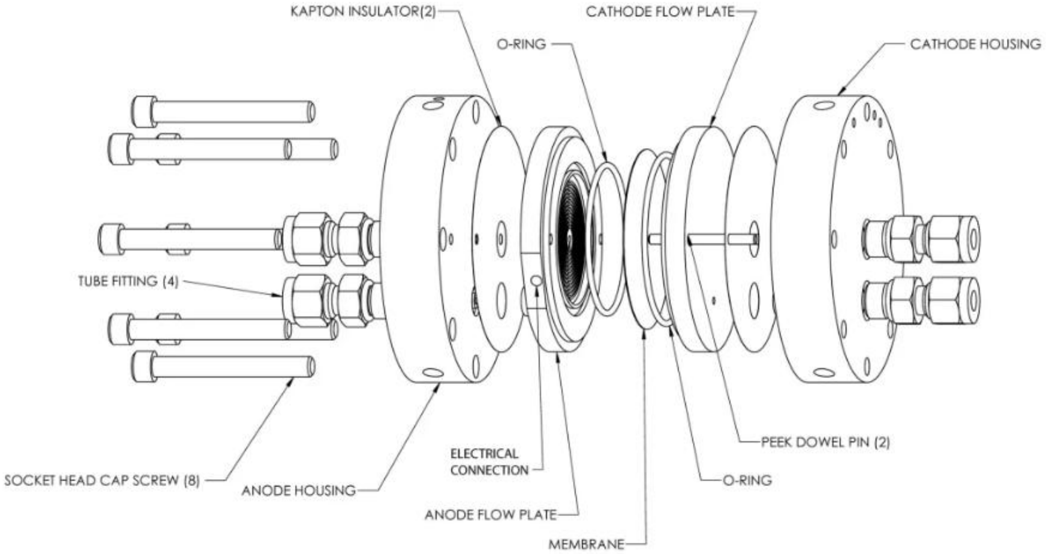

Figure 10 Exploded view of the Parr Instrument Company electrochemical cell

3.4. Cathode Preparation

The cathode was prepared using the ultrasonic spray coating technique with Exacta-Coat system from Sono Tek, **Figure 11**. The starting ink consisted of copper nanoparticles (APS 20-50 nm, 99.9% metal basis, Alfa Aesa), isopropanol and Nafion^{TM} 520 Solution (Ion Power GmbH) which was sonicated for 20 minutes to ensure a uniform dispersion. The coating was deposited onto a carbon paper gas diffusion layer (thickness: 325 +- 25 micron, Sigracet 39BB, Fuel Cell Store). The temperature of the substrate plate was kept at 90°C to ensure solvent evaporation.

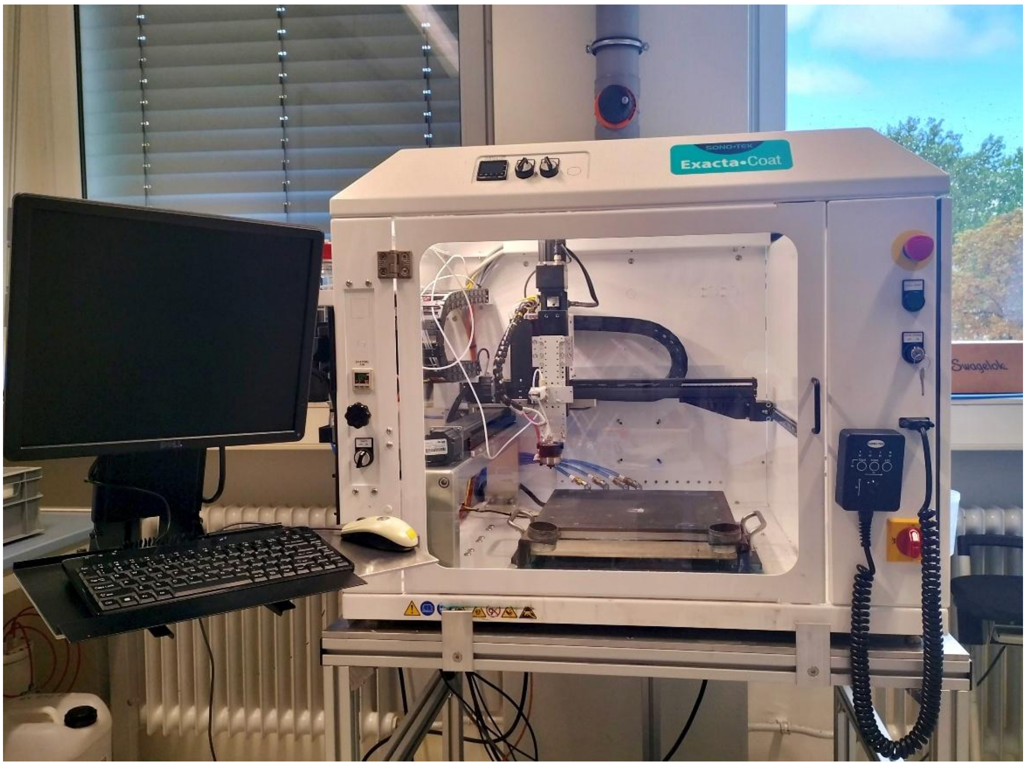

Figure 11 *Exacta-Coat ultrasonic spray coater by Sono-Tek*

At first, a spiral pattern of the nozzle was employed for the spray deposition, but it was discovered that controlling the nozzle pressure was challenging. This approach led to an uneven deposition.

Figure 12 *Cathode ink spray coated using spiral pattern*

It was then decided to switch to a rectangular pattern. A rectangular piece of carbon paper was cut and spray coated. From this piece, a circular shape with an area of 12 cm2 was obtained. This method resulted in a uniform catalyst distribution.

Figure 13 *Cathode ink spray coated using rectangular pattern*

During all deposition processes, catalyst sedimentation was observed inside the tubing of the spray coating system and in the ink collection bottle.

3.5. Anode preparation

The anode was also prepared using the ultrasonic spray coating technique with Exacta-Coat system from Sono-Tek. The starting ink was composed of platinum (10% on carbon, dry, Thermo Scientific), isopropanol and Nafion™ 520 solution (Ion Power GmbH), which was sonicated for 20 minutes to achieve complete homogenization of the mixture. The deposition was carried out on a rectangular carbon paper gas diffusion layer (thickness: 325 +- 25 micron, Sigracet 39BB, Fuel Cell Store). A rectangular pattern was used for the spray coating.

During the spray coating phase, the formation of sparks was observed, followed by the ignition of a flame that caused the combustion of part of the carbon paper, as shown in the **Figure 14** indicated by the arrows.

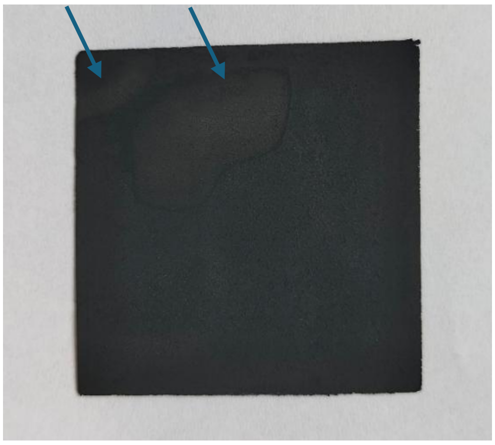

Figure 14 Sample damaged by flame

Following this event, it was decided to modify the solvent used while keeping the same platinum-based catalyst (10% on carbon, dry, Thermo Scientific), Nafion™ 520 solution (Ion Power GmbH) and the same carbon paper (thickness: 325 +- 25 microm, Sigracet 39BB, Fuel Cell Store).

A first attempt was carried out using a solvent composed of distilled water and absolute ethanol in a 1:1 (v/v) ratio, while maintaining the substrate temperature at 60°C. However, since the microporous layer of the carbon paper is highly hydrophobic, droplet formation was observed in certain areas. These droplets, due to the surface properties of the material, tended to move toward the edges. As show in the **Figure 15**, this resulted in a non-uniform catalyst distribution, particularly near the corners.

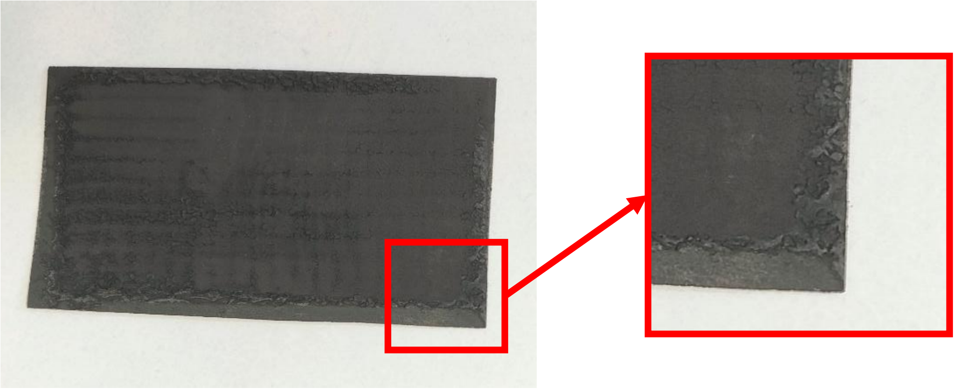

Figure 15 Sample prepared with 1:1 (v/v) water/ethanol solvent

A second attempt was then performed using absolute ethanol as the only solvent. In this cas, no droplet formation observed, and the catalyst coating appeared uniform across the entire carbon paper surface.

Under both experimental conditions, with the distilled water/ethanol (1:1 v/v) mixture and with pure ethanol, no sparks or flames were detected during the spray coating process.

During anode preparation, catalyst sedimentation was also noticed inside the tubing of the spray coating system and in the ink collection bottle, regardless of the solvent used.

3.6. Membrane preparation

The BASF Celtec®-P PBI membrane was used in this work. This commercial membrane comes already pre-doped with phosphoric acid to enable proton conduction, making it ready for immediate use, eliminating the pre-use acidification step. It was cut to a 52 mm diameter using the punching tool show in **Figure 16**.

Figure 16 Punching tool: smaller-diameter punch (diameter 40 mm) for electrode cutting and larger-diameter punch (52 mm) for membrane cutting.

4. Experiments and Results

Three different samples were tested, and their main characteristics are summarised in the **Table 2**.

The first sample, referred to as Sample A, features Pt as catalyst on both cathode and anode, each with a loading of 0.51 mg/cm2. The membrane used is a PBI Celtec®-P supplied by BASF already mentioned above. Since both electrodes are made of the same catalytic material, this configuration represents a symmetric cell, hereafter also referred to as Symmetric Cell.

The second sample, named Sample B, uses copper as cathode catalyst with a loading of 0.81 mg/cm2 and Pt as anode catalyst with a loading of 0.28 mg/cm2, using the same PBI Celtec®-P membrane.

The third sample, named Sample C, features copper as cathode catalyst with a loading of 1.17 mg/cm2 and Pt as anode catalyst with a loading of 0.27 mg/cm2. In this case as well, the PBI Celtec®-P membrane provided by BASF was used.

Sample Name	Cathode Catalyst	Cathode loading [mg/cm2]	Membrane	Anode Catalyst	Anode loading [mg/cm2]
Sample A	Pt/C	0.51	PBI	Pt/C	0.51
Sample B	Cu	0.81	PBI	Pt	0.28
Sample C	Cu	1.17	PBI	Pt	0.27

Table 2 Characteristics of the tested samples

4.1. Pt/Pt Cell Sample A results

In this chapter the results for the Pt/Pt Cell Sample A are shown.

Scanning electron microscopy (SEM) analyses were carried out on the Pt/Pt cell in order to investigate the sample morphology. Before the electrochemical tests, both surface and cross-section analyses were performed, to characterize the initial state of the material. After the electrochemical tests were performed, only cross-section analyses were conducted on the tested sample (**Figure 17**), since the opening of the casing caused a partial destruction of the electrodes, which remained attached to the flow fields. Moreover, due to the pressure applied during the cell assembly, the electrodes also attached to the memr7brane, preventing further surface analysis.

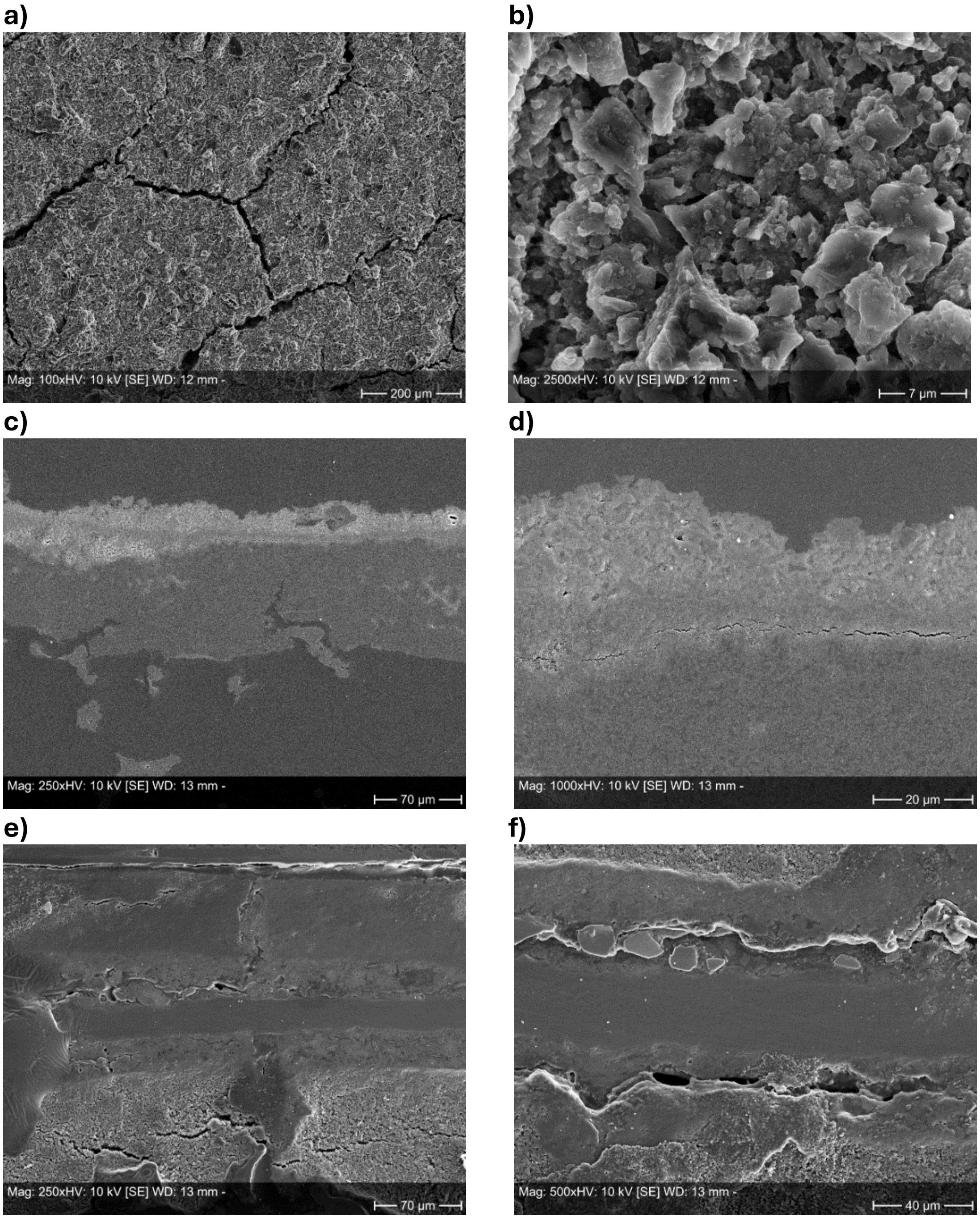

Figure 17 a) pre-test top view Mag:100xHV, b) pre-test top view Mag: 250xHV, c) pre-test cross-section Mag: 250xHV, d) pre-test cross-section Mag:1000xHV, e) post-test cross-section Mag: 250xHV, f) post-test cross section Mag:500HV

The **Table 3** provides a detailed overview of the electrochemical experiments carried on the Pt/Pt Cell Sample A, reporting for each test day the gas feeds, temperature, pressure and the techniques employed (LSV, CA, PEIS). The field ‘Test Day’ indicates the sequential number of the day on which the experiment was performed, regardless of the calendar date.

Test day	Feed	T [°C]	P [bar]	Type of experiments
1	Humidified N2 (Cathode), Humidified H2 (Anode)	120	1	LSV, CA, PEIS
		150		
		180		
2	Dry N2 (Cathode), Dry H2 (Anode)	150	1	LSV, CA, PEIS
		180		
		120		
3	Dry N2 (Cathode), Dry H2 (Anode)	25	1	LSV, CA, PEIS
			2	
			5	
			10	
			20	
			1	
4	Dry N2 (Cathode), Dry H2 (Anode)	50	1	LSV, CA, PEIS
			2	
			5	
			10	
			20	
5	Dry N2 (Cathode), Dry H2 (Anode)	25	1	LSV, CA, PEIS
		80	1	
			2	
			5	
			10	
			20	
6	Dry N2 (Cathode), Dry H2 (Anode)	25	1	LSV, CA, PEIS
		120	1	
			2	
			5	
			10	
			20	
7	Dry N2 (Cathode), Dry H2 (Anode)	25	1	LSV, CA, PEIS
		150	1	
			2	
			5	
			10	
			20	
8	Dry N2 (Cathode), Dry H2 (Anode)	25	1	LSV, CA, PEIS
		180	1	
			2	
			5	
			10	
			20	
9	Dry N2 (Cathode), Dry H2 (Anode)	25	1	LSV, CA, PEIS
		25	20	
		50		
		80		
		120		
		150		
		180		
10	Dry N2 (Cathode), Dry H2 (Anode)	25	1	LSV, CA, PEIS

Table 3 Operating conditions and electrochemical experiments performed on the Pt/Pt Cell Sample A

Figure 18 shows the linear sweep voltammetry (LSV) curves recorded during the first day of analysis at 1 bar and at the three investigated temperatures (120°C, 150°C and 180°C), obtained by feeding **humidified** H2 to the anode and **humidified** N2 to the cathode, thus ensuring an inert atmosphere at the cathode. The corresponding Tafel plots are also reported, determined by plotting the base-10 logarithm of the absolute value of the current density as a function of the cathode (working electrode) vs. the reference electrode. In this study, the potentiostat leads were connected such that the working electrode lead was attached to the cathode, whereas the counter and reference leads were connected on the anode side.

Figure 19 shows the i-V (current density-voltage) curves obtained from chronoamperometric measurements, obtained by stepping constant potentials from lower to higher voltages and then in reverse direction. The applied potentials were -0.05V, -0.1V, -0.15V and -0.2V. For each potential value, the steady-state current was measured after signal stabilisation to characterise the electrochemical response of the system under steady-state conditions. This forward-reverse protocol verifies the absence of hysteresis and measurement reproducibility. The corresponding Tafel plots are also reported for the forward direction only.

Potentiostatic Electrochemical Impedance Spectroscopy (PEIS) measurements were conducted at the same potential values used for chronoamperometry, Nyquist plots are shown in **Figure 20** for the different temperatures tested (120°C, 150°C, 180°C). Blue points correspond to PEIS performed at -0.05V, orange points at -0.1V, grey points at -0.15V and yellow points at -0.2V.

The LSV recorded at the different temperatures show an overall similar behaviour, indicating that the voltametric response of the electrode does not change significantly under the investigated conditions. The i-V curves at 120 and 150°C are essentially overlapped, whereas at 180°C the maximum current density reaches slightly lower values (about -170 mA/cm2 compared to ~ -200 mA/cm2 at 120 and 150°C). Moreover, the almost complete overlap between forward and backward scans highlights a negligible hysteresis.

The Nyquist plots show a progressive shift on the spectra towards higher Re(z) values with increasing temperature, while at fixed temperature the spectra obtained at different potentials are very similar to each other, with noticeable differences only in the low frequency tail.

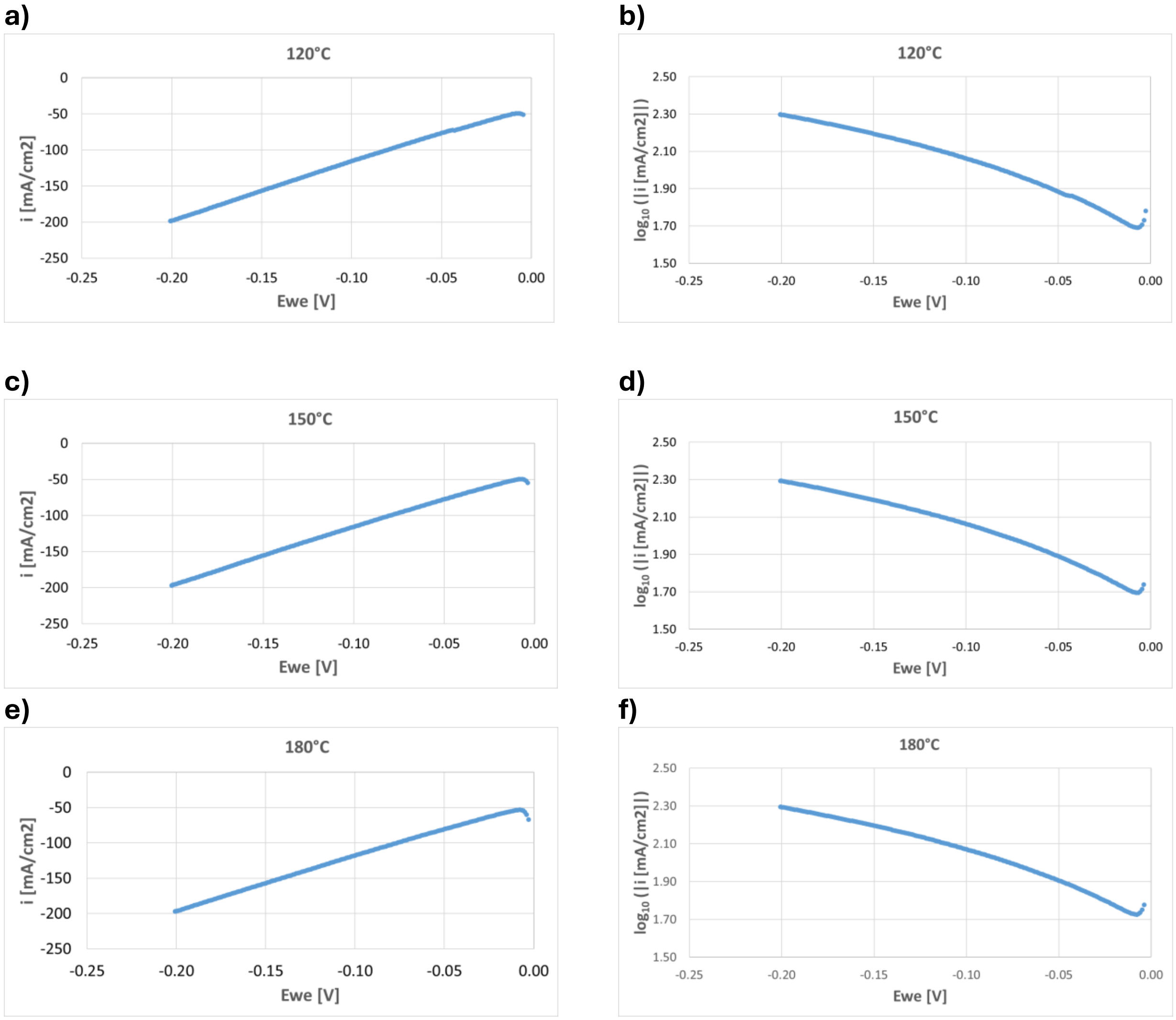

Figure 18 LSV Curves (left) and corresponding Tafel plots (right) under humid gas conditions: a,b) 120°C; c,d) 150°C; e,f) 180°C.

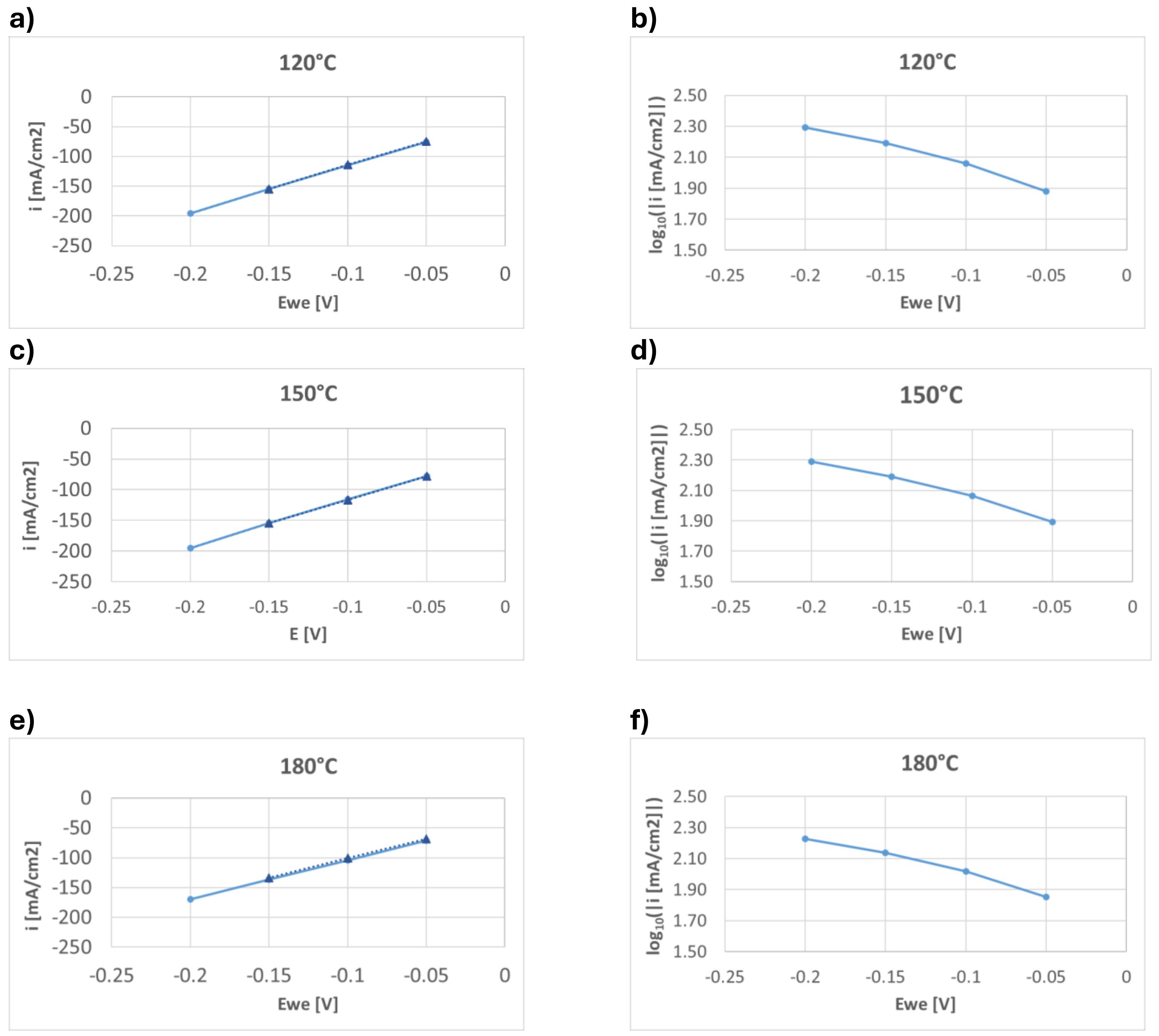

Figure 19 i-V curves (left) and corresponding Tafel plots (right, forward scan only) under humid gas conditions: a,b) 120°C; c,d) 150°C; e,f) 180°C. For the i-V curves, solid lines indicate the forward scans, while dotted lines indicate backward scans.

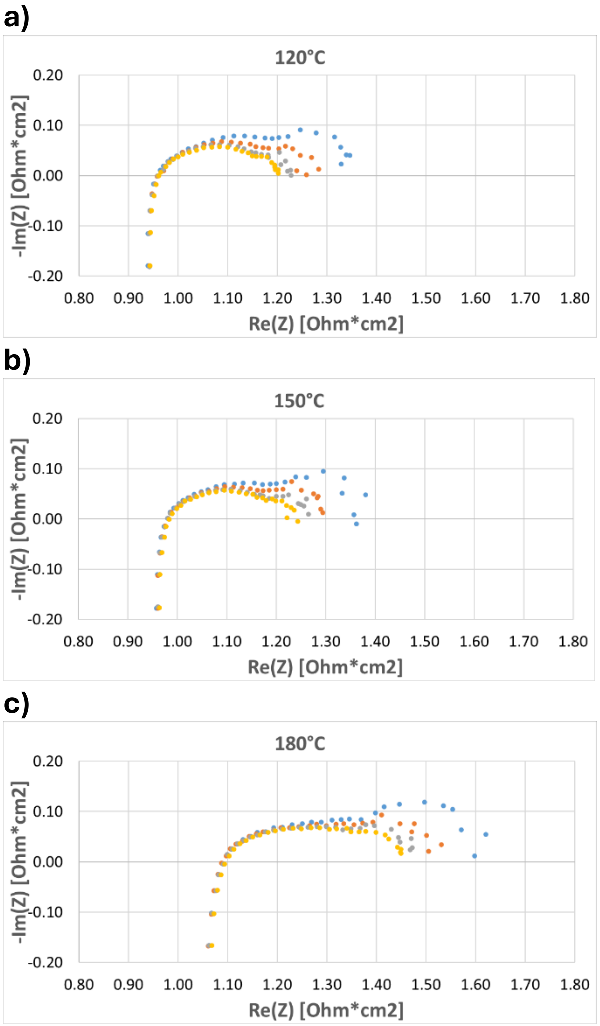

Figure 20 Nyquist plots at different potentials and temperatures under humid gas conditions: a) 120°C; b) 150°C; c) 180°C. Colour legend: blue symbols (-0.05V), orange (-0.1V), grey (-0.15V), yellow (-0.2V).

The same analyses were repeated on the second day under identical pressure (1 bar) and temperature (120°C, 150°C, 180°C) conditions but using **dry gases**. The related LSV curves and Tafel plots are shown in **Figure 21.**

The i-V curves with their respective Tafel plots (forward direction only) under dry gas conditions are shown in **Figure 22.**

The Nyquist plots from PEIS analyses with dry gases are presented in **Figure 23**.

Under dry gas conditions, the LSV scans show that increasing the temperature leads to a decrease in the maximum current density: at 120°C a value of approximately -120 mA/cm2 is reached, whereas at 150 and 180°C it drops to about -80 mA/cm2. The i-V curves at the three temperatures are largely similar, showing only a slight increase in current density at a given potential as the temperature rises. The Nyquist plots display a moderate decrease in the diameter of the semicircles with increasing temperature. At fixed temperature, the spectra recorded at different potentials remain similar, except in the low frequency tail where more pronounced differences appear.

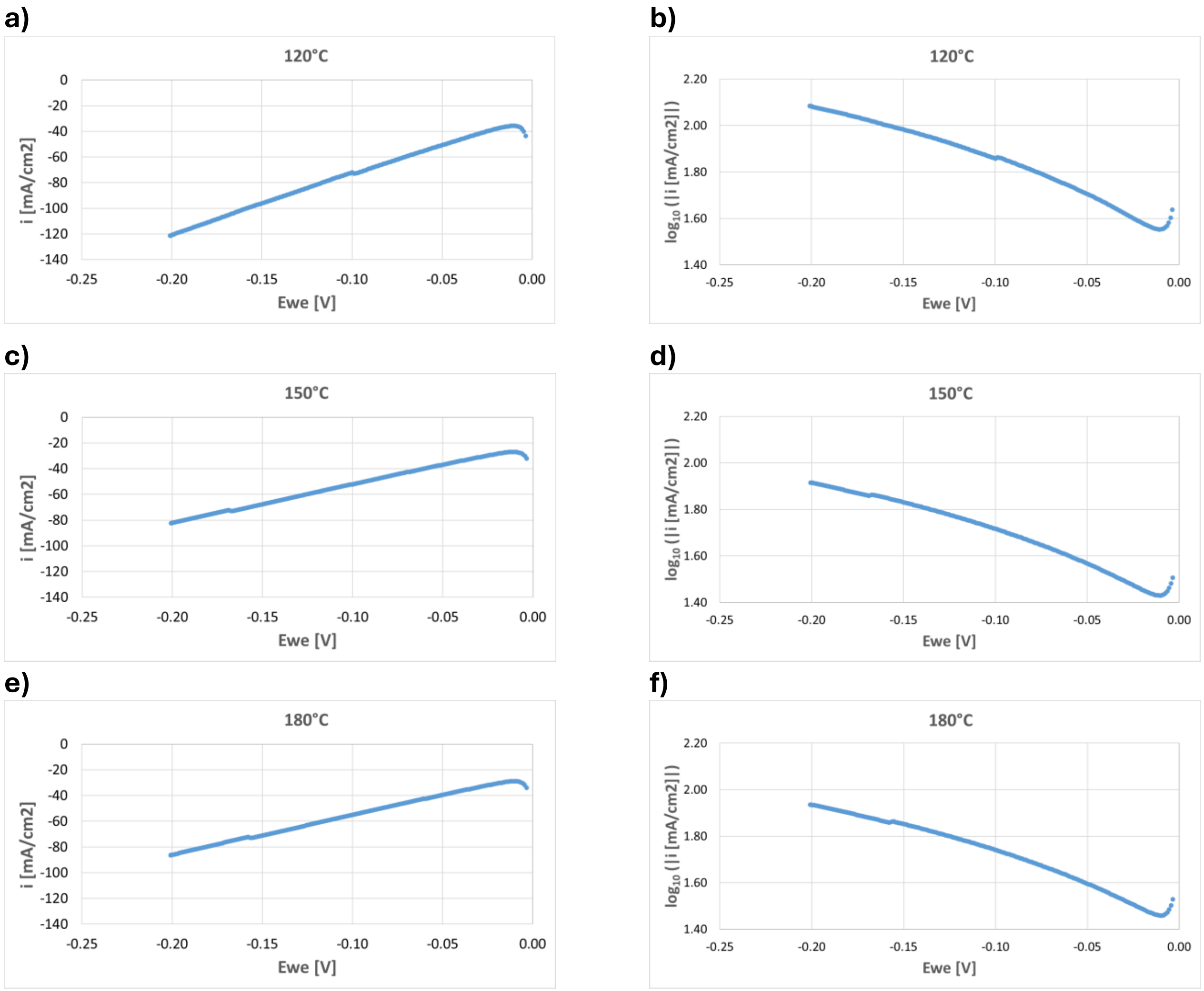

Figure 21 LSV Curves (left) and corresponding Tafel plots (right) under dry gas conditions: a,b) 120°C; c,d) 150°C; e,f) 180°C.

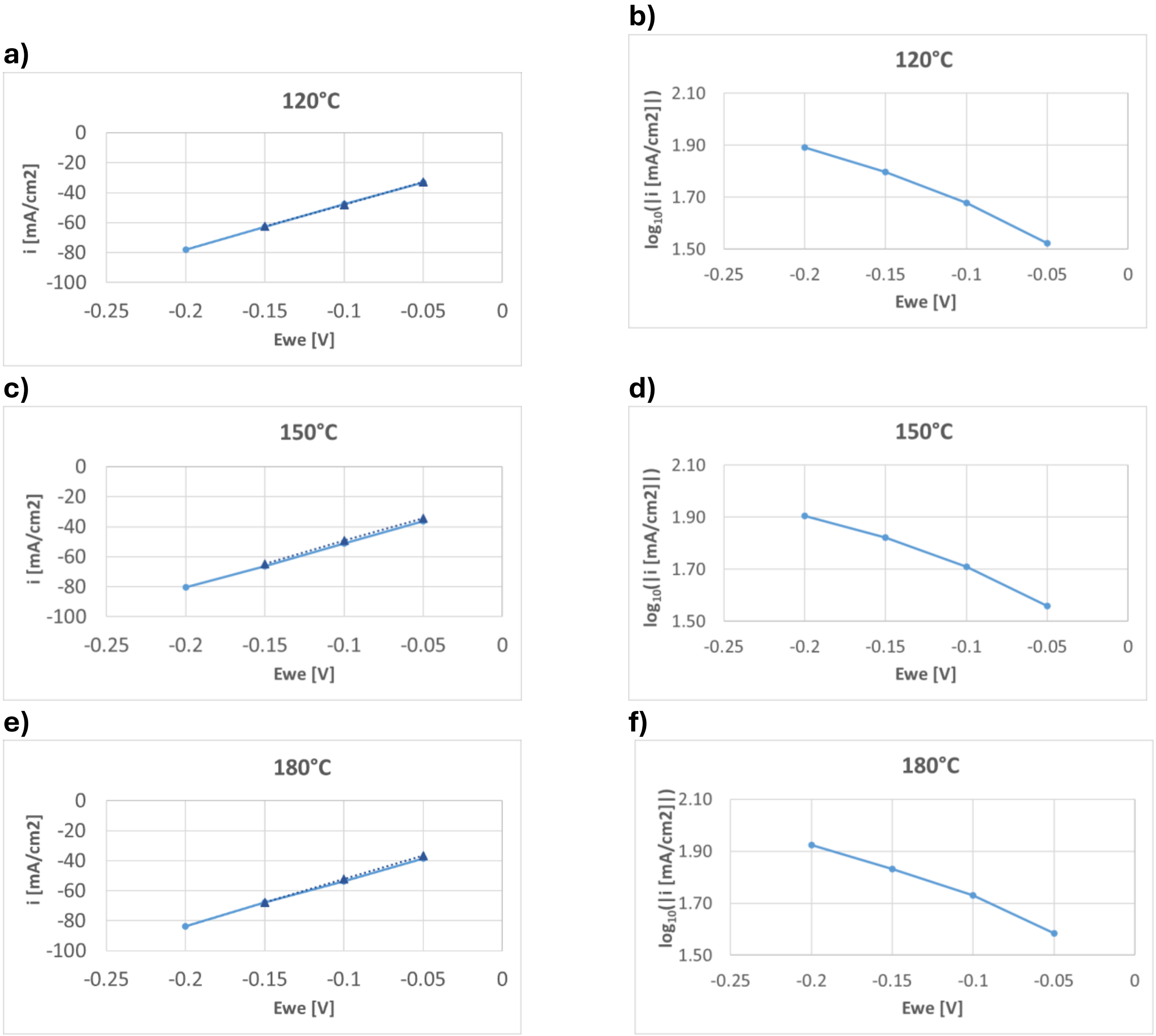

Figure 22 i-V curves (left) and corresponding Tafel plots (right, forward scan only) under dry gas conditions: a,b) 120°C; c,d) 150°C; e,f) 180°C. For the i-V curves, solid lines indicate the forward scans, while dotted lines indicate backward scans.

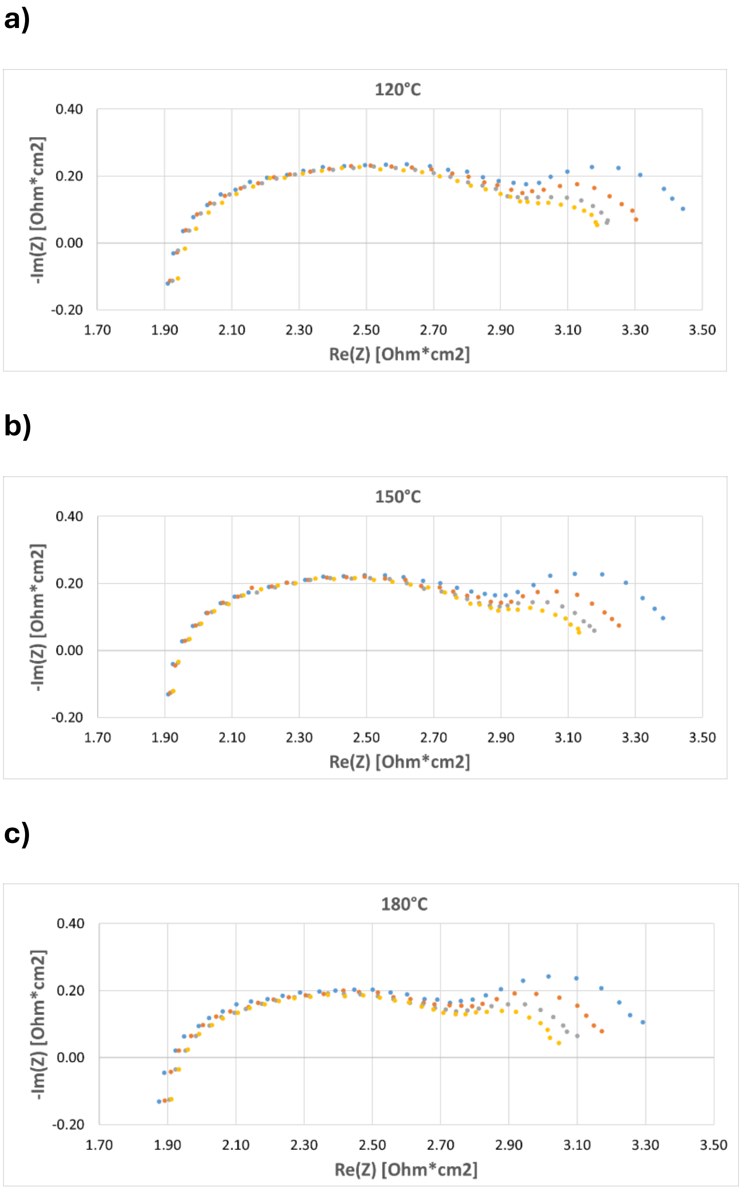

Figure 23 Nyquist plots at different potentials and temperatures under dry gas conditions: a) 120°C; b) 150°C; c) 180°C. Colour legend: blue symbols (-0.05V), orange (-0.1V), grey (-0.15V), yellow (-0.2V).

During days 3-8, a second series of tests was carried out, in which the same types of experiments (LSV, CA, PEIS) previously performed were repeated, while maintaining dry N2 at the cathode and dry H2 at the anode. The operating temperature was systematically varied, specifically at 25, 50, 80, 120, 150, 180°C. For each of these temperatures, kept constant during the measurements, the pressure was incrementally increased in steps to 1, 2, 5, 10, 20 bar. This procedure allowed the influence of pressure on the electrochemical performance to be evaluated.

Figure 24, **Figure 25**, **Figure 26**, show, respectively, the LSV curves with corresponding Tafel plots, the i-V curves with the related Tafel plots (forward only), and the Nyquist plots, all acquired at 25°C under different pressures (1, 2, 5, 10, 20 bar).

Figure 27, Figure 28, Figure 29, show, respectively, the LSV curves with corresponding Tafel plots, the i-V curves with the related Tafel plots (forward only), and the Nyquist plots, all acquired at 50°C under different pressures (1, 2, 5, 10, 20 bar).

Figure 30, Figure 31, Figure 32, show, respectively, the LSV curves with corresponding Tafel plots, the i-V curves with the related Tafel plots (forward only), and the Nyquist plots, all acquired at 80°C under different pressures (1, 2, 5, 10, 20 bar).

Figure 33, Figure 34, Figure 35, show, respectively, the LSV curves with corresponding Tafel plots, the i-V curves with the related Tafel plots (forward only), and the Nyquist plots, all acquired at 120°C under different pressures (1, 2, 5, 10, 20 bar).

Figure 36, Figure 37, Figure 38, show, respectively, the LSV curves with corresponding Tafel plots, the i-V curves with the related Tafel plots (forward only), and the Nyquist plots, all acquired at 150°C under different pressures (1, 2, 5, 10, 20 bar).

Figure 39, Figure 40, Figure 41, show, respectively, the LSV curves with corresponding Tafel plots, the i-V curves with the related Tafel plots (forward only), and the Nyquist plots, all acquired at 180°C under different pressures (1, 2, 5, 10, 20 bar).

At 25°C, increasing the pressure up to 20 bar does not significantly affect the electrochemical response: the LSV curves reach a similar maximum current density of about -60 mA/cm2 at all pressures. The i-V curves show the same trend. From the Nyquist plots, a slight decrease in the diameter of the semicircles is observed. In addition, the spectra recorded at different potentials become similar with pressure, including in the low frequency tail.

At 50°C, the LSV curves as function of pressure show only minor differences: at 1 bar the maximum current density measured is about -50 mA/cm2, while at higher pressures it settles at slightly lower values, around -40 mA/cm2. The i-V curves exhibit almost no variation among the different pressures investigated. From the Nyquist plots, an increase in pressure leads to a slight increase in the Re(Z) values at the high frequency intercept and a reduction in the diameter. Moreover, the spectra recorded at different potentials tend to overlap more closely as the pressure increases.

At 80°C, increasing the pressure does not lead to any significant changes in either the LSV or the i-V curves, which are nearly identical in both shapes and slopes for all conditions. From the Nyquist plots, a decrease in the diameter of the semicircles is observed, and the curves recorded at different potentials become increasingly close to one another as the pressure rises.

A qualitatively similar behaviour can be identified in the measurements at 120, 150 and 180°C.

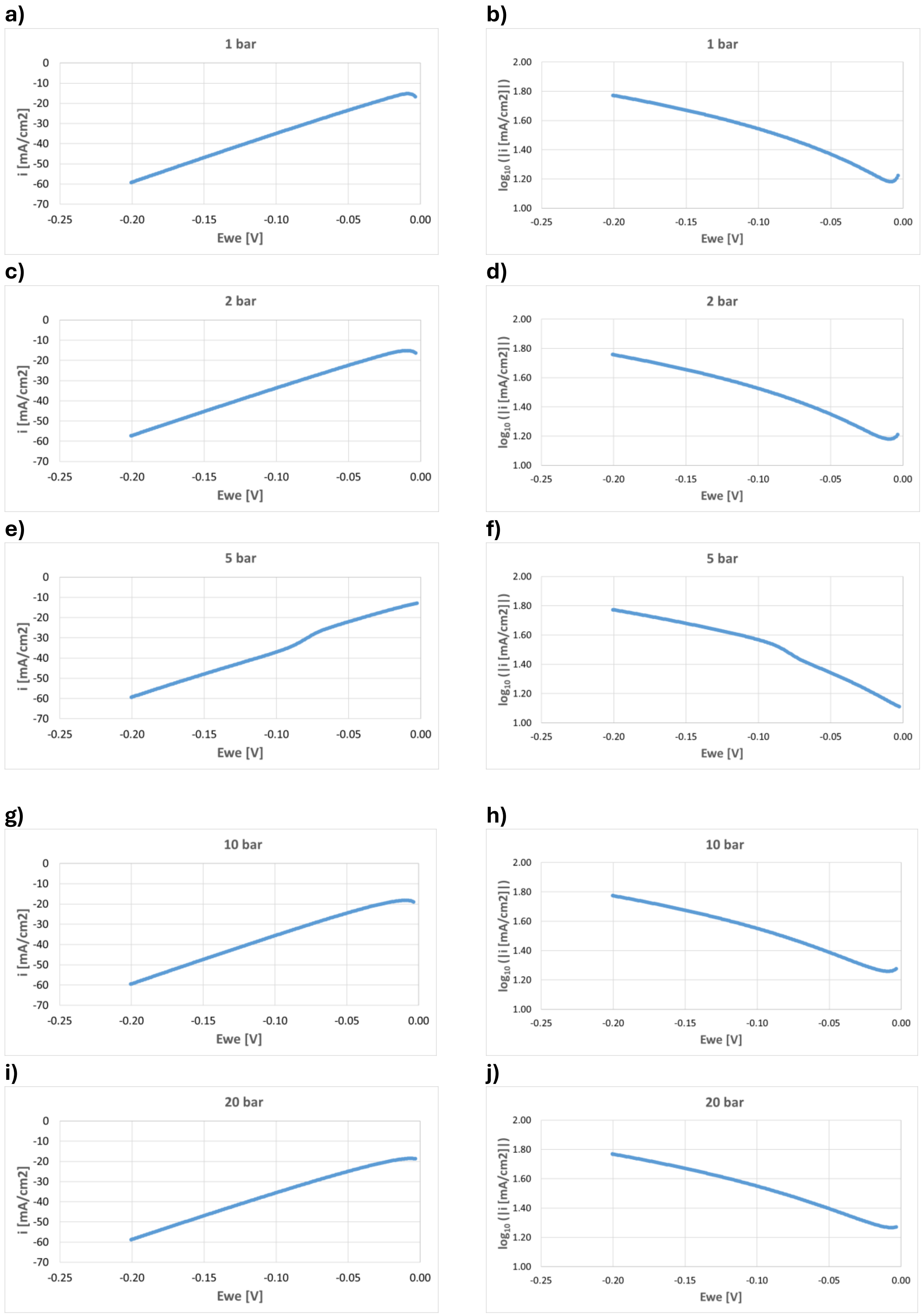

Figure 24 LSV curves (left) and corresponding Tafel plots (right) obtained at 25°C under varying pressures: a,b)1 bar; c,d) 2 bar; e,f) 5 bar; g,h) 10 bar; i,j) 20 bar.

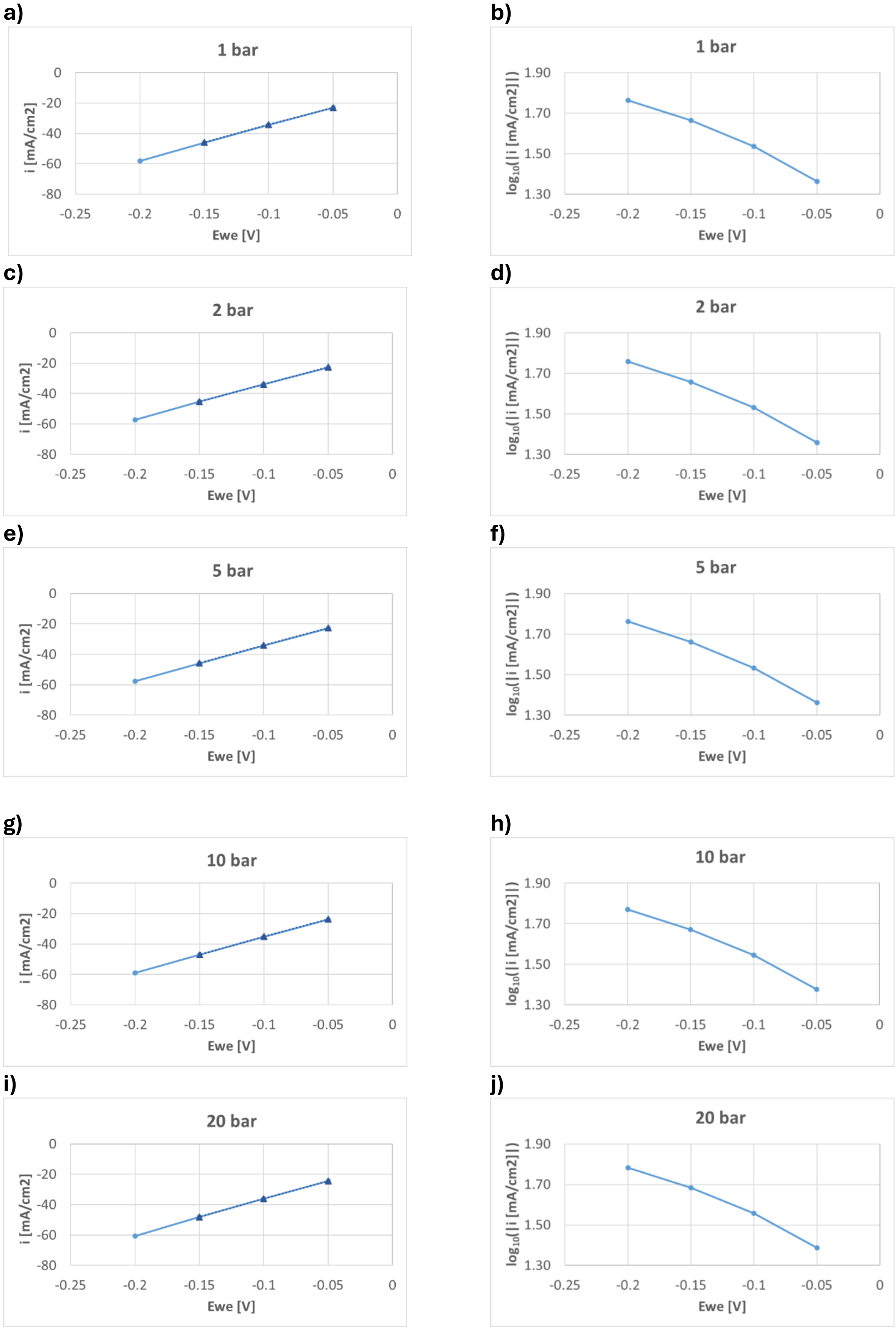

Figure 25 i-V curves (left) and corresponding Tafel plots (right, forward scan only) obtained at 25°C under varying pressures: a,b) 1 bar; c,d) 2 bar; e,f) 5 bar; g,h) 10 bar; i,j) 20 bar. For i-V curves, solid lines with circle symbols indicate forward scans while dotted lines with triangle symbols indicate backward scans.

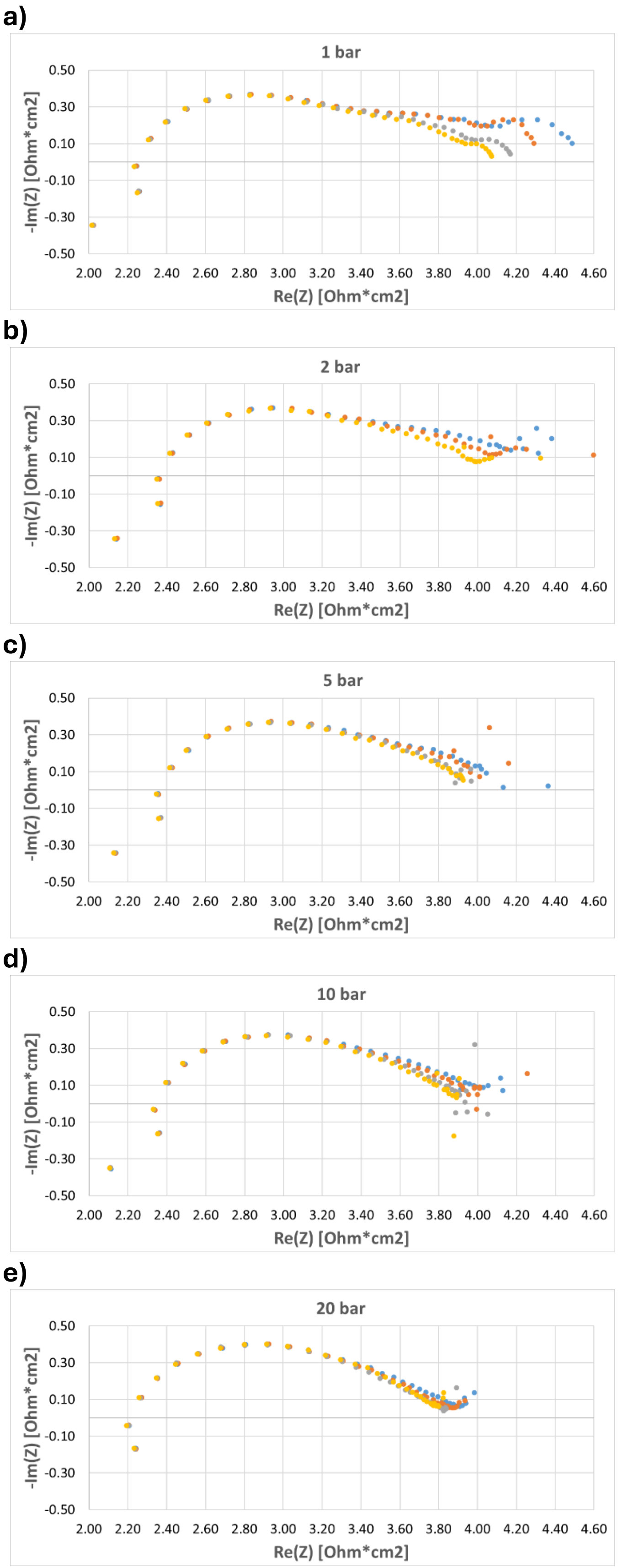

Figure 26 Nyquist plots at 25°C under varying pressures: a) 1 bar; b) 2 bar; c) 5 bar; d) 10 bar; e) 20 bar. Colour legend: blue (-0.05V), orange (-0.1V), grey (-0.15V), yellow (-0.2V).

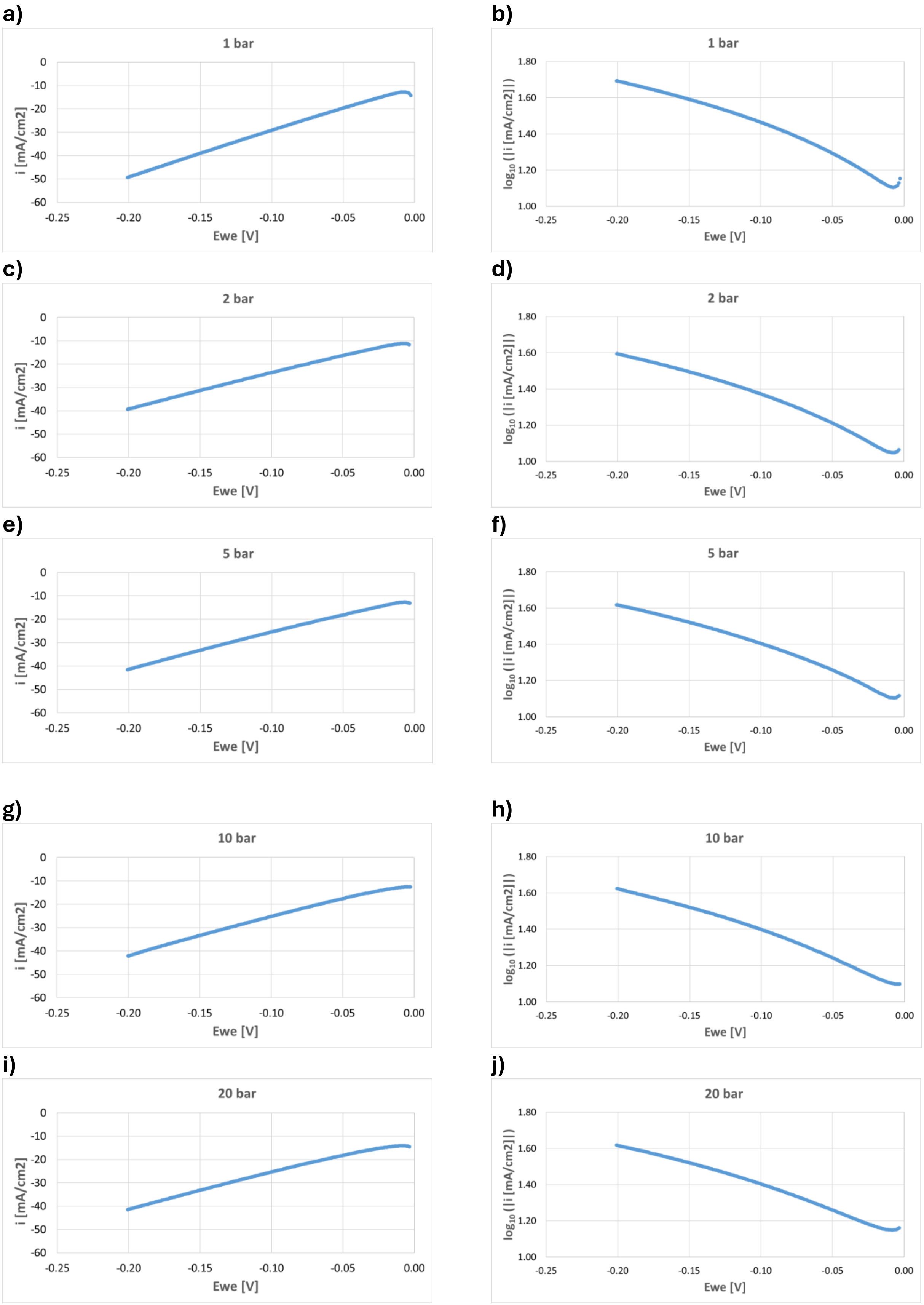

Figure 27 LSV curves (left) and corresponding Tafel plots (right) obtained at 50°C under varying pressures: a,b)1 bar; c,d) 2 bar; e,f) 5 bar; g,h) 10 bar; i,j) 20 bar.

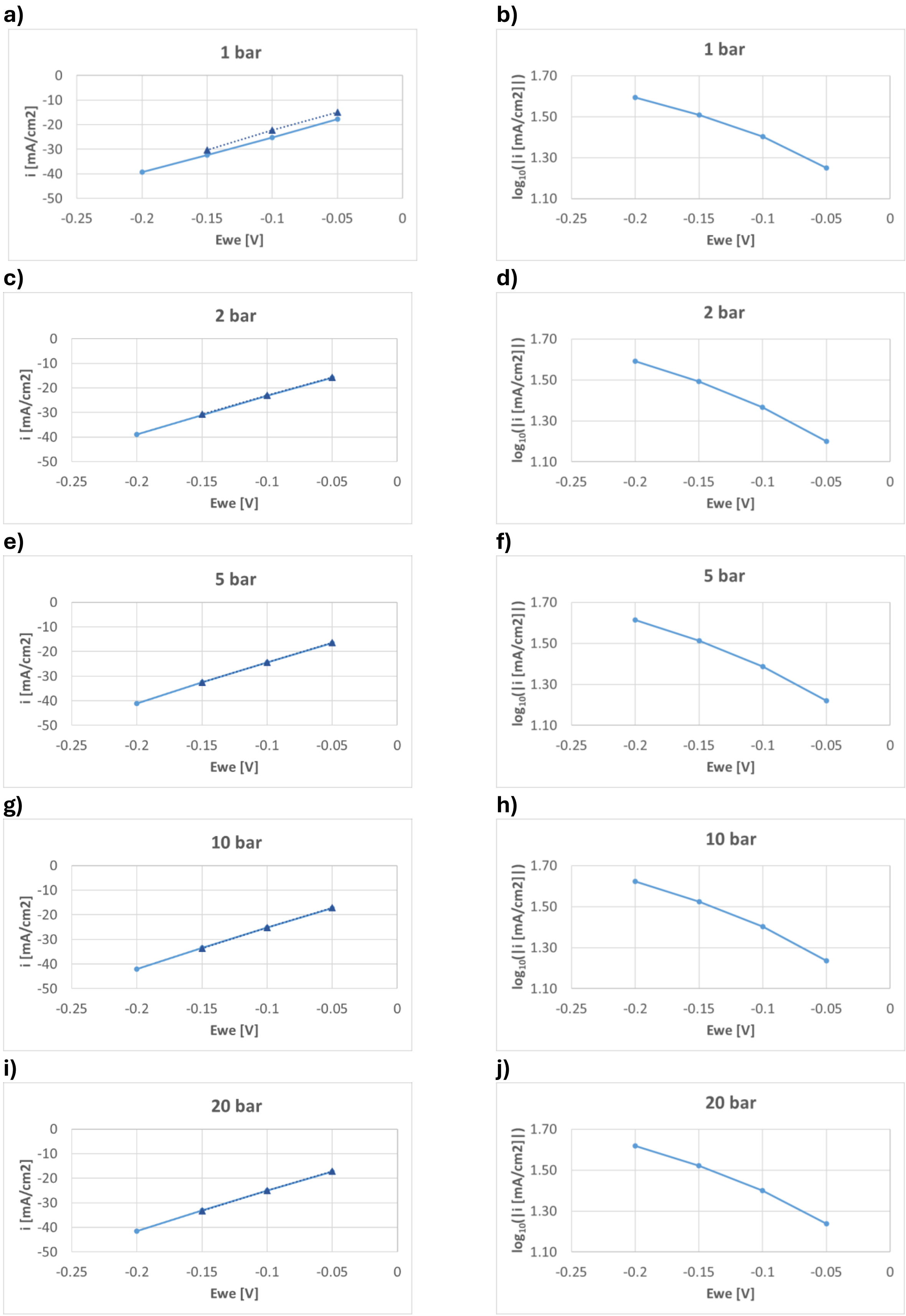

Figure 28 i-V curves (left) and corresponding Tafel plots (right, forward scan only) obtained at 50°C under varying pressures: a,b) 1 bar; c,d) 2 bar; e,f) 5 bar; g,h) 10 bar; i,j) 20 bar. For i-V curves, solid lines with circle symbols indicate forward scans while dotted lines with triangle symbols indicate backward scans

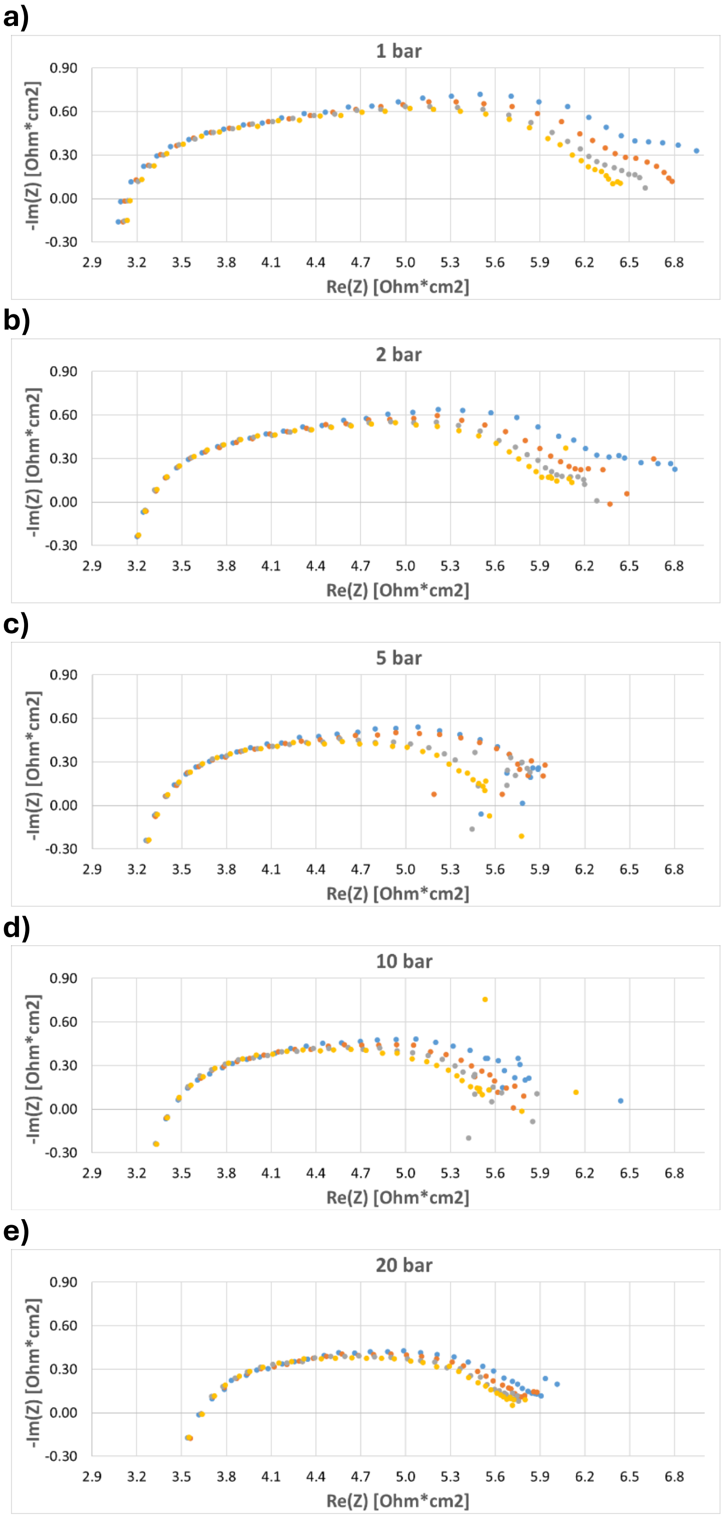

Figure 29 Nyquist plots at 50°C under varying pressures: a) 1 bar; b) 2 bar; c) 5 bar; d) 10 bar; e) 20 bar. Colour legend: blue (-0.05V), orange (-0.1V), grey (-0.15V), yellow (-0.2V).

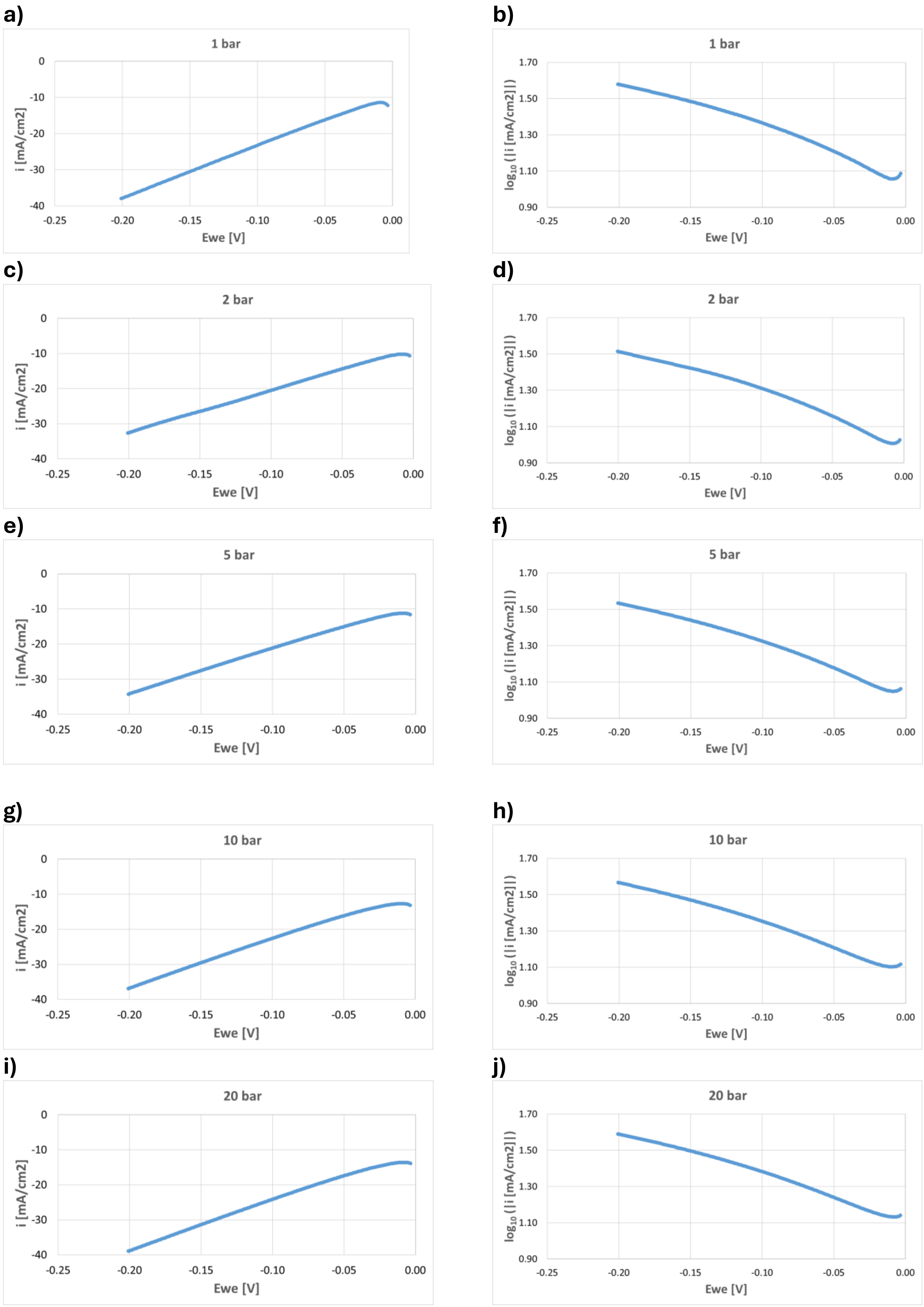

Figure 30 LSV curves (left) and corresponding Tafel plots (right) obtained at 80°C under varying pressures: a,b)1 bar; c,d) 2 bar; e,f) 5 bar; g,h) 10 bar; i,j) 20 bar.

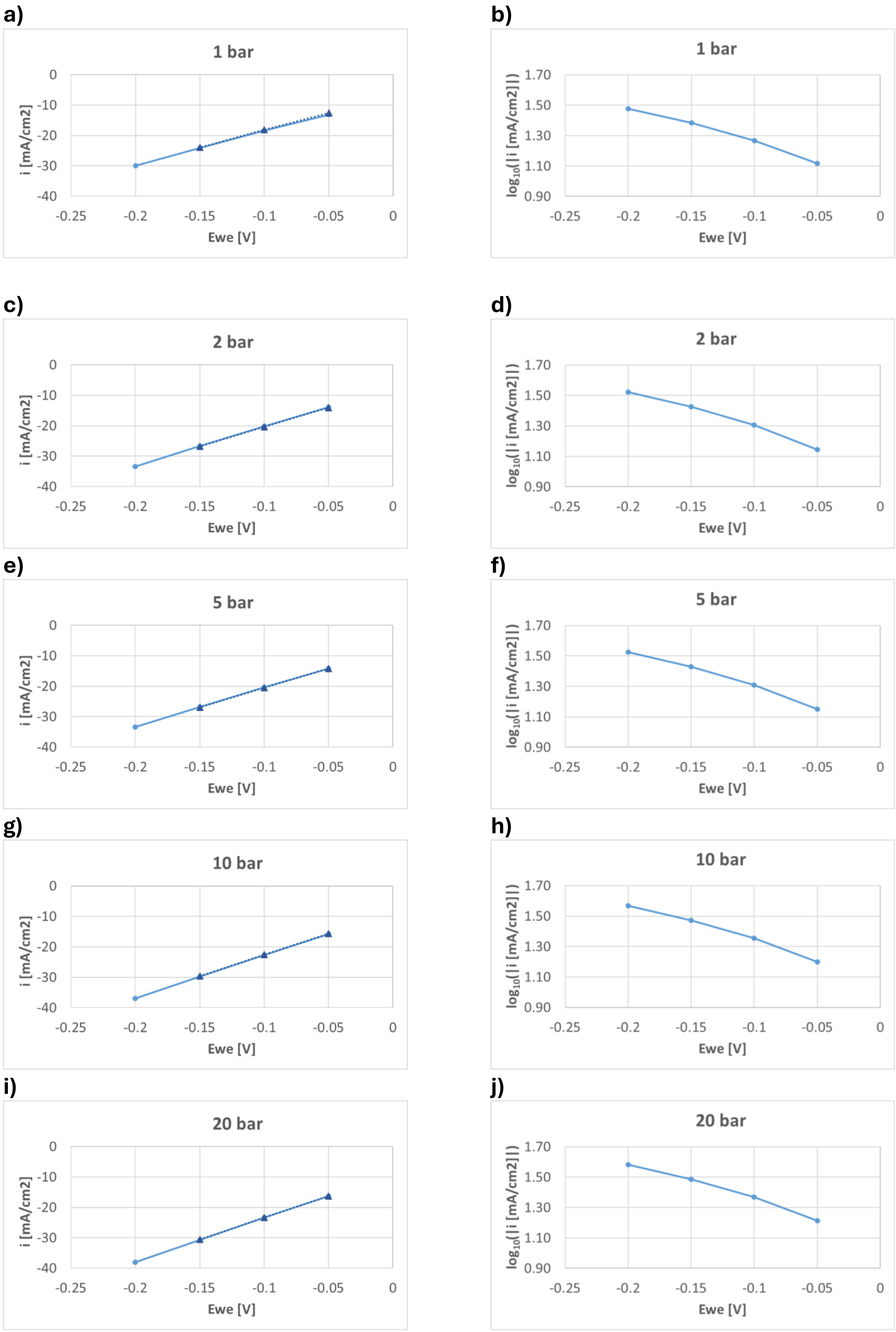

Figure 31 i-V curves (left) and corresponding Tafel plots (right, forward scan only) obtained at 80°C under varying pressures: a,b) 1 bar; c,d) 2 bar; e,f) 5 bar; g,h) 10 bar; i,j) 20 bar. For i-V curves, solid lines with circle symbols indicate forward scans while dotted lines with triangle symbols indicate backward scans.

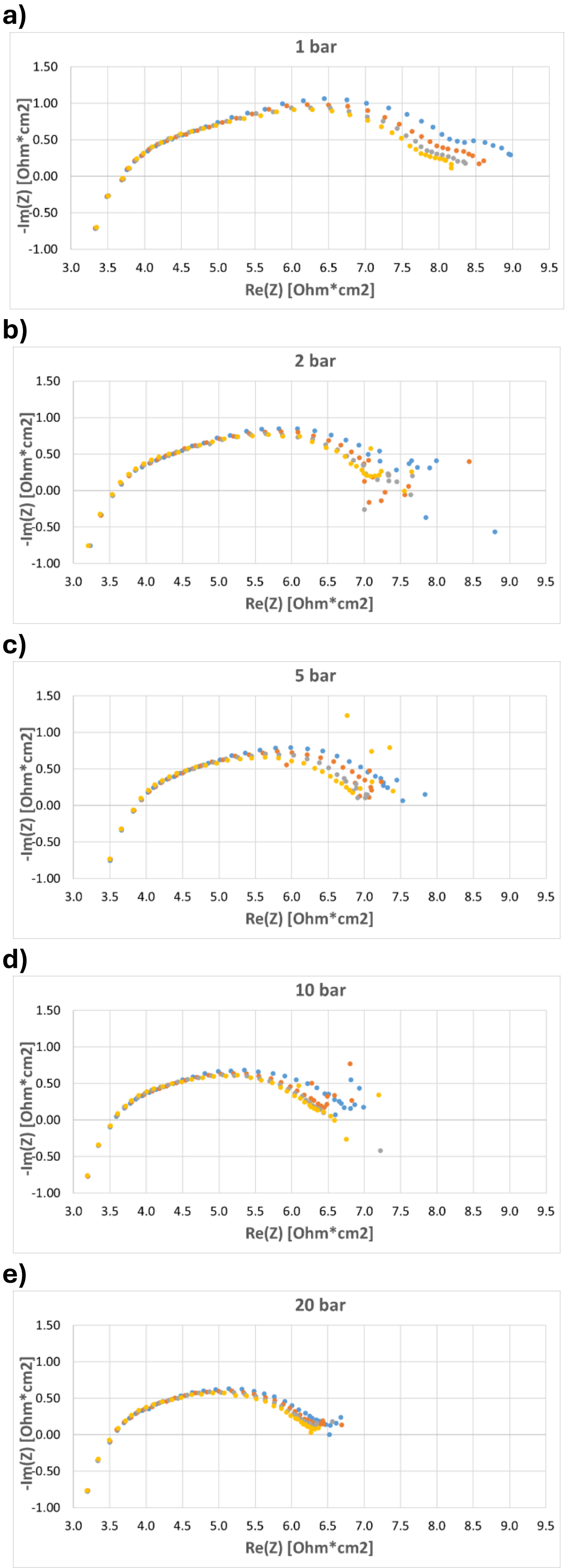

Figure 32 Nyquist plots at 80°C under varying pressures: a) 1 bar; b) 2 bar; c) 5 bar; d) 10 bar; e) 20 bar. Colour legend: blue (-0.05V), orange (-0.1V), grey (-0.15V), yellow (-0.2V).

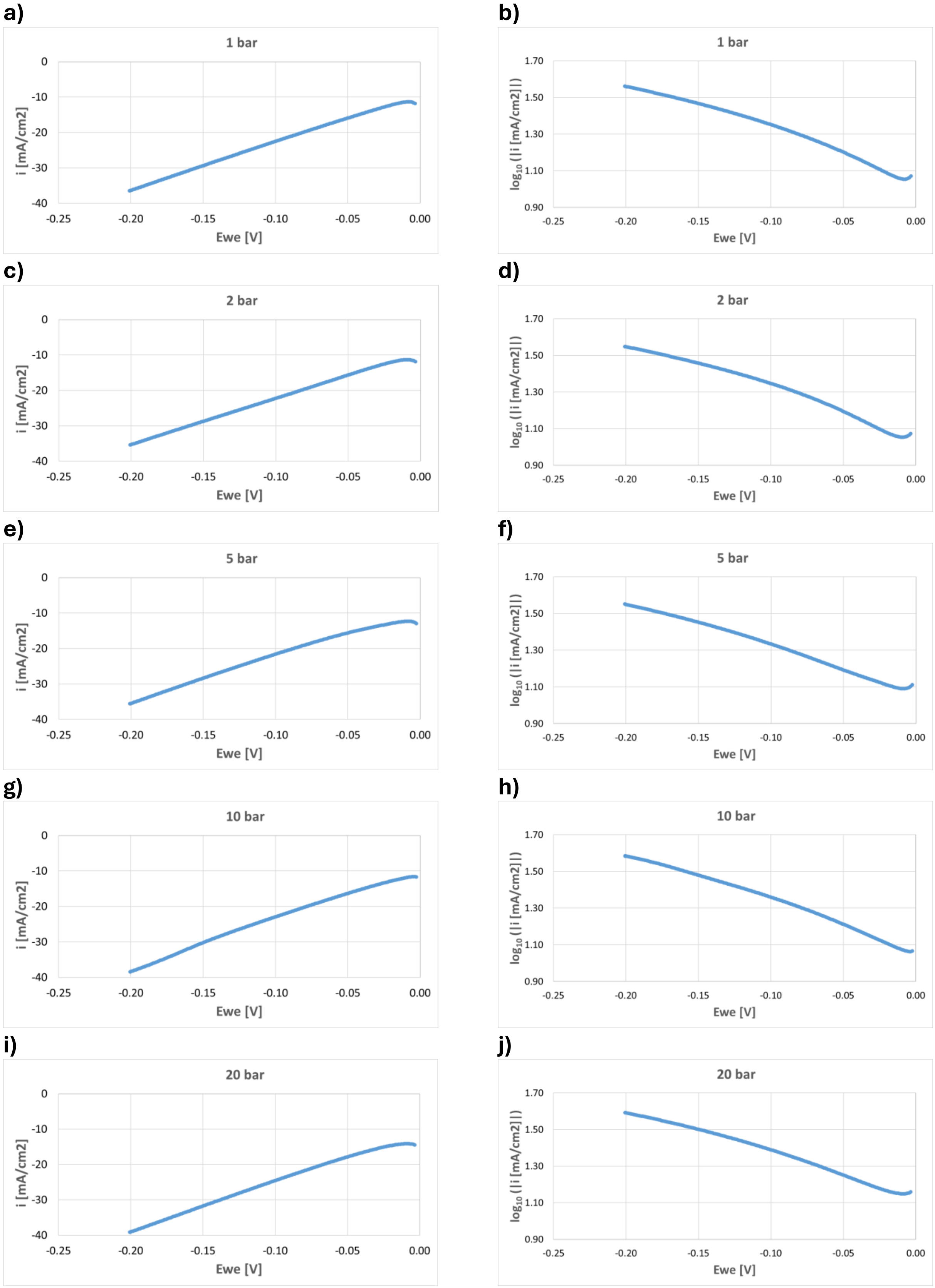

Figure 33 LSV curves (left) and corresponding Tafel plots (right) obtained at 120°C under varying pressures: a,b)1 bar; c,d) 2 bar; e,f) 5 bar; g,h) 10 bar; i,j) 20 bar.

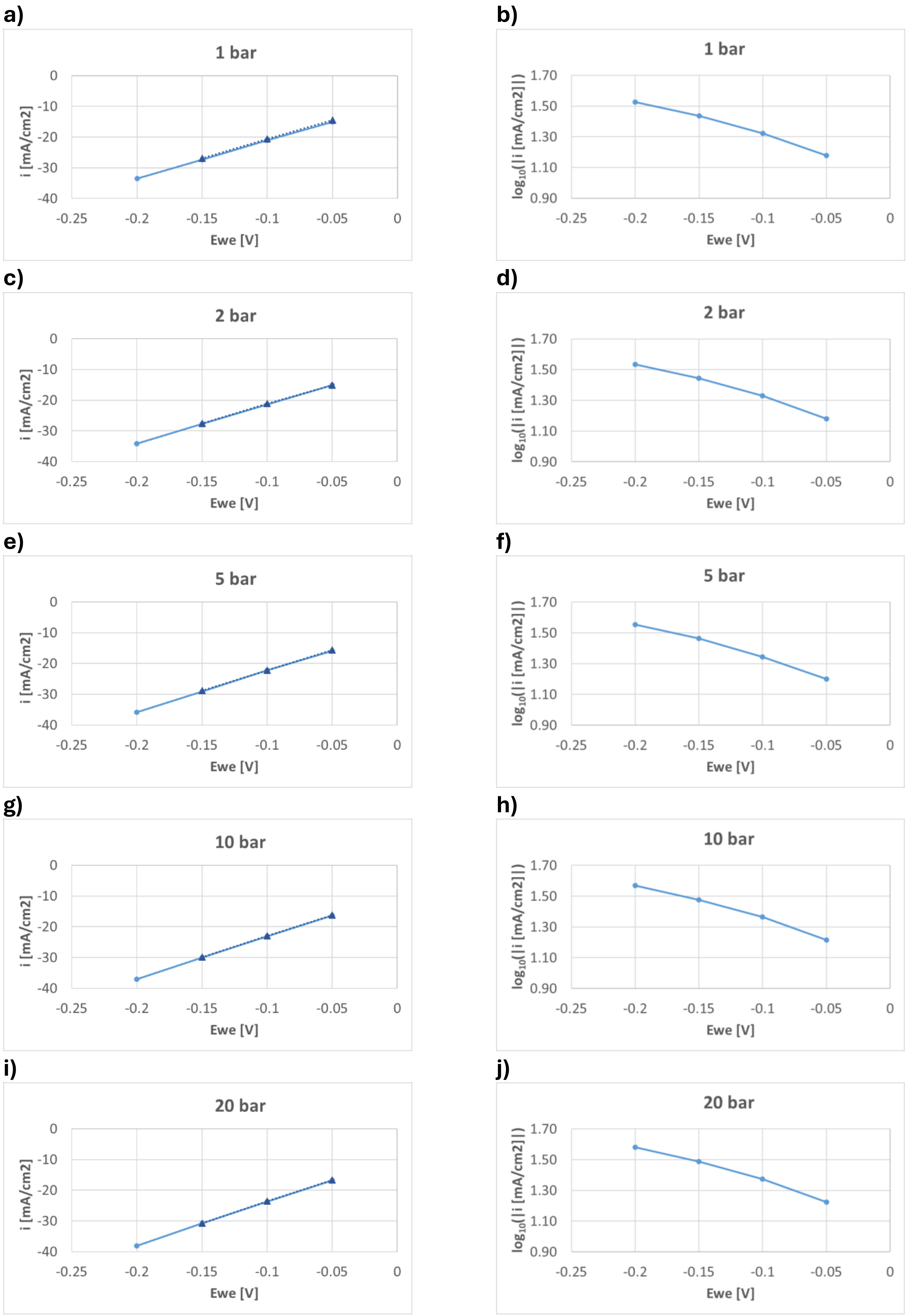

Figure 34 i-V curves (left) and corresponding Tafel plots (right, forward scan only) obtained at 120°C under varying pressures: a,b) 1 bar; c,d) 2 bar; e,f) 5 bar; g,h) 10 bar; i,j) 20 bar. For i-V curves, solid lines with circle symbols indicate forward scans while dotted lines with triangle symbols indicate backward scans.

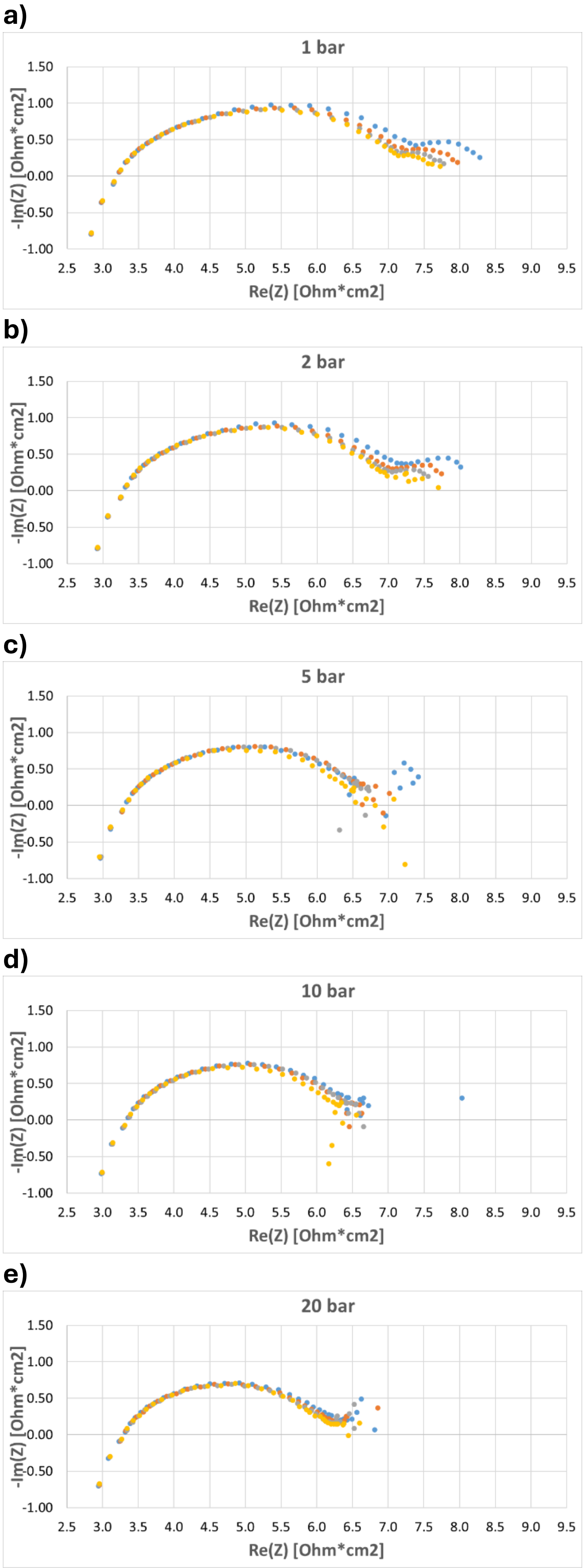

Figure 35 Nyquist plots at 120°C under varying pressures: a) 1 bar; b) 2 bar; c) 5 bar; d) 10 bar; e) 20 bar. Colour legend: blue (-0.05V), orange (-0.1V), grey (-0.15V), yellow (-0.2V).

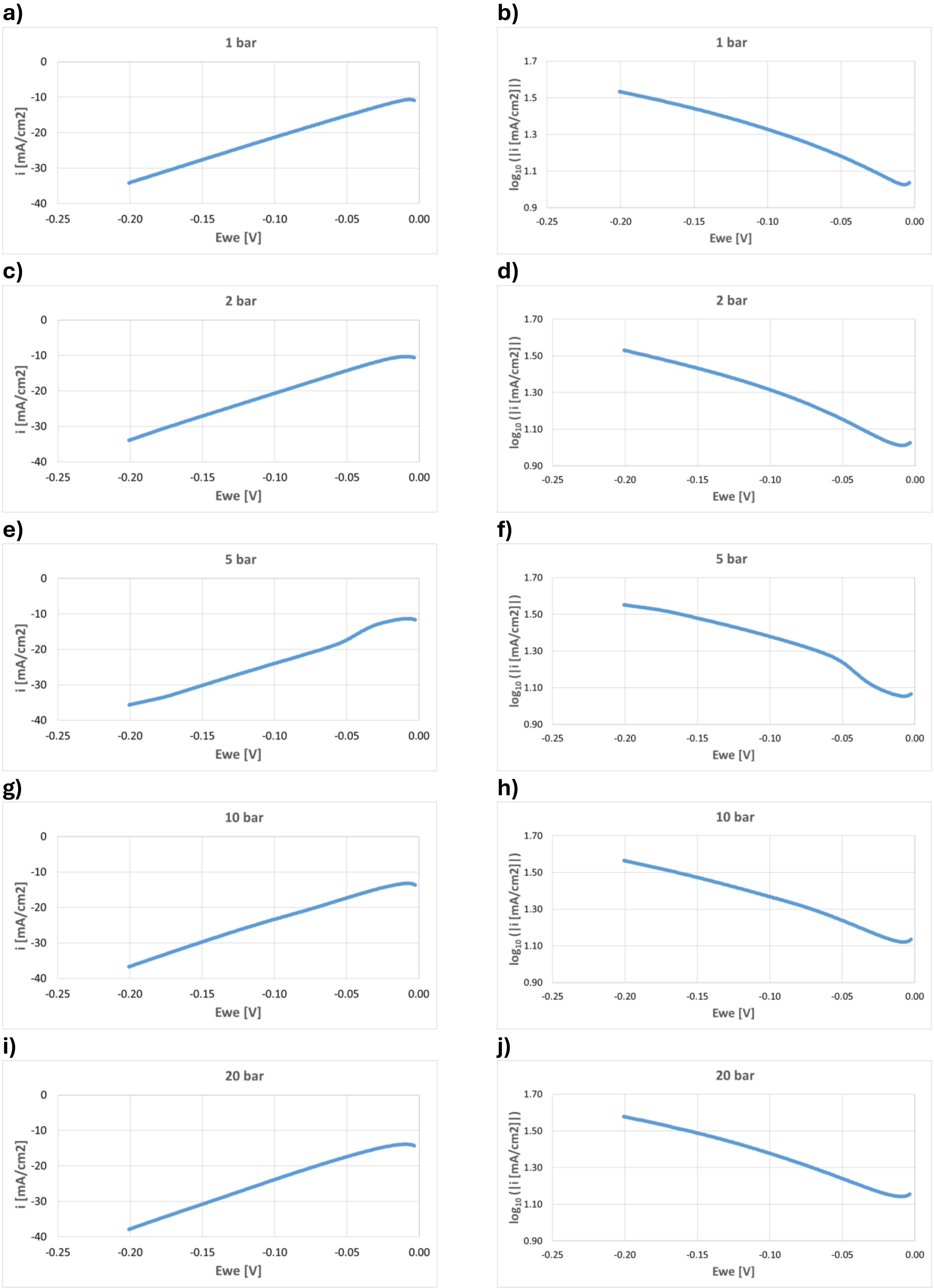

Figure 36 LSV curves (left) and corresponding Tafel plots (right) obtained at 150°C under varying pressures: a,b)1 bar; c,d) 2 bar; e,f) 5 bar; g,h) 10 bar; i,j) 20 bar.

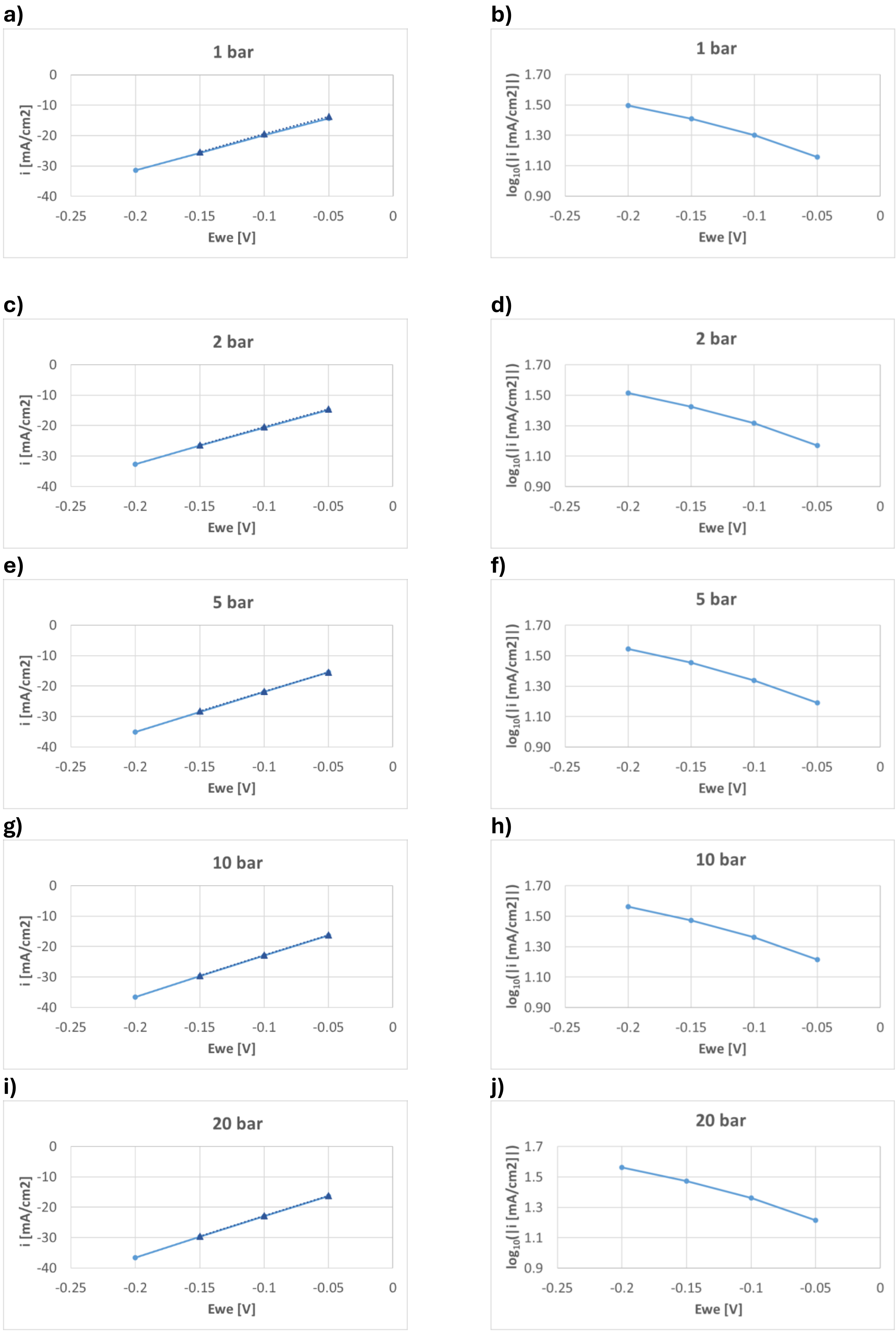

Figure 37 i-V curves (left) and corresponding Tafel plots (right, forward scan only) obtained at 150°C under varying pressures: a,b) 1 bar; c,d) 2 bar; e,f) 5 bar; g,h) 10 bar; i,j) 20 bar. For i-V curves, solid lines with circle symbols indicate forward scans while dotted lines with triangle symbols indicate backward scans.

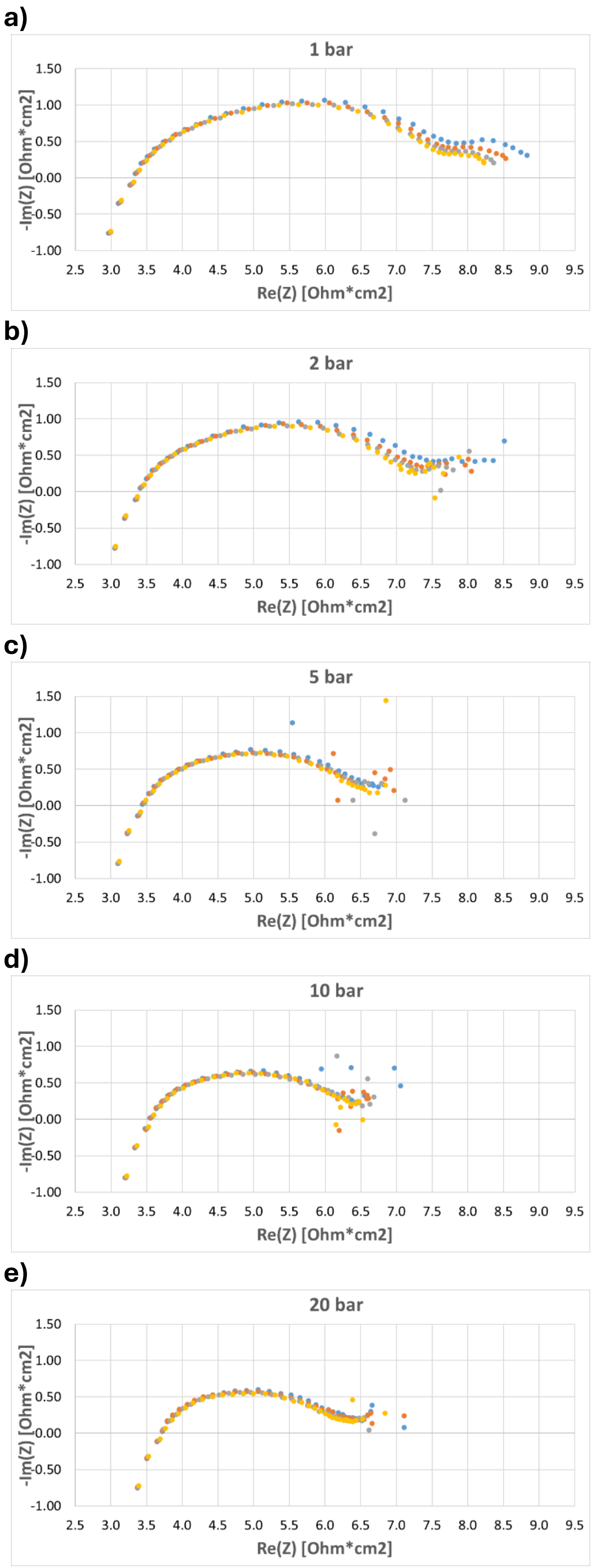

Figure 38 Nyquist plots at 150°C under varying pressures: a) 1 bar; b) 2 bar; c) 5 bar; d) 10 bar; e) 20 bar. Colour legend: blue (-0.05V), orange (-0.1V), grey (-0.15V), yellow (-0.2V).

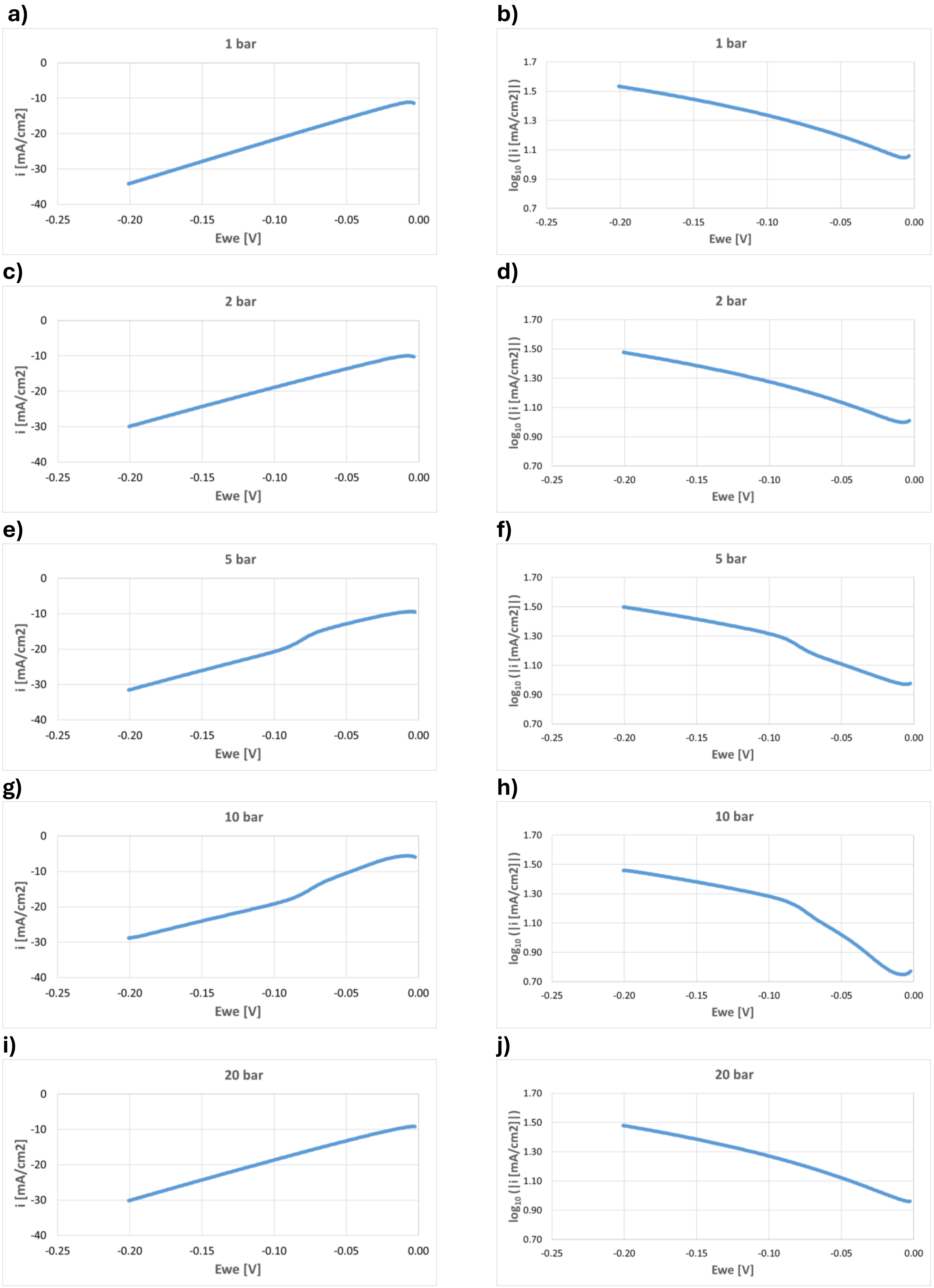

Figure 39 LSV curves (left) and corresponding Tafel plots (right) obtained at 180°C under varying pressures: a,b)1 bar; c,d) 2 bar; e,f) 5 bar; g,h) 10 bar; i,j) 20 bar.

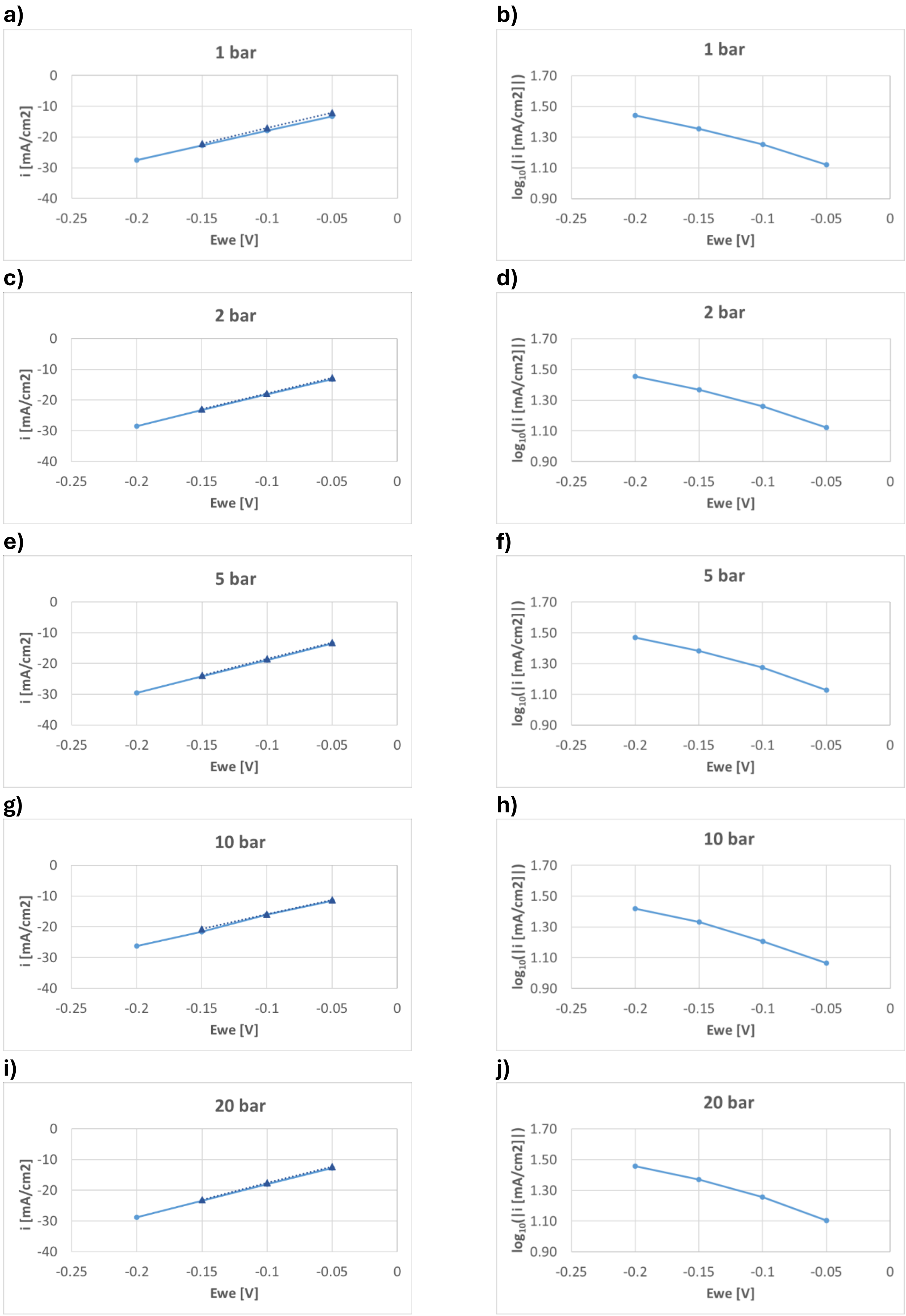

Figure 40 i-V curves (left) and corresponding Tafel plots (right, forward scan only) obtained at 180°C under varying pressures: a,b) 1 bar; c,d) 2 bar; e,f) 5 bar; g,h) 10 bar; i,j) 20 bar. For i-V curves, solid lines with circle symbols indicate forward scans while dotted lines with triangle symbols indicate backward scans.

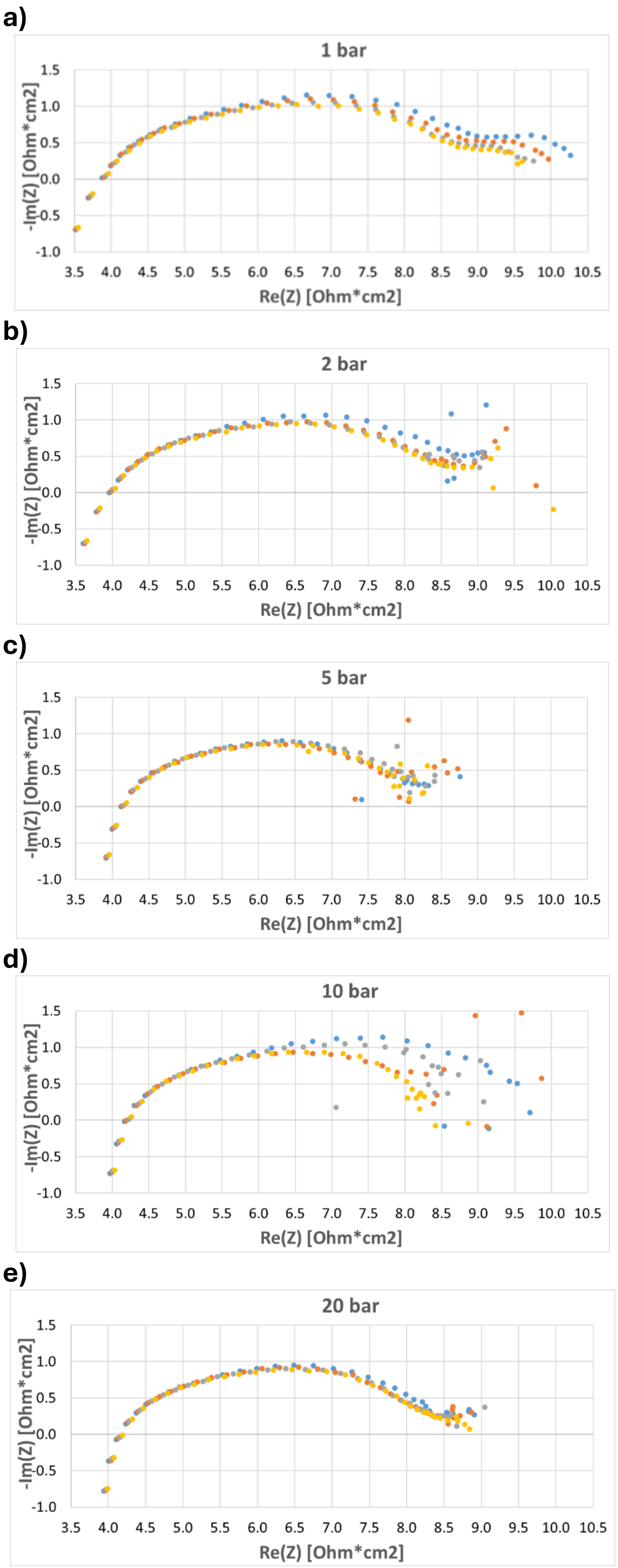

Figure 41 Nyquist plots at 180°C under varying pressures: a) 1 bar; b) 2 bar; c) 5 bar; d) 10 bar; e) 20 bar. Colour legend: blue (-0.05V), orange (-0.1V), grey (-0.15V), yellow (-0.2V).

To investigate the effect of temperature, analyses were conducted at constant pressure by varying the temperature. Specifically, the same electrochemical analyses previously performed (LSV, CA, PEIS) were replicated at 20 bar and temperatures of 25, 50, 80, 120, 150, 180 °C.

Figure 42, Figure 43, Figure 44, show, respectively, the LSV curves with corresponding Tafel plots, the i-V curves with the related Tafel plots (forward only), and the Nyquist plots, all acquired at 20 bar under different temperatures (25, 50, 80, 120, 150, 180 °C).

The LSV curves indicate that the current density increases as the temperature is raised from 25 to 50°C and then to 80°C, whereas at 120°C a decrease in the maximum measured current is observed. The i-V curves follow a similar pattern: the current density increases from 25 to 50°C, the curves at 50°C and 80°C are nearly identical, and a further decrease in current density appears when temperature is raised to 120°C. The Tafel plots are essentially parallel to each other.

The Nyquist plots at 20 bar show that at 25°C the spectrum suggests the presence of two overlapping arcs, which at 50°C tend to merge into a single, more regular semicircle shifted to lower Re(Z) values. As the temperature is further increased to 80°C and 120°C, the diameter of the semicircles grows, whereas at 150 and 180°C it decreases again.

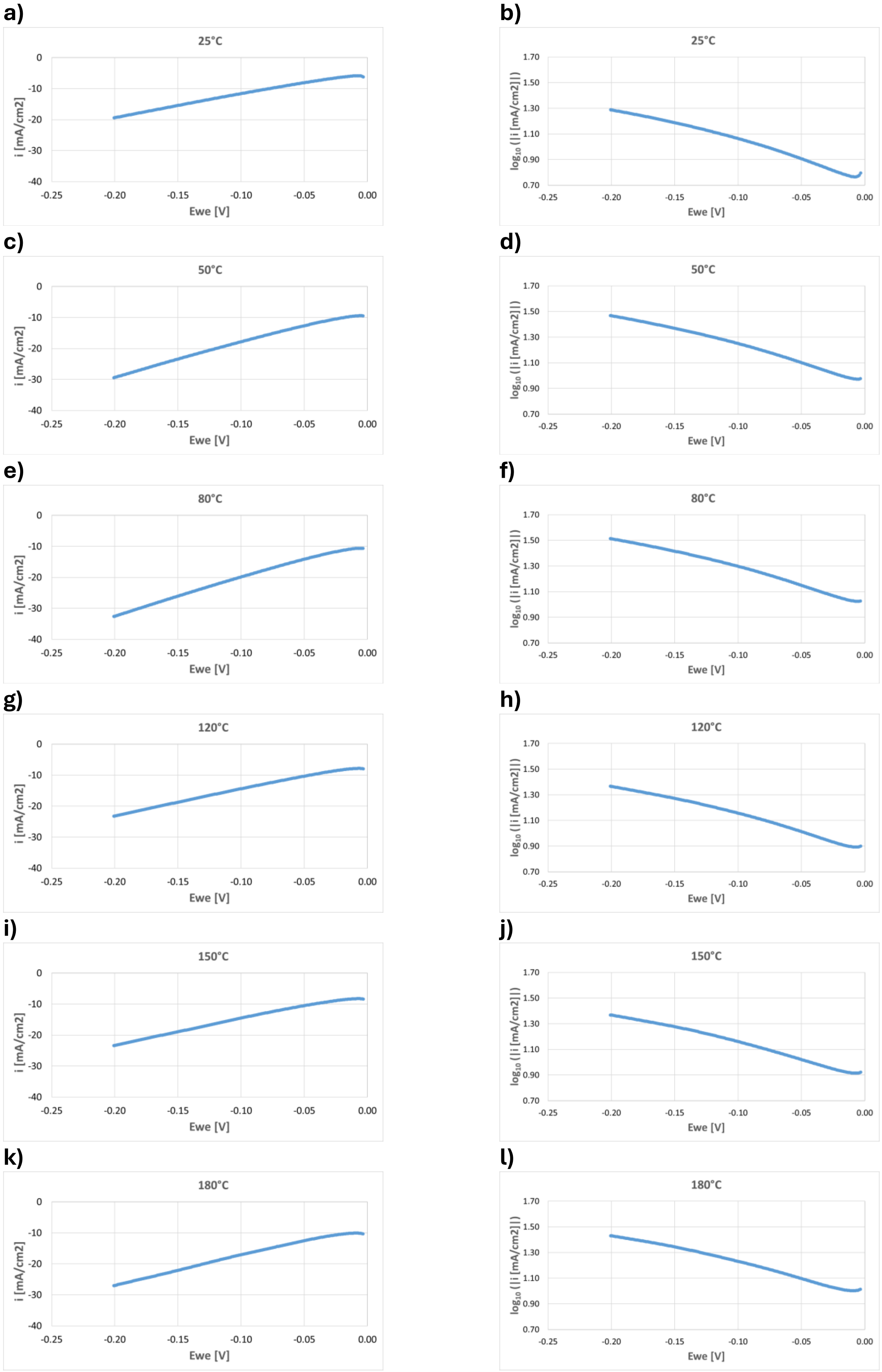

Figure 42 LSV curves (left) and corresponding Tafel plots (right) obtained at 20 bar under varying temperatures: a,b) 25°C; c,d) 50°C; e,f) 80°C; g,h) 120°C; i,j) 150°C, k,l) 180°C.

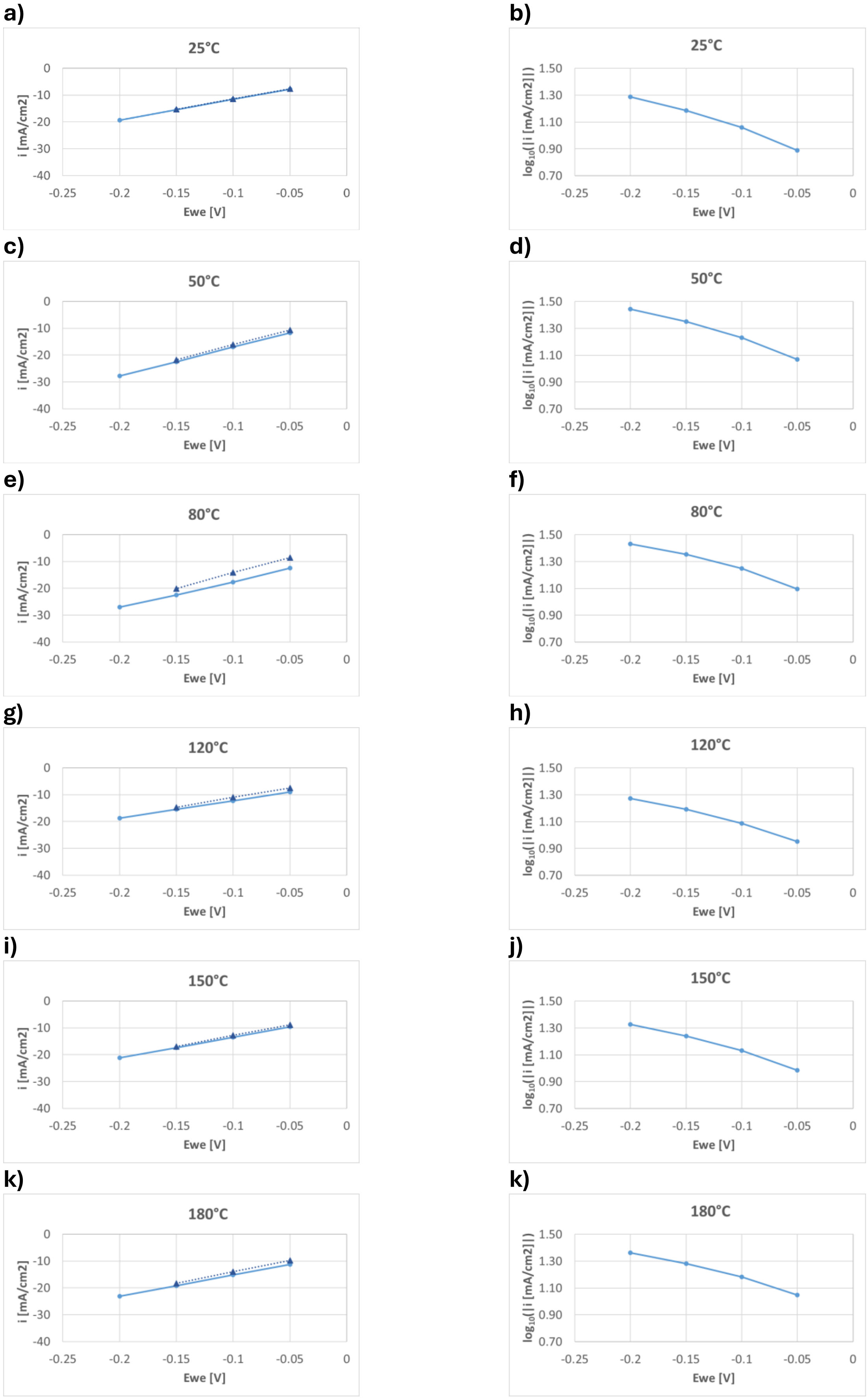

Figure 43 i-V curves (left) and corresponding Tafel plots (right, forward scan only) obtained at 20 bar under varying temperatures: a,b) 25°C; c,d) 50°C; e,f) 80°C; g,h) 120°C; i,j) 150°C, k,l) 180°C. For i-V curves, solid lines with circle symbols indicate forward scans while dotted lines with triangle symbols indicate backward scans.

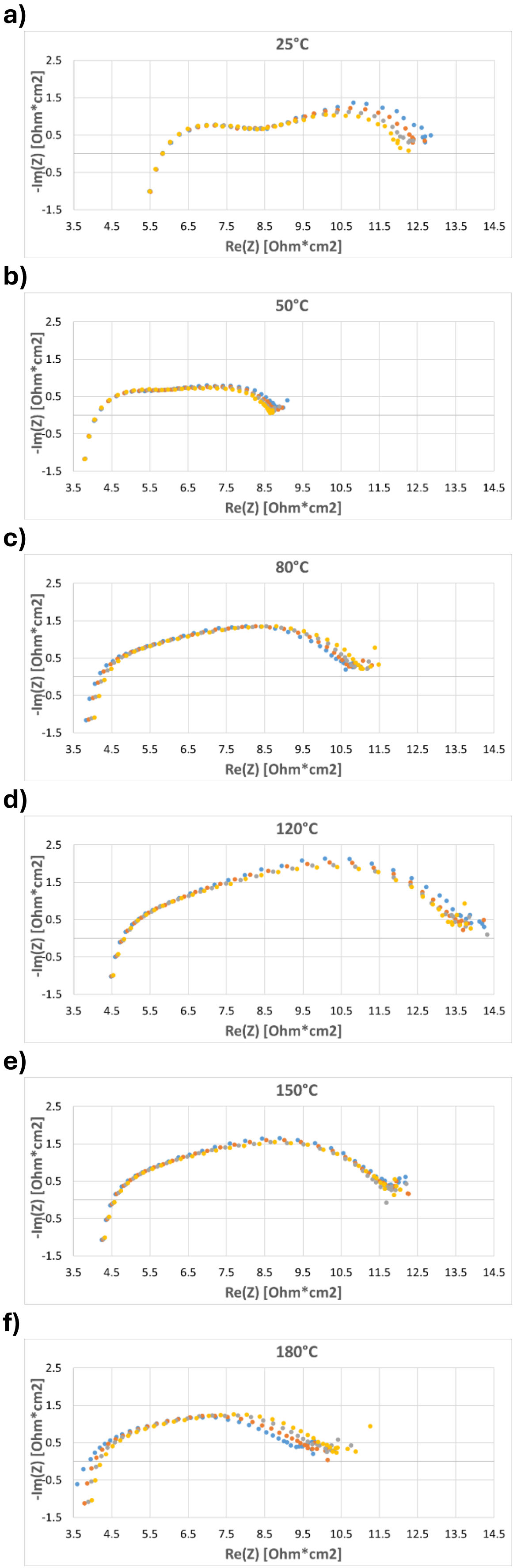

Figure 44 Nyquist plots at 20 bar under varying temperatures: a) 25°C; b) 50°C; c) 80°C; d) 120°C; e) 150°C; f)180°C. Colour legend: blue symbols (-0.05V), orange (-0.1V), grey (-0.15V), yellow (-0.2V).

Among the experiments conducted at variable pressures (1 to 20 bar) at constant temperatures and those at constant pressure (20 bar) with increasing temperature, specific reference tests at 25°C and 1 bar were included, performed sequentially after each cycle of pressure and temperature increase. Specifically: after the experiments at 25°C with progressive pressure up to 20 bar, after those at 50°C with pressure increase up to 20 bar, after those at 80°C up to 20 bar, after those at 120°C up to 20 bar, after those at 150°C up to 20 bar, after those at 180°C with pressure increase up to 20 bar, and finally after the experiments at constant pressure of 20 bar with temperature increased from 25 to 180°C. Returning to the reference conditions allowed evaluation of the cell’s stability over time.

Figure 45-Figure 50 show, respectively, the LSV curves with their corresponding Tafel plots, the i-V curves with the associated Tafel plots (considering only the forward direction) and the Nyquist plots obtained under different reference conditions.

The reference conditions are defined as followed:

1. Reference condition 1 (Ref. 1): it corresponds to the initial experiments carried out at 1 bar and 25°C.
2. Reference condition 2 (Ref. 2): experiments performed after the first pressure increase (from 1 to 20 bar) at 25°C.
3. Reference condition 3 (Ref. 3): experiments performed after the second pressure increase at 50°C.
4. Reference condition 4 (Ref. 4): experiments performed after the third pressure increase at 80°C.
5. Reference condition 5 (Ref. 5): experiments performed after the fourth pressure increase at 120°C.
6. Reference condition 6 (Ref. 6): experiments performed after the fifth pressure increase at 150°C.
7. Reference condition 7 (Ref. 7): experiments performed after the sixth pressure increase at 180°C.
8. Reference condition 8 (Ref. 8): experiments performed after the series of tests at constant pressure (20 bar) and increasing temperature from 25°C to 180°C.

In the LSV measurements, the curves corresponding to Reference condition 1 and 2 show almost identical profiles, reaching current densities of about -60 mA/cm2, indicating that the initial pressure increase from 1 to 20 bar at 25°C does not lead to any noticeable change in the cell behaviour. Starting from Reference condition 3, a progressive decrease in the maximum current density is observed, from roughly -45 mA/cm2 for Ref. 3 to about -15 mA/cm2 for Ref. 8. This trend suggests that temperature shows a more pronounced influence on the cell performance than pressure alone, in line with the fact that, at constant temperature, pressure variations had only minor effects on the measurements. The Tafel plots show comparable shapes and appear essentially shifted in parallel.

The same trend is found in the i-V curves.

The Nyquist plots exhibit semicircles that progressively shift towards higher values for the real part of the impedance and increase in diameter. For Reference condition 7 and 8, two partially overlapping arcs become evident.

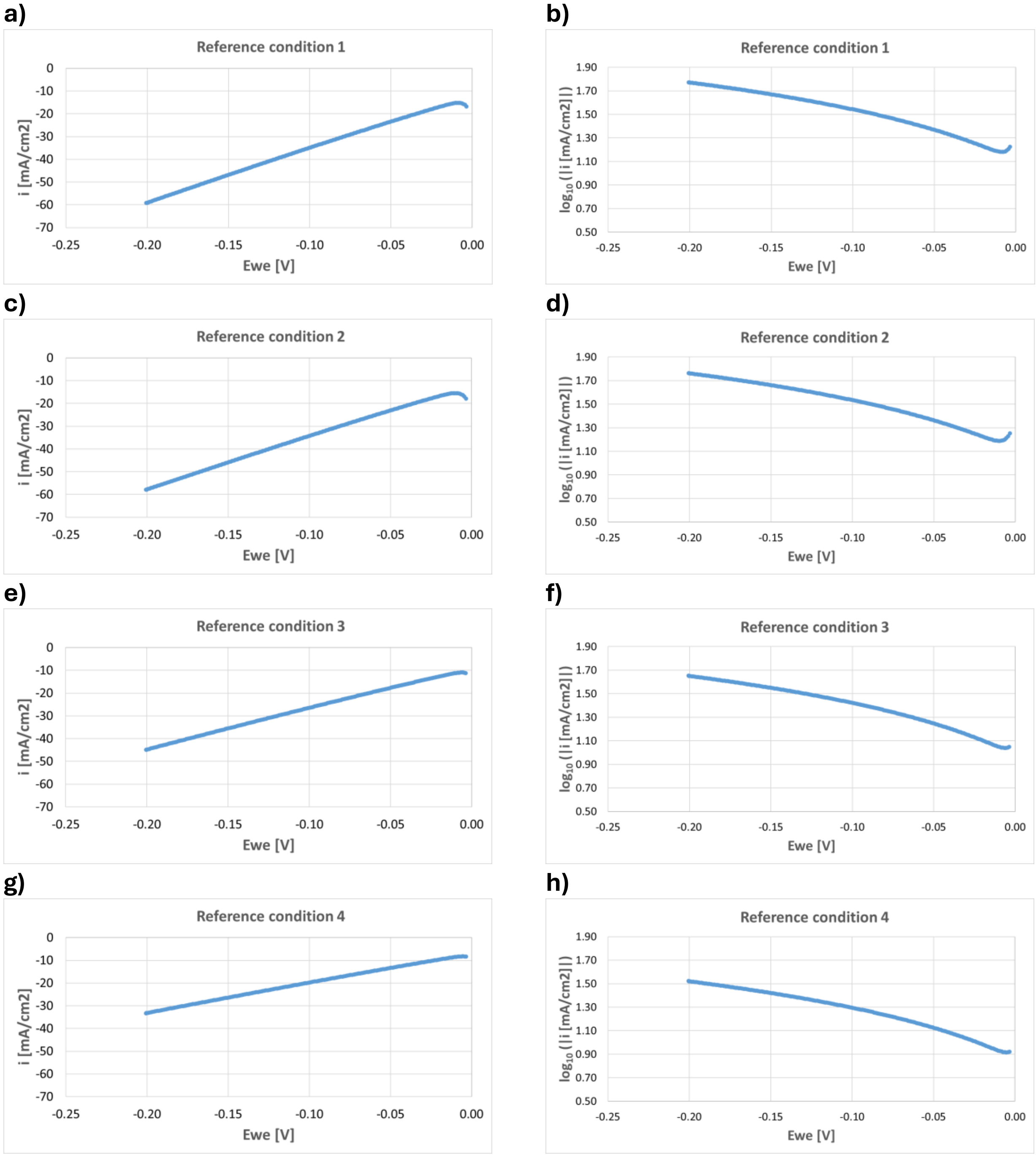

Figure 45 LSV curves (left) and corresponding Tafel plots (right) obtained at 1 bar and 25°C under N2 feed (Reference conditions): a,b) Reference condition 1; c,d) Reference condition 2; e,f) Reference condition 3; g,h) Reference condition 4.

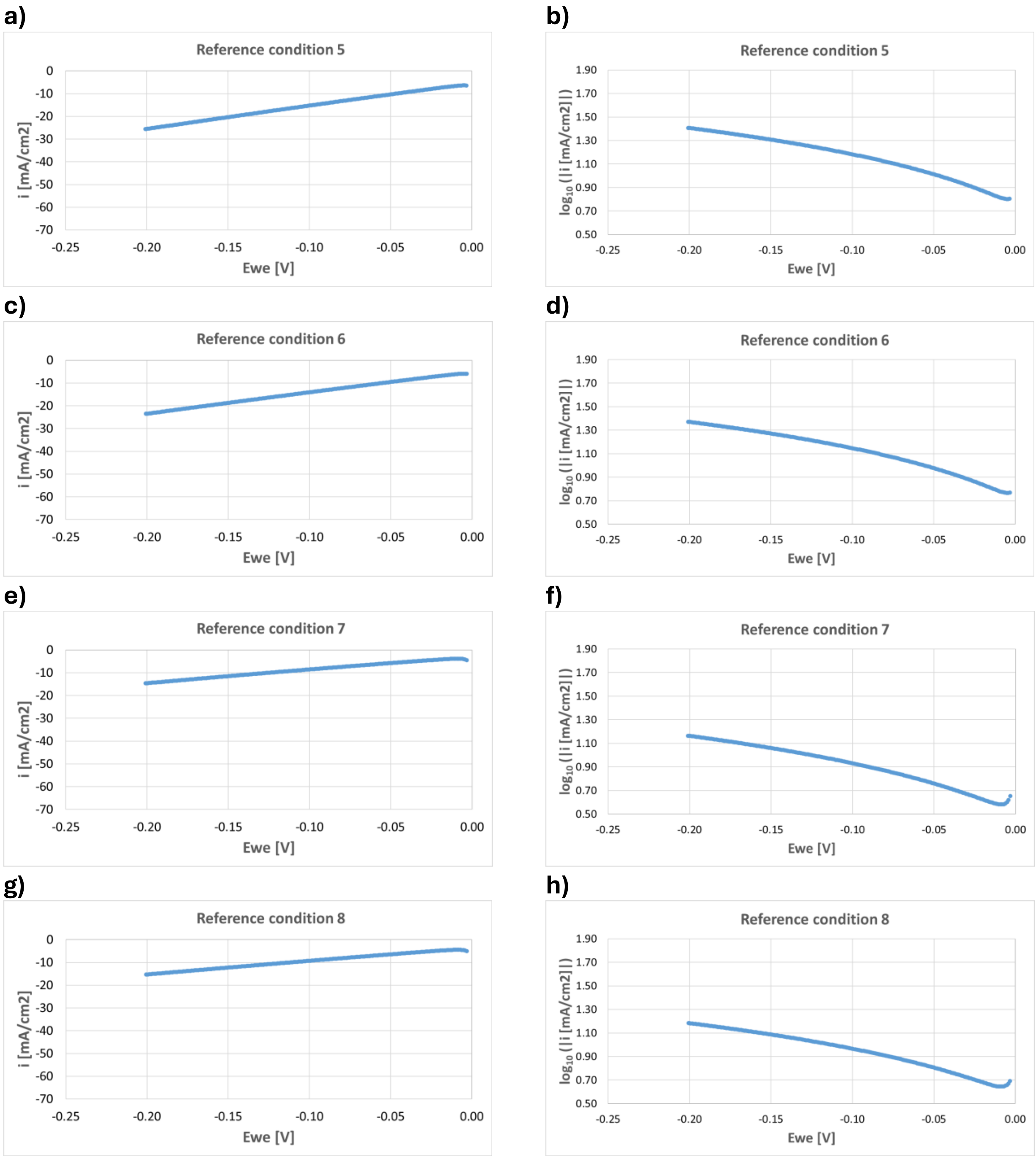

Figure 46 LSV curves (left) and corresponding Tafel plots (right) obtained at 1 bar and 25°C under N2 feed (Reference conditions): a,b) Reference condition 5, c,d) Reference condition 6; e,f) Reference condition 7; g,h) Reference condition 8.

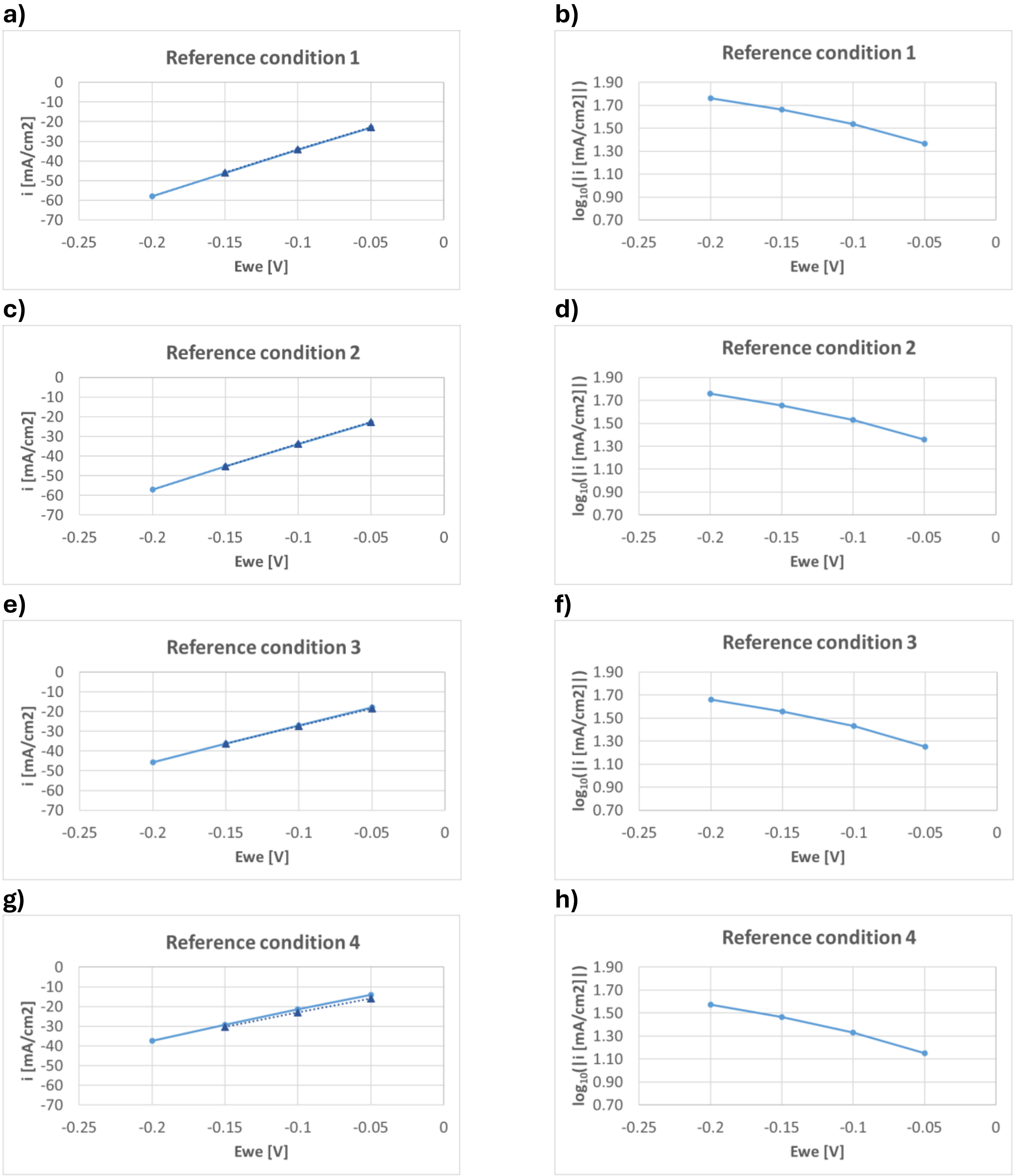

Figure 47 i-V curves (left) and corresponding Tafel plots (right, forward scan only) obtained at 1 bar and 25°C under N2 feed (Reference conditions): a,b) Reference condition 1; c,d) Reference condition 2; e,f) Reference condition 3; g,h) Reference condition 4. For i-V curves, solid lines with circle symbols indicate forward scans while dotted lines with triangle symbols indicate backward scans.

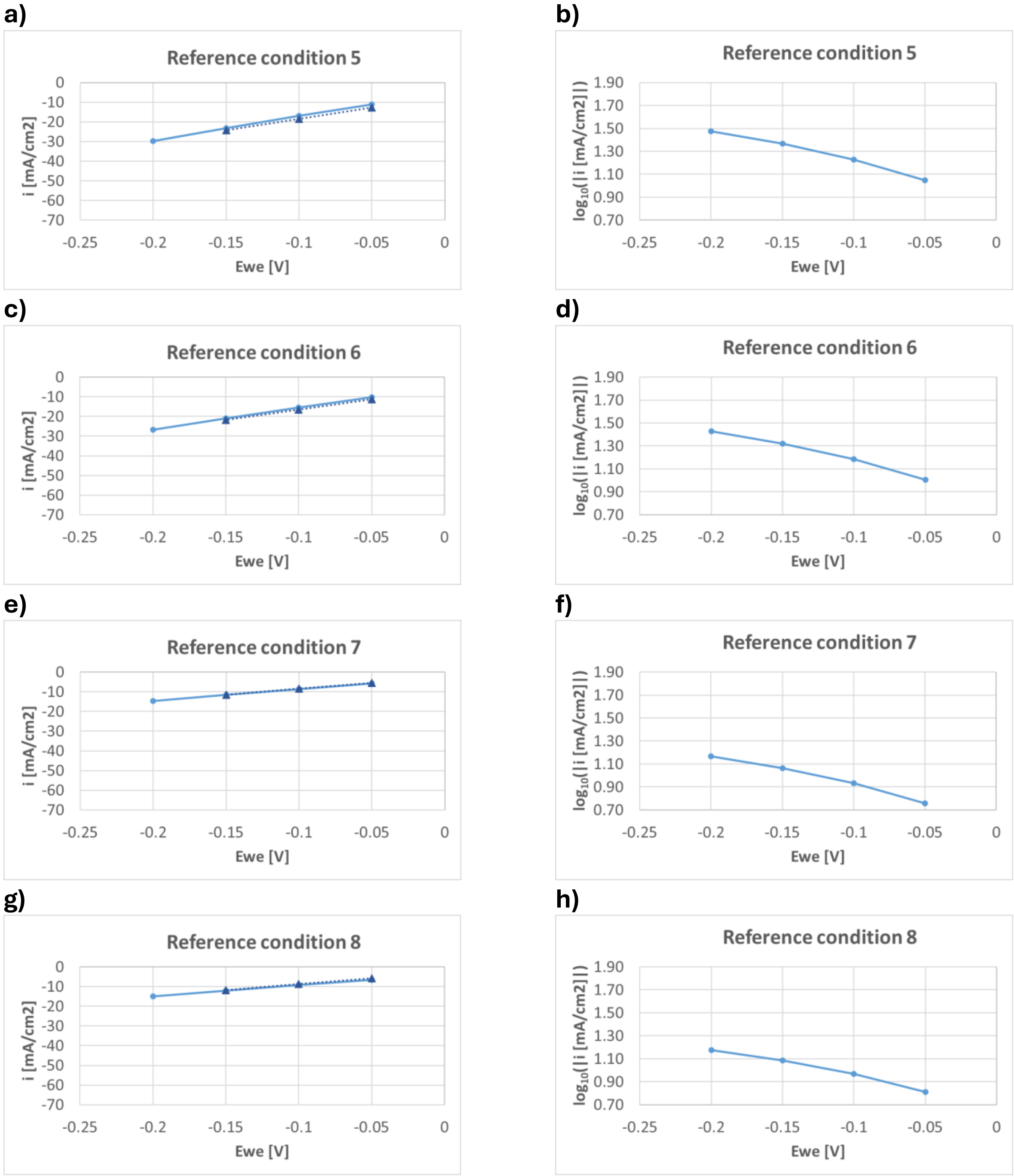

Figure 48 i-V curves (left) and corresponding Tafel plots (right, forward scan only) obtained at 1 bar and 25°C under N2 feed (Reference conditions): a,b) Reference condition 5; c,d) Reference condition 6; e,f) Reference condition 7; g,h) Reference condition 8. For i-V curves, solid lines with circle symbols indicate forward scans, while dotted lines with triangle symbols indicate backward scans.

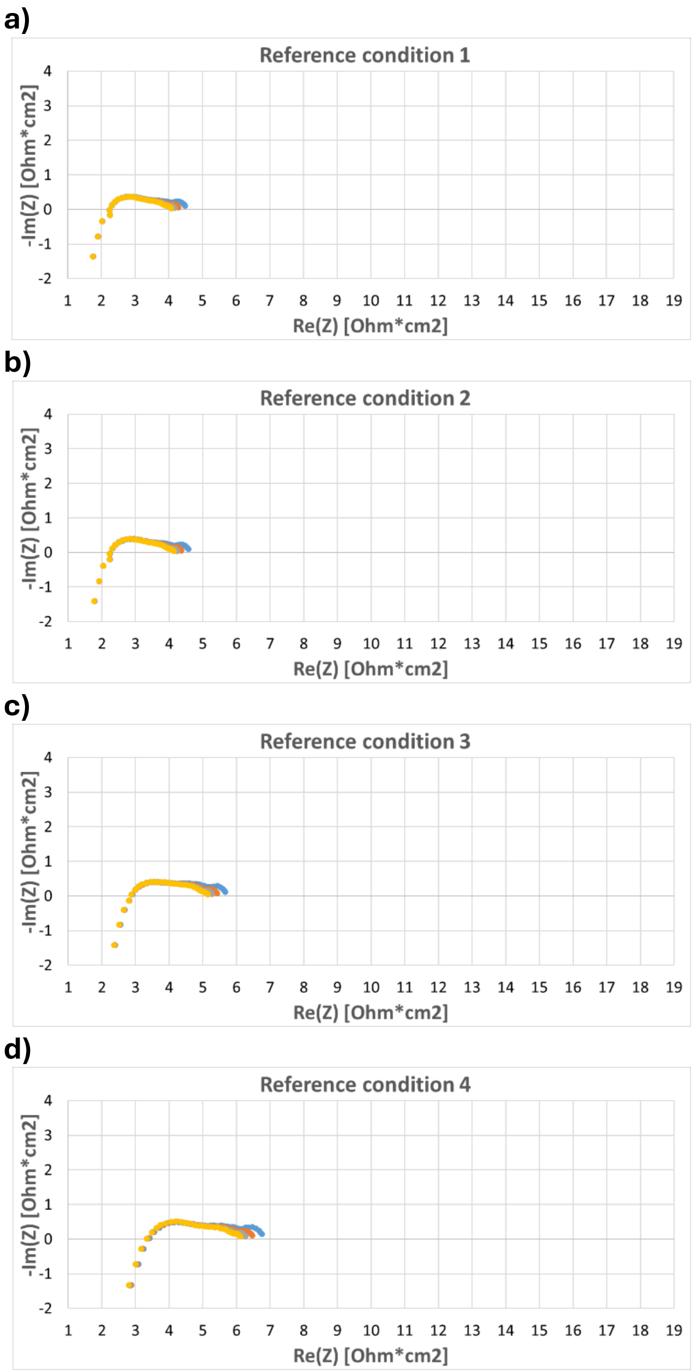

Figure 49 Nyquist plots obtained at 1 bar and 25°C under N2 feed (Reference conditions): a) Reference condition 1; b) Reference condition 2; d) Reference condition 3; e) Reference condition 4. Colour legend: blue symbols (-0.05V), orange (-0.1V), grey (-0.15V), yellow (-0.2V).

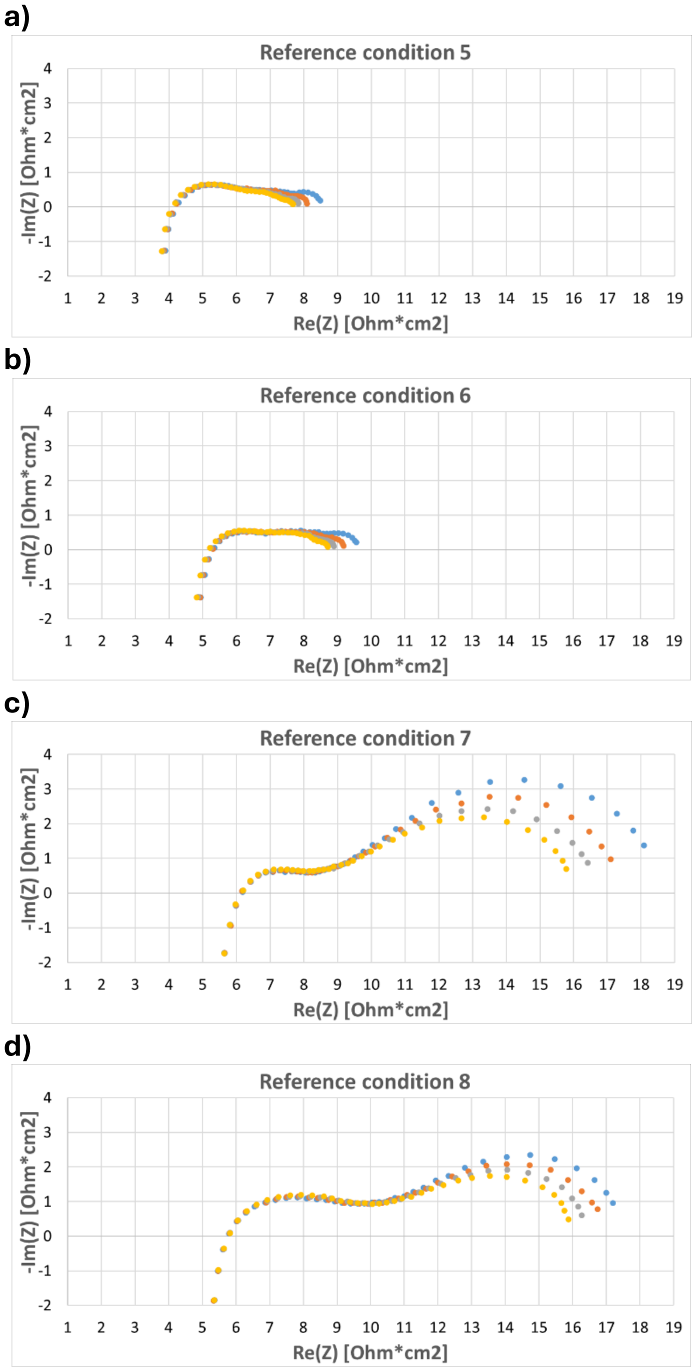

Figure 50 Nyquist plots obtained at 1 bar and 25°C under N2 feed (Reference conditions): a) Reference condition 5; b) Reference condition 6; d) Reference condition 7; e) Reference condition 8. Colour legend: blue symbols (-0.05V), orange (-0.1V), grey (-0.15V), yellow (-0.2V).

4.2. Sample B

In this chapter the results for the Sample B are shown.

Scanning electron microscopy (SEM) analyses were carried out on the Sample B. Before the electrochemical tests, surface and cross-section analyses were performed on both Cu electrode and Pt electrode. After electrochemical tests, only cross-section analyses were conducted on the tested MEA sample (**Figure 51, Figure 52**), since the disassembly caused partial electrode damage and adhesion to the cell components.

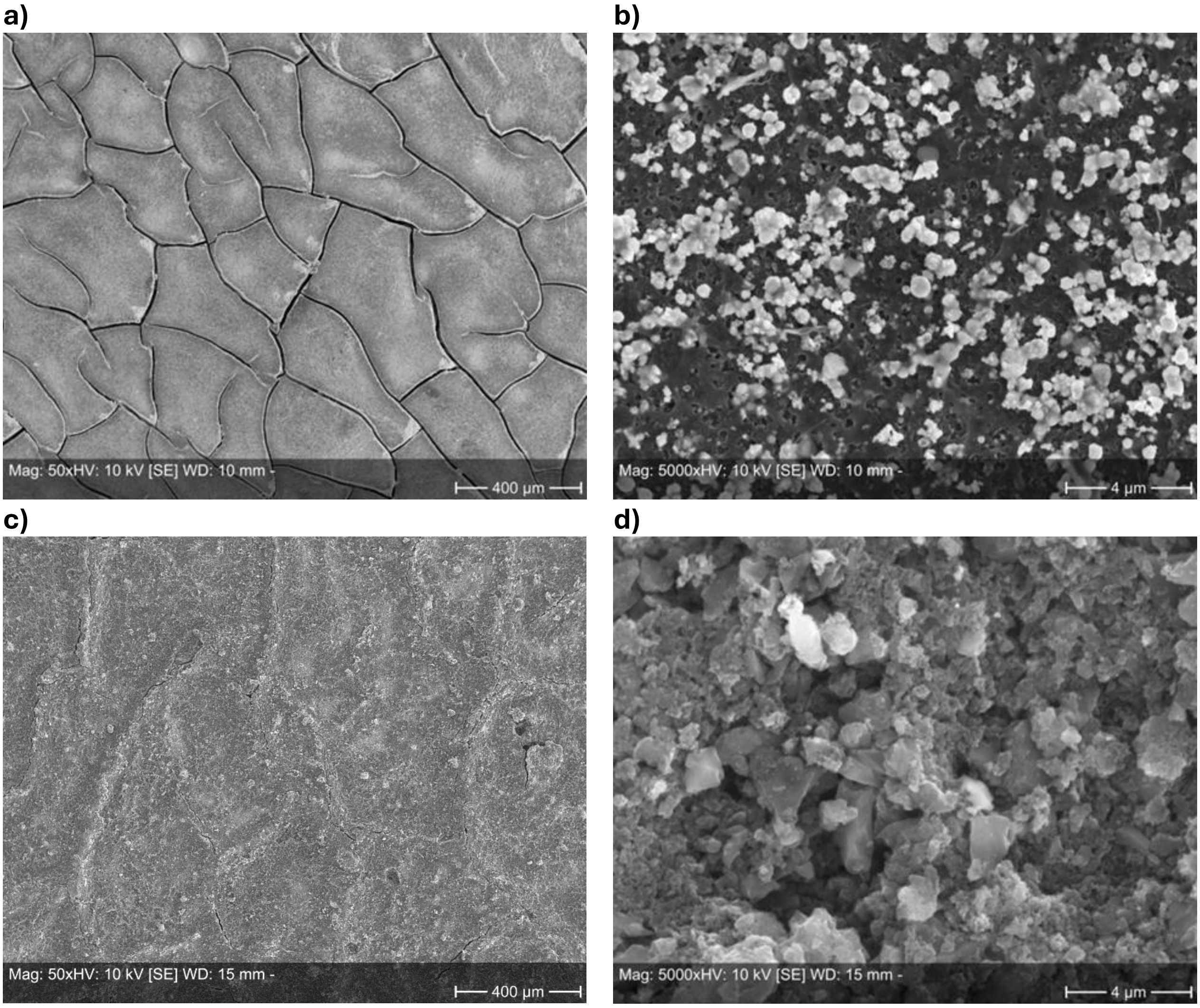

Figure 51 a) Cu Pre-test top view Mag:50xHv, b) Cu Pre-test top view Mag:5000xHV, c) Pt Pre-test top view Mag:50xHv, d) Pt Pre-test top view Mag:5000xHV

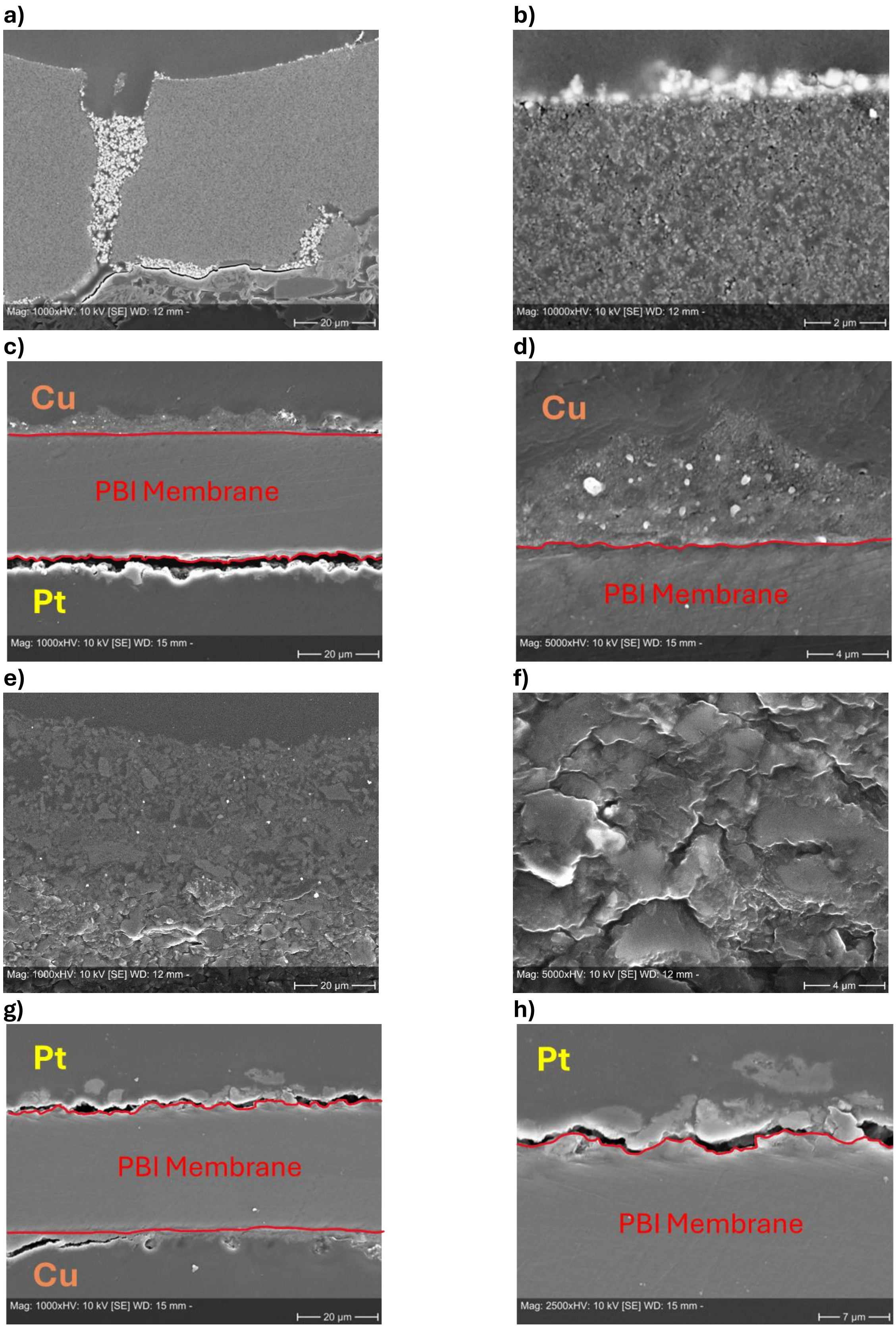

Figure 52 a) Cu pre-test cross section Mag:1000xHV, b) Cu pre-test cross section Mag:1000xHV, c) MEA post-test cross section Mag:1000xHV (Cu side on top), d) MEA post-test cross section Mag:5000xHV (Cu side on top), e) Pt pre-test cross section Mag:1000xHV, f) Pt pre-test cross section Mag:5000xHv, g) MEA post-test cross section Mag:1000xHV (Pt side on top), h) MEA post-test cross section Mag:5000xHV (Pt side on top), e) Pt pre-test cross section Mag:2500xHV.

The **Table 4** provides a detailed overview of the electrochemical experiments carried on the Sample B, reporting for each test day the gas feeds, temperature, pressure and the techniques employed (LSV, CP, GEIS). The field ‘Test Day’ indicates the sequential number of the day on which the experiment was performed, regardless of the calendar date.

Test day	Feed	T [°C]	P [bar]	Type of experiments
1	Humidified N2 (Cathode),	25	1	LSV, CP, GEIS
	Humidified CO2 (Cathode), Humidified H2 (Anode)	25	1	
		25	20	
		120	20	
		180	20	
	Humidified N2 (Cathode),	180	20	
2	Humidified N2 (Cathode),	25	1	LSV, CP, GEIS
	Humidified CO2 (Cathode), Humidified H2 (Anode)	25	1	
		25	20	
		120	20	
		180	20	
	Humidified N2 (Cathode), Humidified H2 (Anode)	180	20	
		120	20	
3	Humidified N2 (Cathode),	25	1	LSV, CP, GEIS
4	Humidified CO2 (Cathode), Humidified H2 (Anode)	25	1	LSV, CP, GEIS
		50		
		80		
		120		
		150		
		180		
5	Humidified N2 (Cathode), Humidified H2 (Anode)	25	1	LSV, CP, GEIS
		50		
		80		
		120		
		150		
		180		
		25		

Table 4 Operating conditions and electrochemical experiments performed on the Sample B

With this cell, experiments were carried out using exclusively humidified gas feeds. In particular, hydrogen was supplied to the anode side and nitrogen to the cathode side, as for previous sample. In addition, experiments were also carried out by feeding only CO2 to the cathode side, while keeping the hydrogen feed to the anode side unchanged.

First, electrochemical measurements (LSV, CP, GEIS) were performed at a pressure of 20 bar and at a temperature of 25, 120, 180°C. Under CO2 feeding at the cathode, tests were carried out at 20 bar and at 25, 120, 180°C, whereas under nitrogen feeding measurements were only performed at 20 bar, but only at 180°C because of the limited available time.

Figure 53 shows the linear sweep voltammetry (LSV) curves acquired under the operating conditions described above. The figure includes both measurements under nitrogen feeding at the cathode and those performed under carbon dioxide feeding.

Figure 54 shows the i-V curves obtained from galvanostatic chronoamperometric measurements, in which a sequence of constant currents was imposed first in the forward (increasing) direction and then in the backward (decreasing) direction. For each current value, the steady state cell potential was recorded after signal stabilisation, in order to characterise the electrochemical response of the cell under steady state conditions. The corresponding Tafel plots are shown only for the forward scan.

For the measurements at 20 bar and 25°C under CO2 feeding, the imposed currents were -2.4 A (-200 mA/cm2), -4.8 A (-400 mA/cm2), -7.2 A (-600 mA/cm2), -9.6 A (-800 mA/cm2). For the experiments at higher temperatures (120 and 180°C), the imposed currents were -2.4 A (-200 mA/cm2), -4.8 A (-400 mA/cm2), -7.4 A (-620 mA/cm2), -10 A (-830 mA/cm2), this last value being the highest current that could be applied, as it corresponds to the upper limit of the amplifier used (BioLogic VMP3B-10 amplifier) and therefore represents the limit of the system. Under nitrogen feeding the measurements were only performed at current densities of -620 mA/cm2 and -830 mA/cm2, and only in the forward (increasing) direction.

For the same current densities used in the chronoamperometric measurements, GEIS analyses were performed, the corresponding Nyquist plots are shown in **Figure 55** for the different temperatures tested (25, 120, 180°C) at 20 bar. Light-blue points correspond to GEIS measurements at -200 mA/cm2, orange points to -400 mA/cm2, grey points to -620 mA/cm2 and yellow points to -830 mA/cm2, while the points marked violet refer to current density of -600 mA/cm2 and those marked green to -800 mA/cm2.

To verify the reproducibility of the electrochemical response of the cell, the same experiments were repeated on the following day under identical operating conditions. In addition, with more time available, further tests were carried out with nitrogen feeding at 20 bar and 120°C. For all these chronoamperometric and GEIS measurements, the imposed currents densities were -200 mA/cm2, -400 mA/cm2, -620 mA/cm2 and -830 mA/cm2. These experiments are shown in **Figure 56**, **Figure 57**, **Figure 58**, which show, respectively, the LSV curves with corresponding Tafel plots, the i-V curves with associated Tafel plots (forward only), and the Nyquist plots.

This cell already delivers from the very first experiments, much higher current densities then the first cell tested (Pt/Pt Cell Sample A). Under CO2 feed (red curves), increasing temperature does not significantly affect the LSV curves, which exceed -1 A/cm2 at potentials of around -0.9 V. The corresponding Tafel plots exhibit very similar slopes and positions among the different temperatures. At 180°C, the curves recorded under N2 feed (blue curves) do not differ substantially from those obtained under CO2.

Chronoamperometric measurements also show that this cell is highly performant, reaching -800 mA/cm2 at about -0.6 V at room temperature. at higher temperatures, current densities of -830 mA/cm2 are reached at approximately -0.7 V, and similar values are obtained even when feeding only CO2 to the cathode. No significant differences are observed between the forward and backward sweeps.

Regarding the Nyquist plots, under CO2 feed the spectra shift to higher real impedance values as the temperature increases, and a clear dependence on the imposed current density can be observed. For the only two measurements carried out under N2 feed, the Nyquist plots are very similar to those obtained under CO2 at the same conditions, i.e., 180°C and applied current densities of -620 and -830 mA/cm2.

Regarding the experiments carried out on Day 2 at 20 bar, under CO2 feed, the LSV at 25°C reaches approximately -1 A/cm2 at about -0.7 V; this current density is achieved at a slightly more negative potential (around -0.8 V) at 120°C, whereas the required small decreases again to around -0.7 V at 180°C. Under N2 feed, comparable current densities to those observed at 180°C under CO2 are obtained; however, the curve shape obtained at 180°C under N2 changes at low potentials, with more pronounced feature at 120°C, where the measurement was performed after the one at 180°C.

Regarding the i-V curves at 20 bar, under CO2 feed at 25°C a potential of about -0.5 V is recorded at -830 mA/cm2, whereas at 120 an180°C the corresponding potential is approximately -0.6V, lower than the ones observed on Day 1. At 180°C under CO2 feed, a clear difference between the forward and backward branches is observed for measurements performed at a fixed current density of -200 mA/cm2, and the shape of backward scan is reproduced in the experiments under N2 feed, where it appears in both the forward and backward scans.

Regarding the Nyquist plots, at 25°C under CO2 feed the spectra shift towards higher real impedance and display an increase diameter as the imposed current density rises. At 120°C a similar behaviour is observed, although the curves recorded at the two highest current densities (-620 and -830 mA/cm2) are almost overlapping. At 180°C, the spectra obtained at -200 and -400 mA/cm2 are very similar to each other, as are those at -620 and -830 mA/cm2, the latter being shifted towards lower real impedance with respect to the former pair. Under N2 feed, the spectra at 120 and 180°C are very similar, and an overall shift of the Nyquist plots towards lower real impedance is observed as the imposed current density increases.

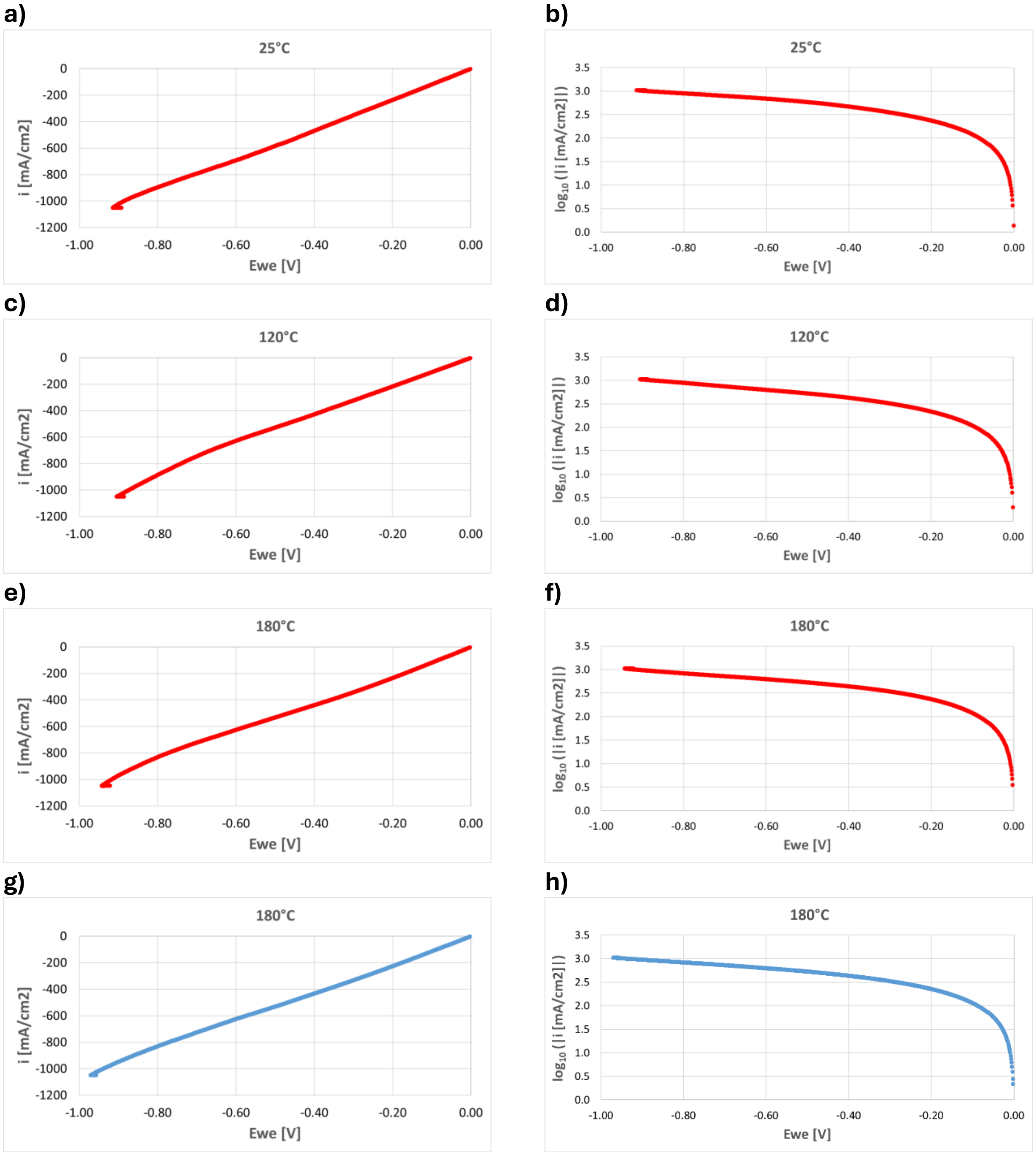

Figure 53 LSV curves (left) and corresponding Tafel plots (right) obtained at 20 bar under varying temperatures (day 1 measurements): a,b) 25°C; c,d) 120°C; e-h) 180°C. Red curves: CO2 feed; blue curves: N2 feed.

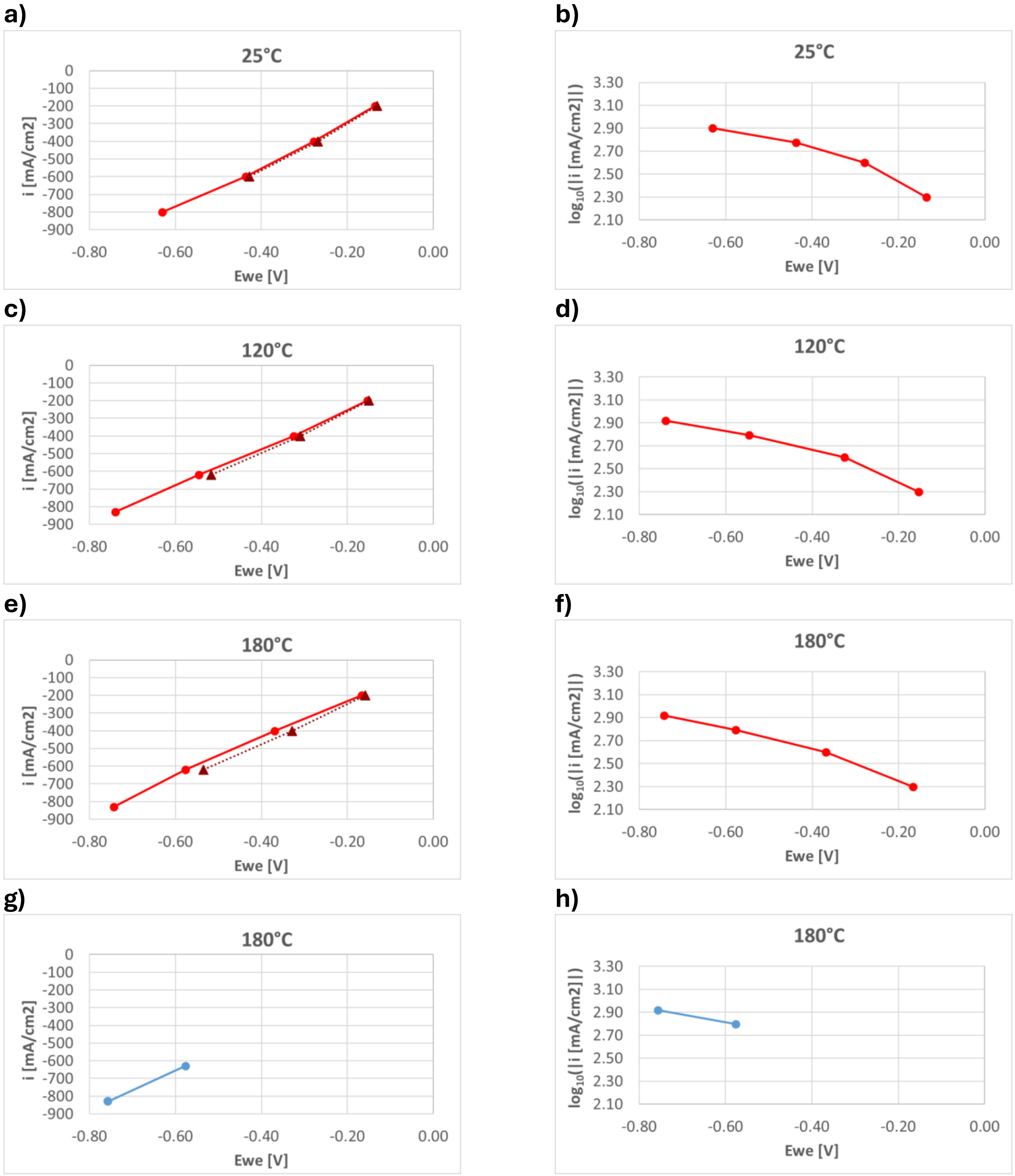

Figure 54 i-V curves (left) and corresponding Tafel plots (right, forward scan only) obtained at 20 bar under varying temperatures (day 1 measurements): a,b) 25°C; c,d) 120°C; e-h) 180°C. Solid lines with circle symbols indicate forward scans; while dotted lines with triangle symbols indicate backward scans. Red curves: CO2 feed; blue curves: N2 feed.

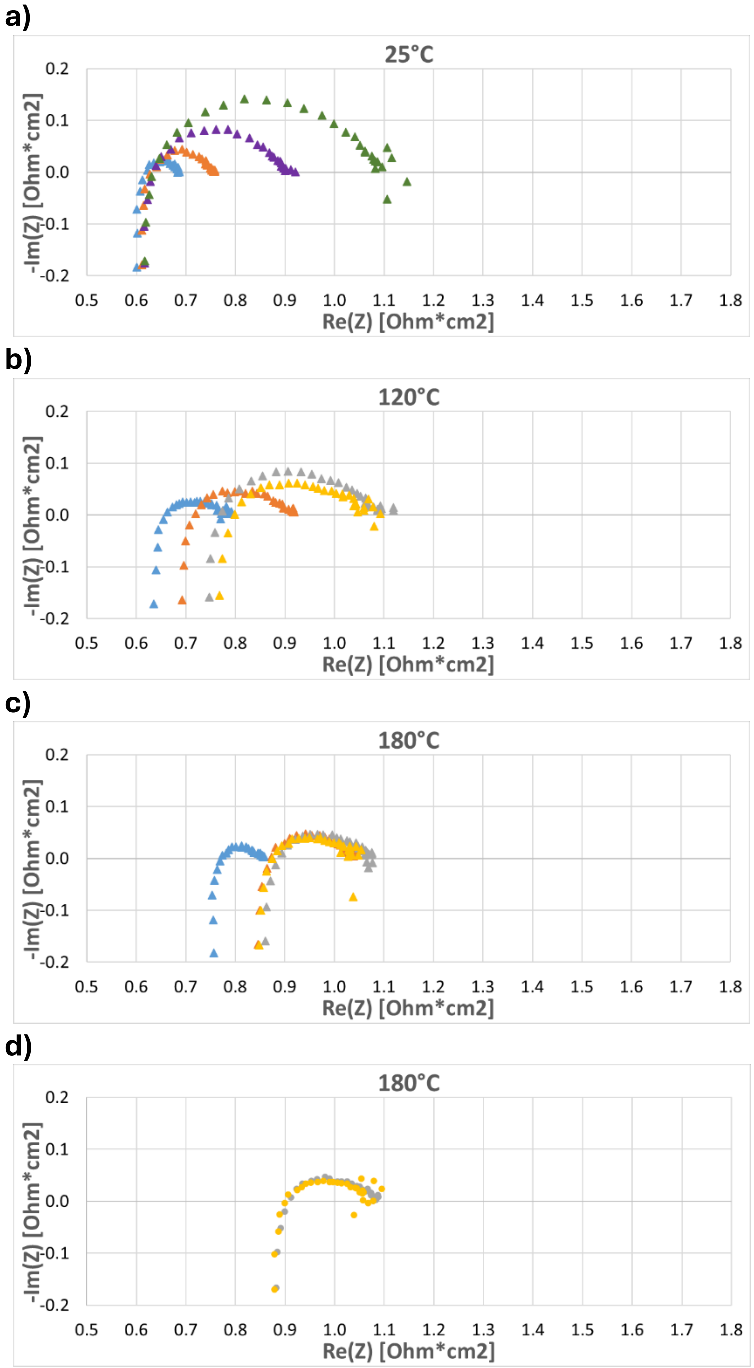

Figure 55 Nyquist plots obtained at 20 bar under varying temperatures (day 1 measurements): a) 25°C; b) 120°C; c,d) 180°C. Colour legend: blue symbols (-200 mA/cm2), orange (-400 mA/cm2), violet (-600 mA/cm2), grey (-630 mA/cm2), green (-800 mA/cm2), yellow (-830 mA/cm2). Circle symbols indicate N2 feed, triangle symbols indicate CO2 feed.

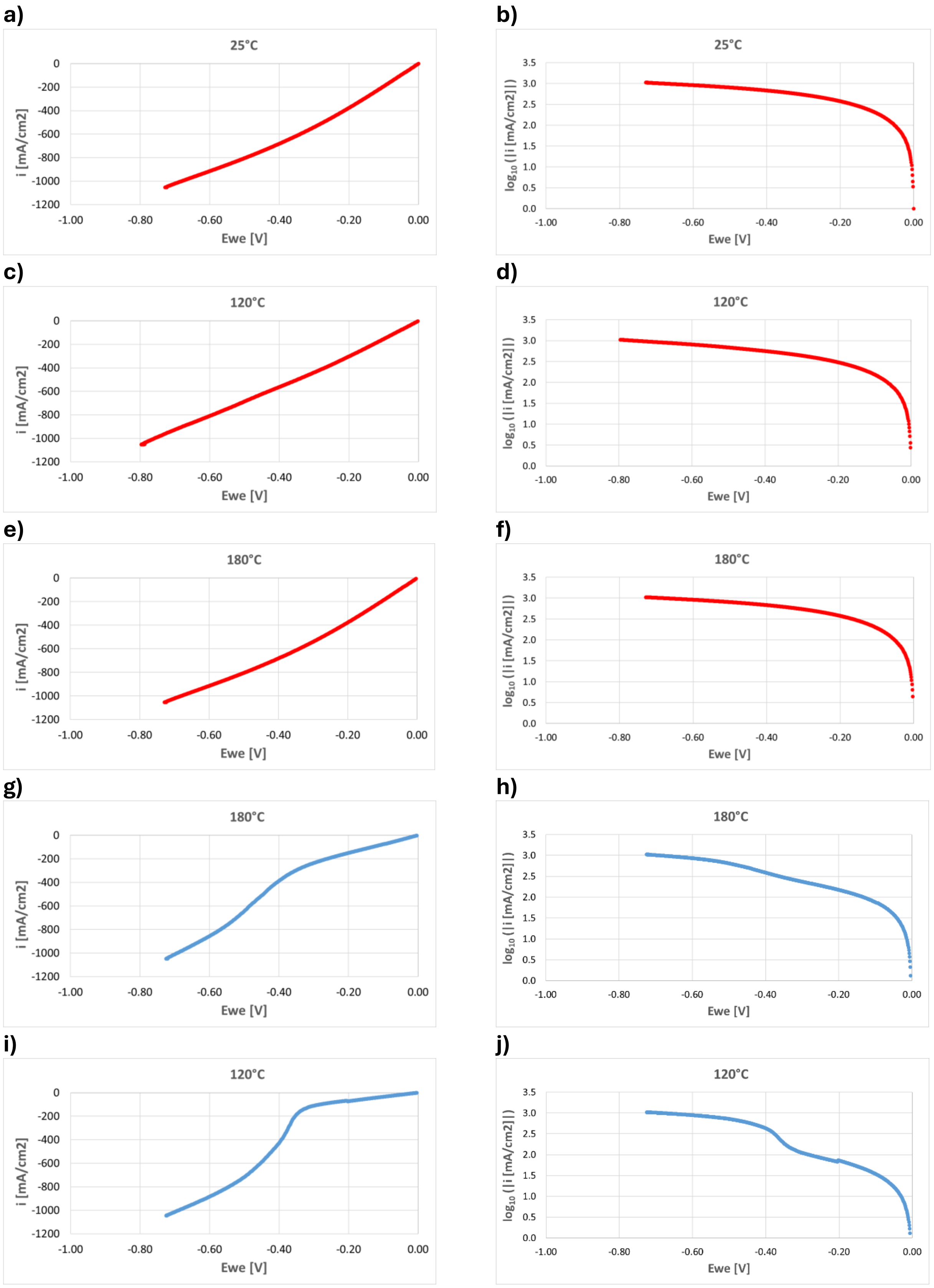

Figure 56 LSV curves (left) and corresponding Tafel plots (right) obtained at 20 bar under varying temperatures (day 2 measurements): a,b) 25°C; c,d,i,j) 120°C; e-h) 180°C. Red curves: CO2 feed; blue curves: N2 feed.

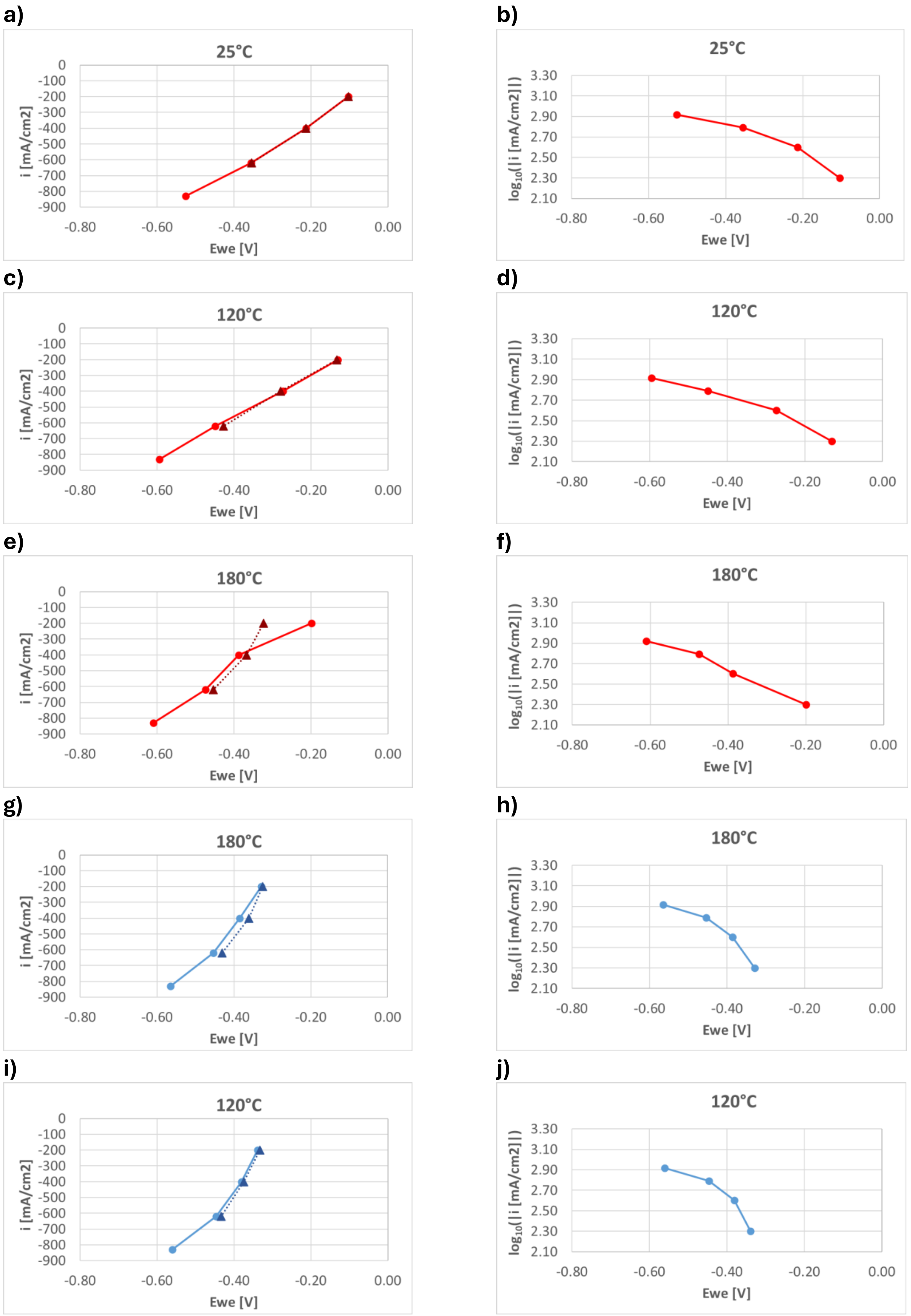

Figure 57 i-V curves (left) and corresponding Tafel plots (right, forward scan only) obtained at 20 bar under varying temperatures (day 2 measurements): a,b) 25°C; c,d, i, j) 120°C; e-h) 180°C. Solid lines with circle symbols indicate forward scans, while dotted lines with triangle symbols indicate backward scans. Red curves: CO2 feed; blue curves: N2 feed.

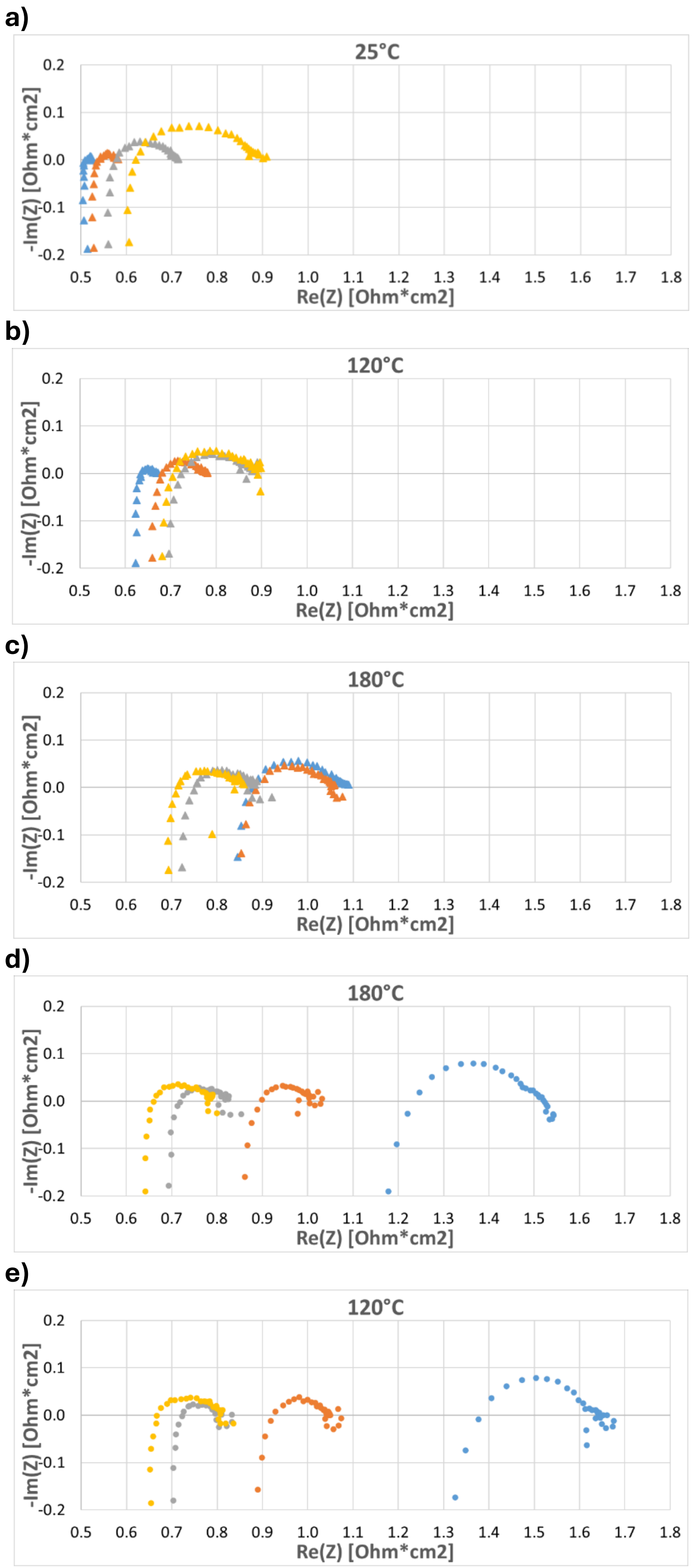

Figure 58 Nyquist plots obtained at 20 bar under varying temperatures (day 2 measurements): a) 25°C; b,e) 120°C; c,d) 180°C. Colour legend: blue symbols (-200 mA/cm2), orange (-400 mA/cm2), grey (-630 mA/cm2), yellow (-830 mA/cm2). Circle symbols: N2 feed; triangle symbols: CO2 feed.

To investigate the effect of temperature, the same type of experiments described above were carried out at 1 bar and 25, 50, 80, 120, 150, 180°C first feeding CO2 to the cathode and then feeding only N2 to the cathode.

The **Figure 59**, **Figure 60**, **Figure 61** show, respectively, the LSV curves with corresponding Tafel plots, the i-V curves with associated Tafel plots (forward only) and the Nyquist plots, all acquired at 1 bar at different temperatures (25, 50, 80, 120, 150, 180°C) under CO2 feeding.

Regarding the LSV curves, the same shape previously observed at 20 bar and 120, 180°C under N2 feed is also found at 1 bar and 25, 50, and 80°C under CO2 feed. At 120, 150 and 180°C the curves show a similar overall shape but exhibit a discontinuity. A current density of -1 mA/cm2 is nevertheless achieved: at 25°C it is reached at about -0.7V, at 50, 80, and 120°C at around -0.8V, and at 150 and 180°C at approximately -1V.

A comparable behaviour is observed for the i-V curves: the shape seen at 20 bar and 120, 180°C under N2 feed is reproduced at 1 bar and 25, 50, 80 and 120°C, where the highest current density is obtained at a potential of roughly -0.6V, whereas at higher temperatures it is reached at a more negative potential, around -0.75V.

Similarly, the Nyquist plots show the same trend as 20 bar and 120, 180°C under N2 feed: for each temperature, the spectra shift towards lower real impedance as the current density increases. At the same time, the high frequency intercept on the real axis grows with temperature, with the curves at 150 and 180°C being very similar.

In addition, **Figure 62**, **Figure 63**, **Figure 64** show the LSV curves with the corresponding Tafel plots, the i-V curves with associated Tafel plots (forward only) and the Nyquist plots, all acquired at 1 bar at different temperatures (25, 50, 80, 120, 150, 180°C), this time under N2 feeding.

If some Nyquist plots are not shown, it indicates that the impedance was not measured under those conditions.

Regarding the LSV curves at 1 bar under N2 feed, the same trends described for CO2 are observed over the investigated temperature range, and a comparable behaviour is also found for the i-V curves.

For the Nyquist plots at 25, 50 and 80°C, some impedance spectra could not be recorded, possibly due to a not suitable perturbation amplitude; however, the impedance at -830 mA/cm2 was always measured and shows only minor changes among these three temperatures. At 120, 150 and 180°C, the spectra appear rather similar, with the only noticeable difference being an increase in the diameter of the curve at -200 mA/cm2 when moving from 120 to 150°C.

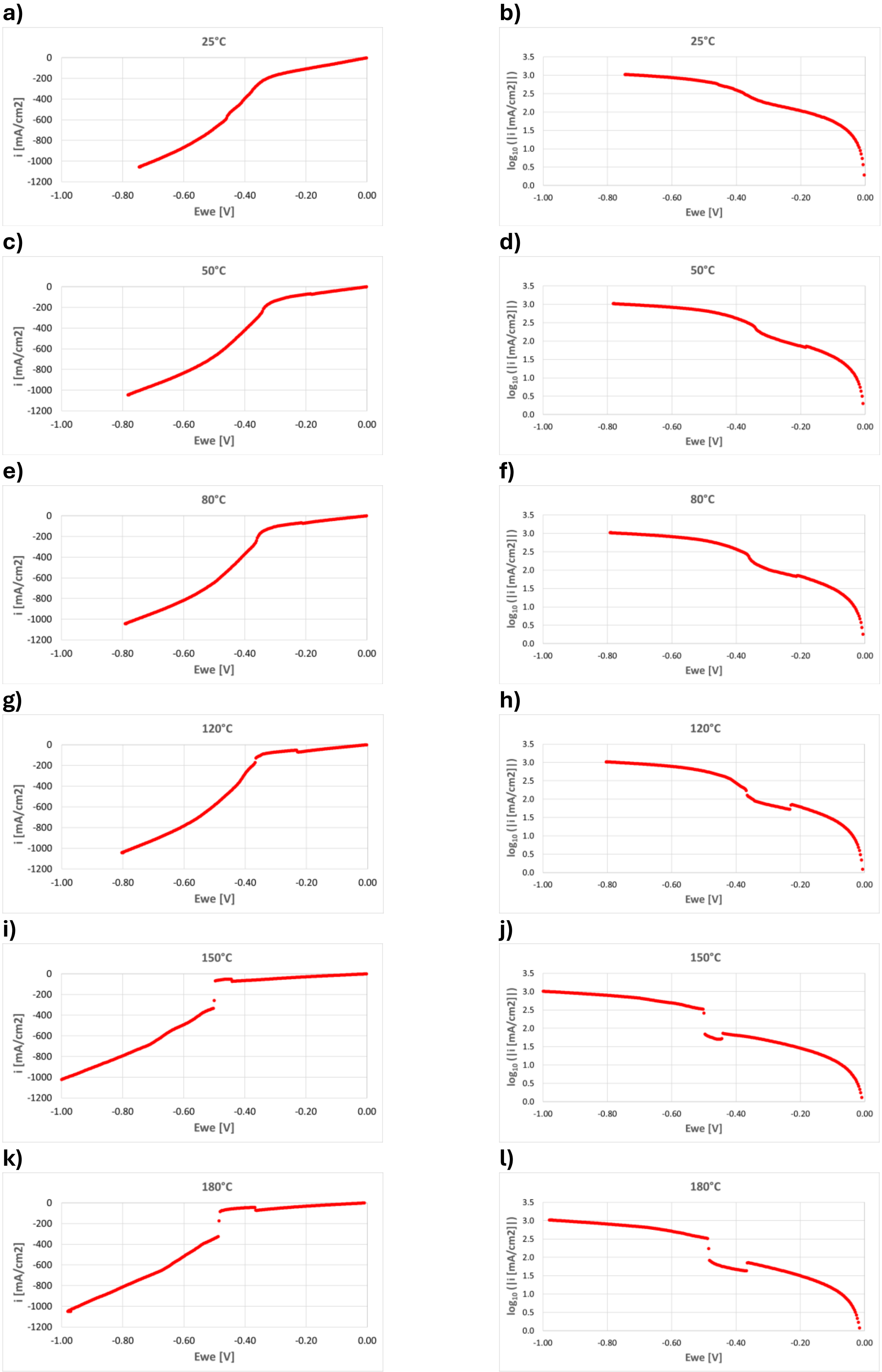

Figure 59 LSV curves (left) and corresponding Tafel plots (right) obtained under CO2 feed at 1 bar and varying temperatures: a,b) 25°C; c,d) 50°C; e,f) 80°C; g,h) 120°C, i,j) 150°C; k,l) 180°C.

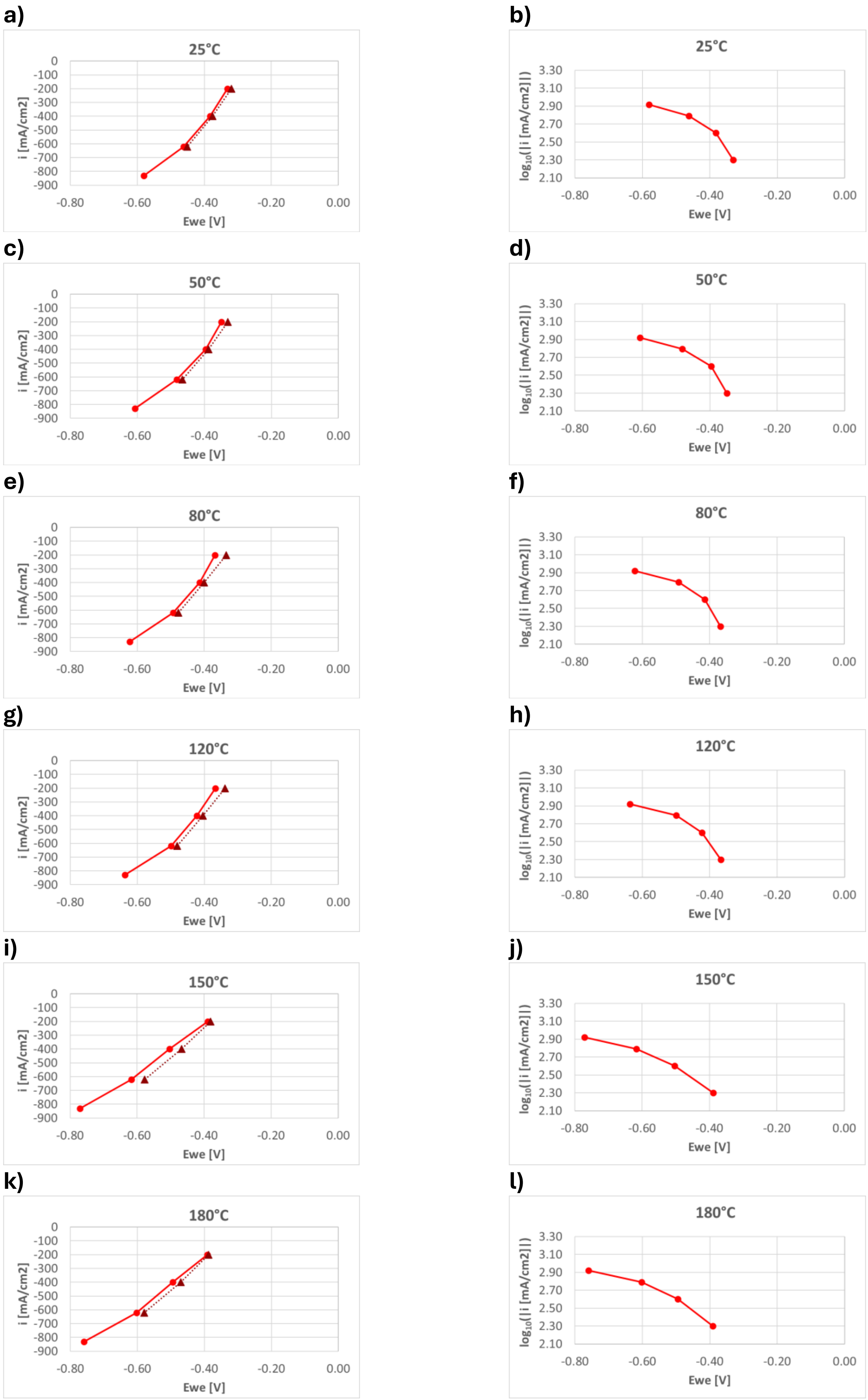

Figure 60 i-V curves (left) and corresponding Tafel plots (right, forward scan only) obtained under CO2 feed at 1 bar and varying temperatures: a,b) 25°C; c,d) 50°C; e,f) 80°C; g,h) 120°C; i,j) 150°C; k,l) 180°C. Solid lines with circle symbols indicate forward scans, while dotted lines with triangle symbols indicate backward scans.

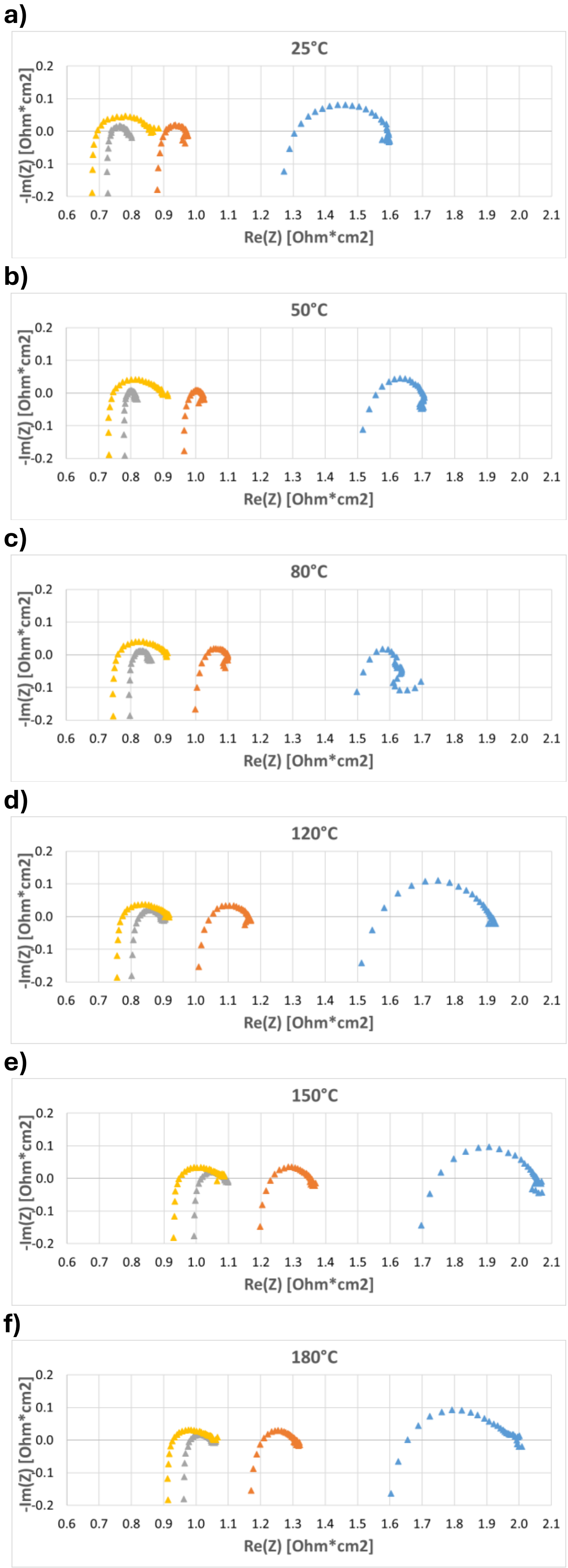

Figure 61 Nyquist plots obtained under CO2 feed at 1 bar and varying temperatures: a) 25°C; b) 50°C; c) 80°C; d) 120°C; e) 150°C; f) 180°C. Colour legend: blue symbols (-200 mA/cm2), orange (-400 mA/cm2), grey (-630 mA/cm2), yellow (-830 mA/cm2).

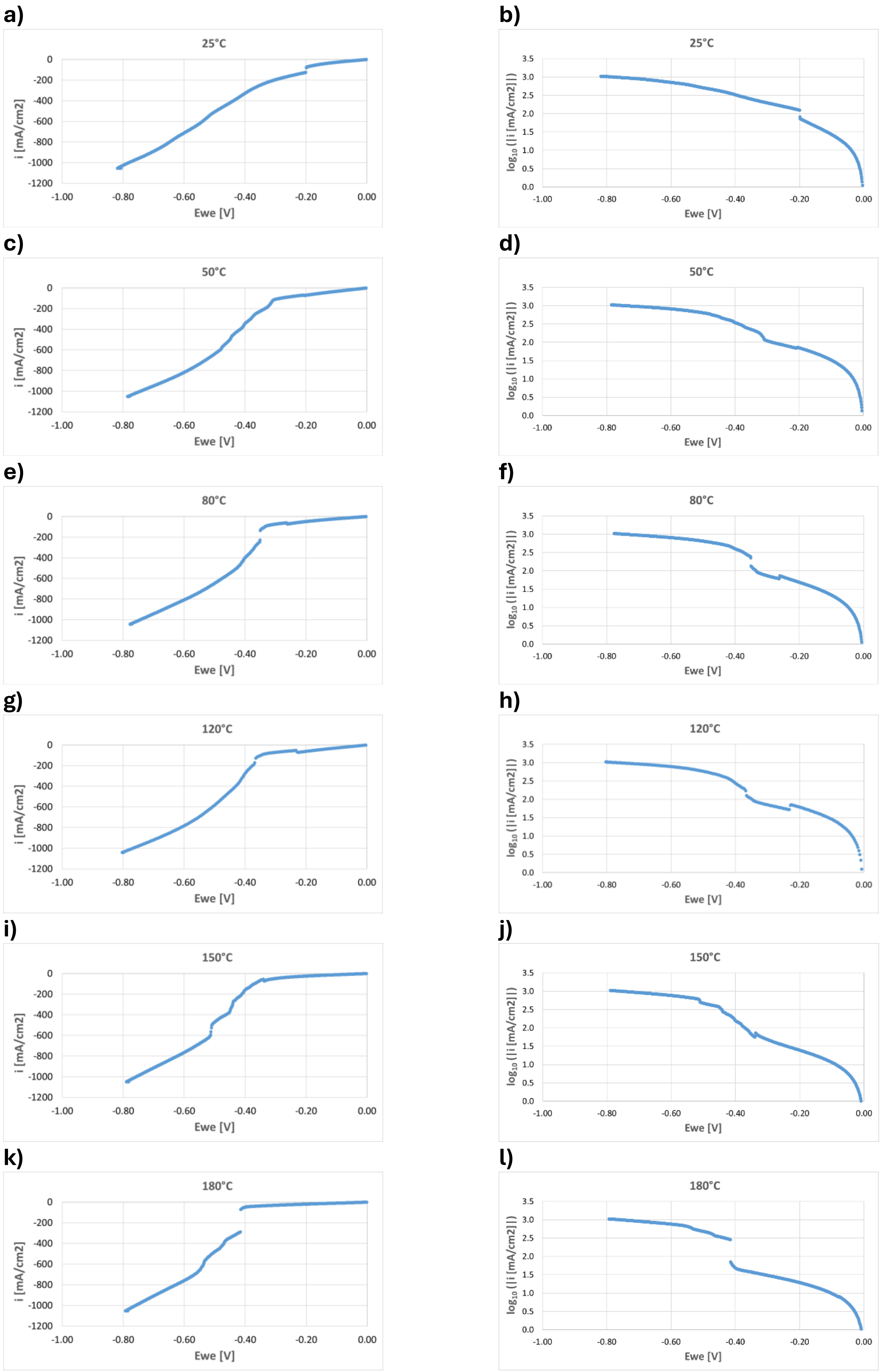

Figure 62 LSV curves (left) and corresponding Tafel plots (right) obtained under N2 feed at 1 bar and varying temperatures: a,b) 25°C; c,d) 50°C; e,f) 80°C; g,h) 120°C, i,j) 150°C; k,l) 180°C.

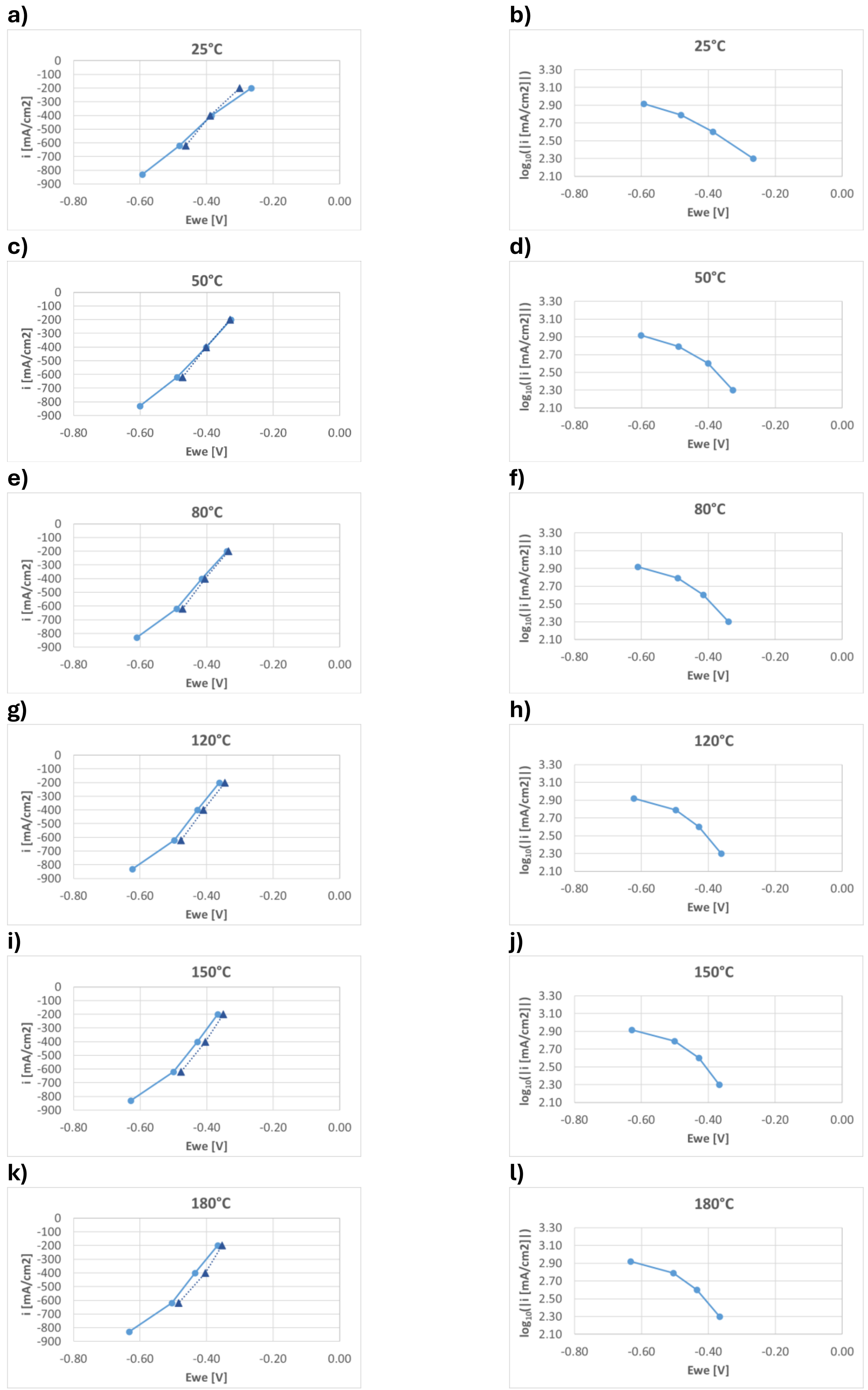

Figure 63 i-V curves (left) and corresponding Tafel plots (right, forward scan only) obtained under N2 feed at 1 bar and varying temperatures: a,b) 25°C, c,d) 50°C, e,f) 80°C, g,h) 120°C, I,j) 150°C, k,l) 180°C. Solid lines with circle symbols indicate forward scans, while dotted lines with triangle symbols indicate backward scans.

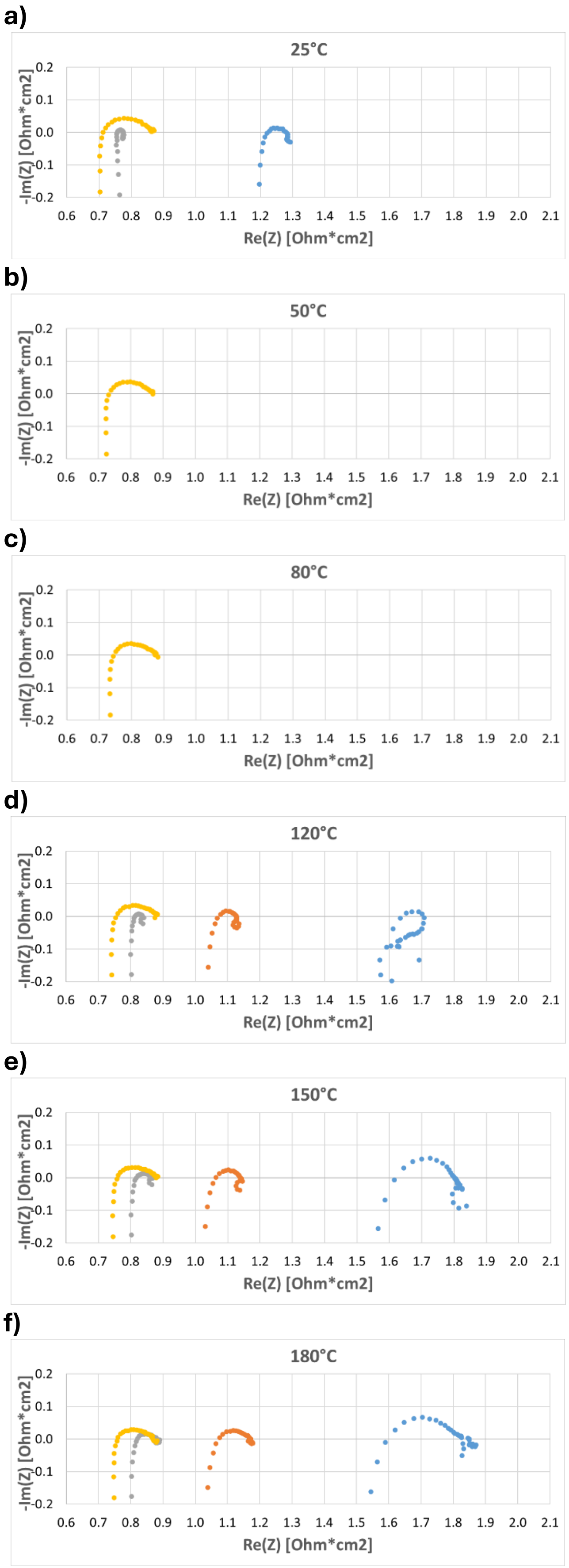

Figure 64 Nyquist plots obtained under N2 feed at 1 bar and varying temperatures: a) 25°C; b) 50°C; c) 80°C; d) 120°C; e) 150°C; f) 180°C. Colour legend: blue symbols (-200 mA/cm2), orange (-400 mA/cm2), grey (-630 mA/cm2), yellow (-830 mA/cm2).

Reference experiments were also performed with this cell (25°C, 1 bar with nitrogen fed to the cathode), after each of the two pressurisation steps of the system and after each of the two temperature increases.

Figure 65, **Figure 66**, **Figure 67** show, respectively, the LSV curves with their corresponding Tafel plots, the i-V curves with the associated Tafel plots (only forward direction) and the Nyquist plots obtained under different reference conditions.

In this case the reference conditions are defined as followed:

1. Reference condition 1 (Ref. 1): it corresponds to the initial experiments carried out at 1 bar and 25°C.
2. Reference condition 2 (Ref. 2): experiments carried out after the first set of experiments at 20 bar and 25, 120, 180°C.
3. Reference condition 3 (Ref. 3): experiments carried out after the second set of experiments at 20 bar and 25, 120, 180°C.
4. Reference condition 4 (Ref. 4): experiments carried out after the series of experiments at 1 bar and 25, 50, 80, 120, 150, 180°C with CO2 feeding to the cathode.
5. Reference condition 5 (Ref. 5); experiments carried out after the series of experiments at 1 bar and 25, 50, 80, 120, 150, 180°C with N2 feeding to the cathode.

From the measurements carried out under the different reference conditions, a clear change in the shape of both the LSV and the i-V curves is observed when moving from Ref. 2 to Ref. 3, that is, between the experiments performed after the first and second set of tests at 20 bar and 25, 120, and 180°C . This change in behaviour was first detected at 20 bar and 180°C under N2 feed during the second experimental day and is then reproduced in the later measurements at Ref. 3. A similar evaluation is observed for the Nyquist plots, which at Ref. 3 are consistent with those obtained at 20 bar and 180° under N2 feed.

Despite these changes, the cell did not exhibit any big performance loss, unlike Sample A. The current density of -830 mA/cm2 is still reached at around -0.6V during Reference condition measurements, with only minor evaluation, and the impedance spectra do not show any significant shift or drastic change in shape.

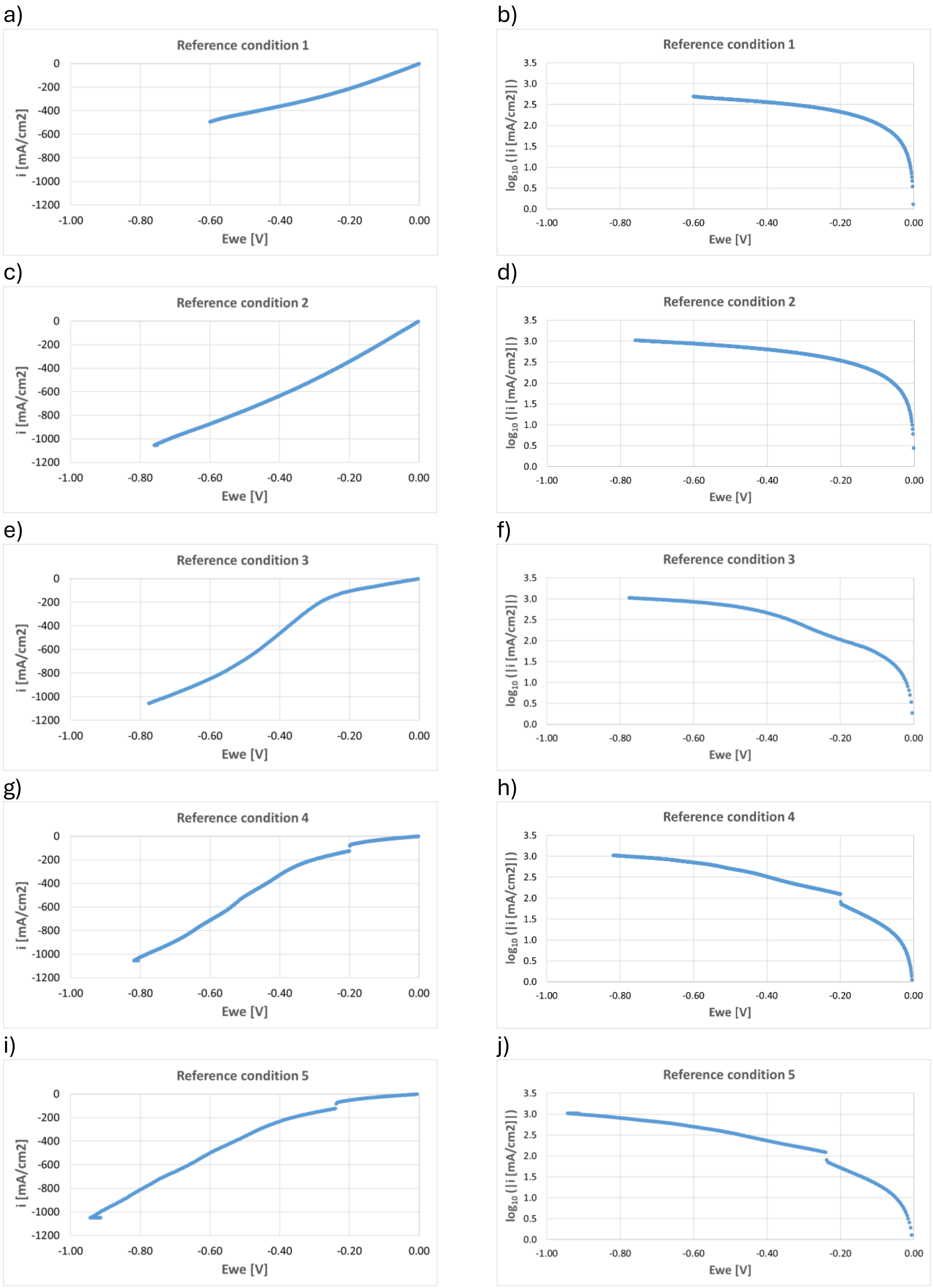

Figure 65 LSV curves (left) and corresponding Tafel plots (right) obtained at 1 bar and 25°C under N2 feed (Reference conditions): a,b) Reference condition 1; c,d) Reference condition 2; e,f) Reference condition 3; g,h) Reference condition 4; i,j) Reference condition 5.

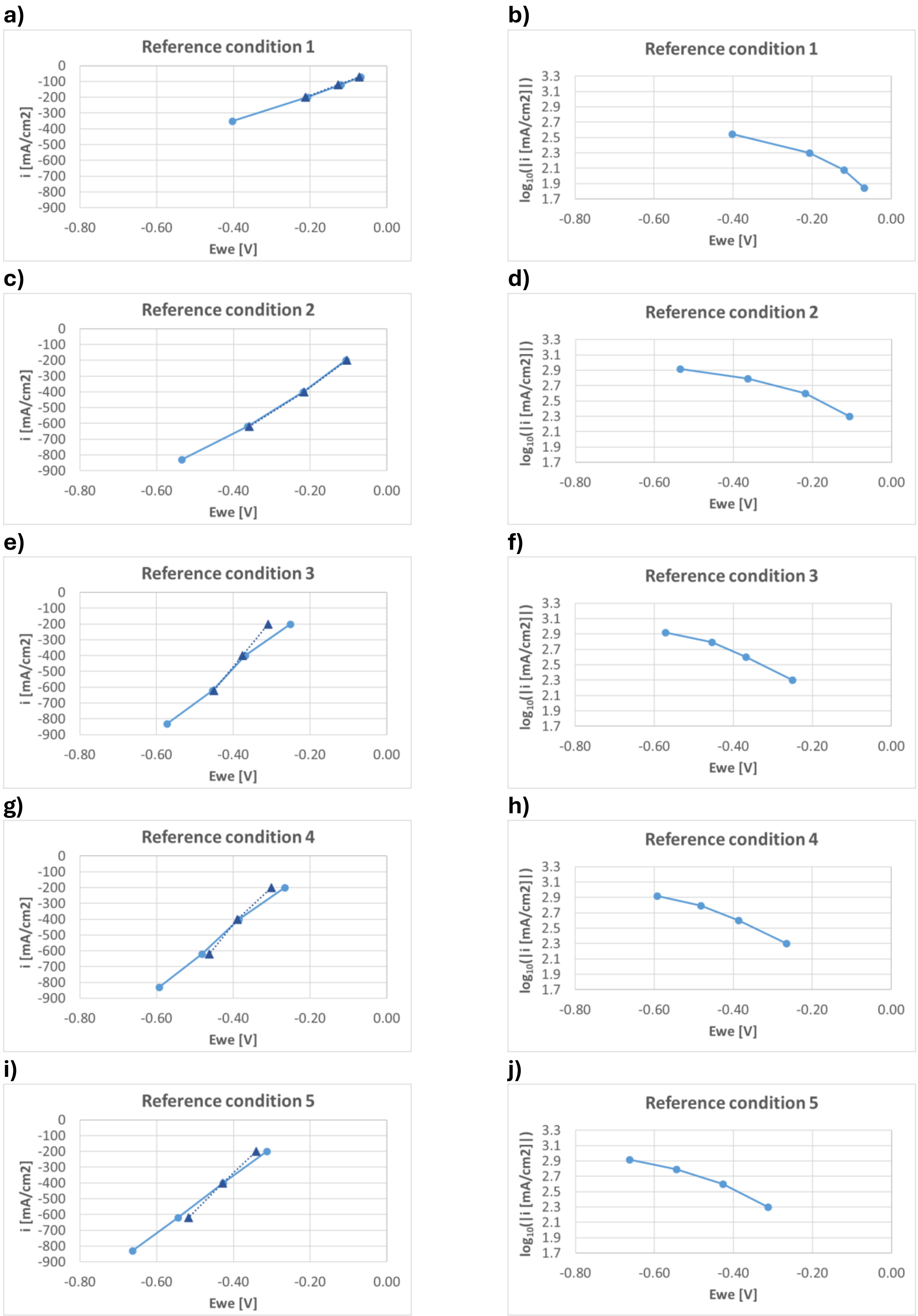

Figure 66 i-V curves (left) and corresponding Tafel plots (right, forward scan only) obtained at 1 bar and 25°C under N2 feed (Reference conditions): a,b) Reference condition 1; c,d) Reference condition 2; e,f) Reference condition 3; g,h) Reference condition 4; i,j) Reference condition 5. Solid lines with circle symbols indicate forward scans, while dotted lines with triangle symbols indicate backward scans.

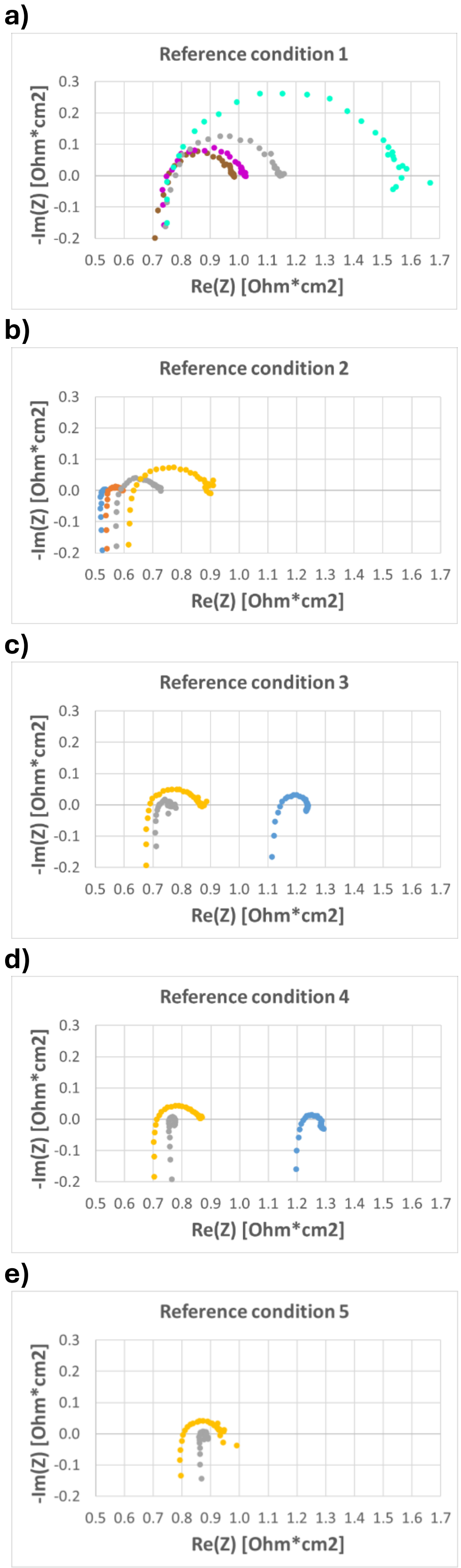

Figure 67 Nyquist plots obtained at 1 bar and 25°C under N2 feed (Reference conditions): a,b) Reference condition 1; c,d) Reference condition 2; e,f) Reference condition 3; g,h) Reference condition 4; i,j) Reference 5. Colour legend: brown symbols (-70 mA/cm2), pink (-120 mA/cm2), blue (-200 mA/cm2), turquoise (-350 mA/cm2), orange (-400 mA/cm2), grey (-630 mA/cm2), yellow (-830 mA/cm2).

4.3. Cu/Pt Cell2 Sample C

Scanning electron microscopy (SEM) analyses were carried out on the Sample C. Before the electrochemical tests, surface and cross-section analyses were performed on both Cu electrode and Pt electrode. After electrochemical tests, only cross-section analyses were conducted on the tested MEA sample. No visible sign of degradation is observed.

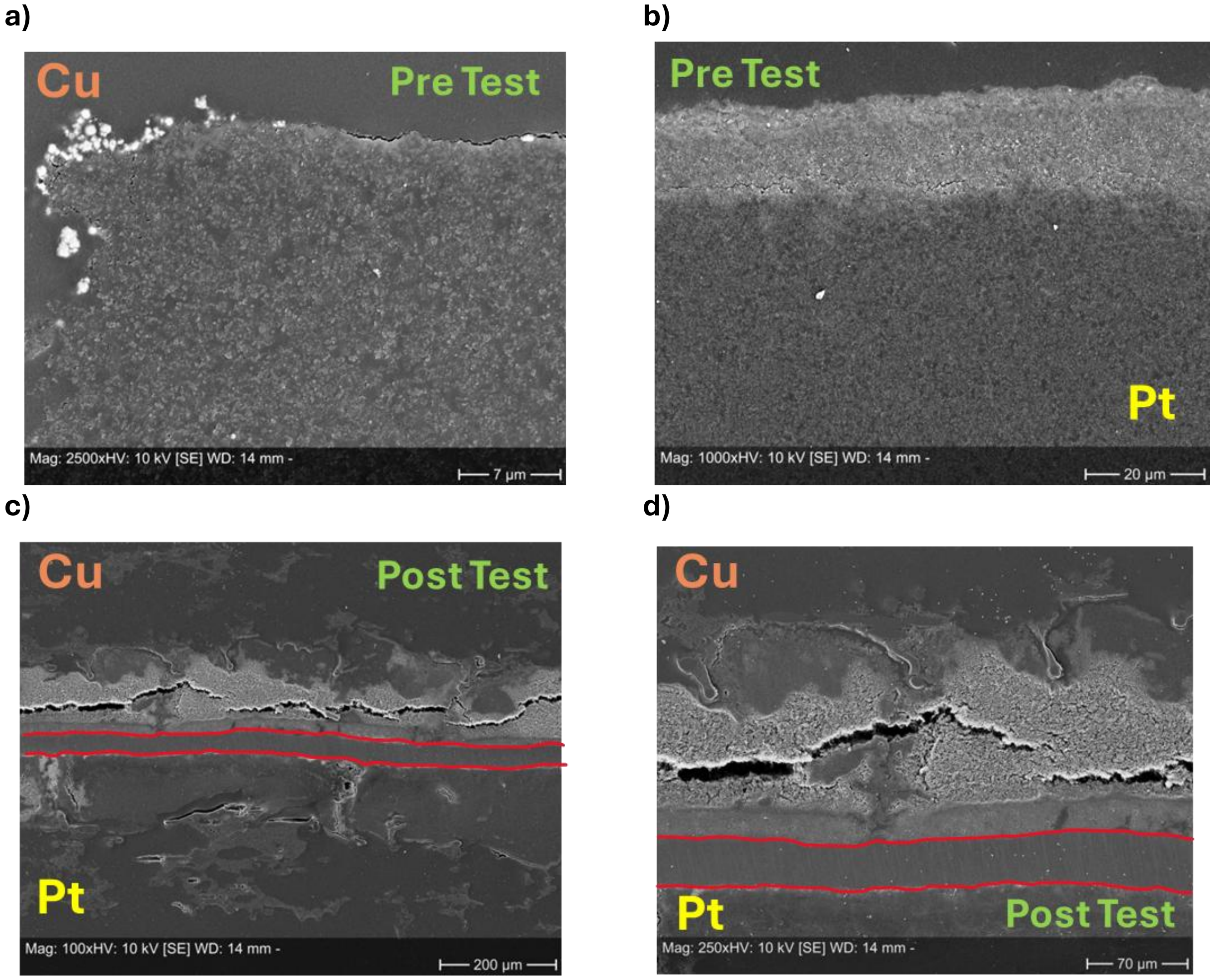

Figure 68 a) Cu pre-test cross section Mag:2500xHV, b) Pt pre-test cross section Mag:1000xHV, c) MEA post-test cross section Mag:100xHV (Cu side on top), d) MEA post-test cross section Mag:250xHV (Cu side on top)

The **Table 5** provides a detailed overview of the electrochemical experiments carried on the Sample C, reporting for each test day the gas feeds, temperature, pressure and the techniques employed (LSV, CP, GEIS).

Test day	Feed	T [°C]	P [bar]	Type of experiments
1	Humidified N2 (Cathode), Humidified H2 (Anode)	25	1	LSV, CP, GEIS
	Humidified CO2 (Cathode), Humidified H2 (Anode)	25	1	
		25	20	
		120	20	
		180	20	
	Humidified N2 (Cathode), Humidified H2 (Anode)	180	20	
2	Humidified N2 (Cathode), Humidified H2 (Anode)	25	1	LSV

Table 5 Operating conditions and electrochemical experiments performed on the Sample C

In order to validate the experimental results obtained for Sample B, a new series of tests was performed on Sample C, conducted under the same experimental conditions applied to Sample B.

The **Figure 69**, **Figure 70**, **Figure 71**, show, respectively, the LSV curves with corresponding Tafel plots, the i-V curves with associated Tafel plots (forward only) and the Nyquist plots, all acquired at 20 bar increasing temperature (25, 120, 180°C). The figure includes both measurements under nitrogen feeding at the cathode, blue curves, and those performed under carbon dioxide feeding, red curves.

Reference experiments were also performed with this cell (25°C, 1 bar with nitrogen fed to the cathode).

In this case the reference conditions are defined as followed:

1. Reference condition 1 (Ref. 1): it corresponds to the initial experiments carried out at 1 bar and 25°C.
2. Reference condition 2 (Ref. 2): experiments carried out after the set of experiments at 20 bar and 25, 120, 180°C.

Figure 72 shows, respectively, the LSV curves with their corresponding Tafel plots obtained under these reference conditions. From this figure, a faster degradation van be observed compared to Sample B.

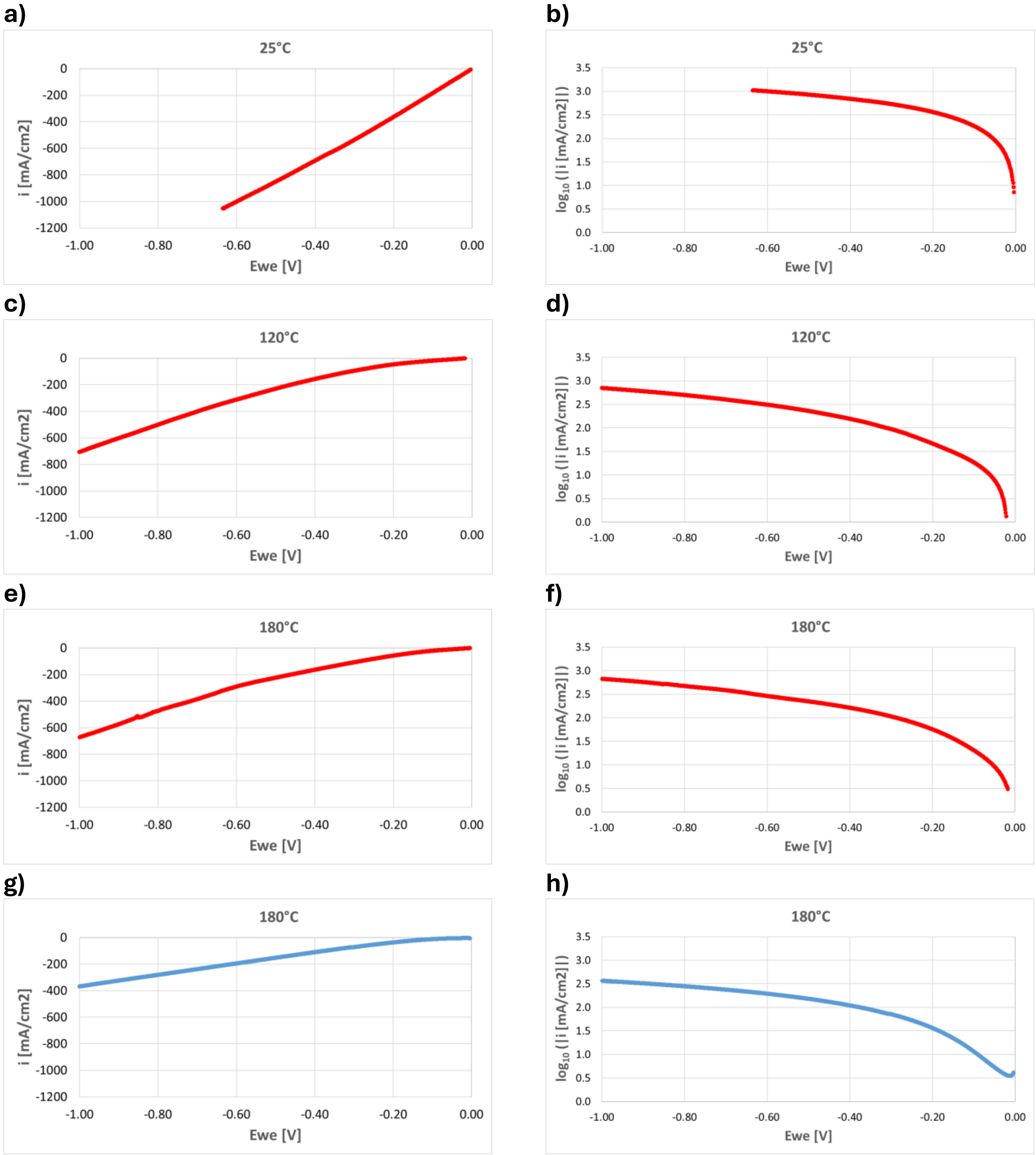

Figure 69 LSV curves (left) and corresponding Tafel plots (right) obtained at 20 bar under varying temperatures: a,b) 25°C; c,d) 120°C; e-h) 180°C. Red curves: CO2 feed; blue curves: N2 feed.

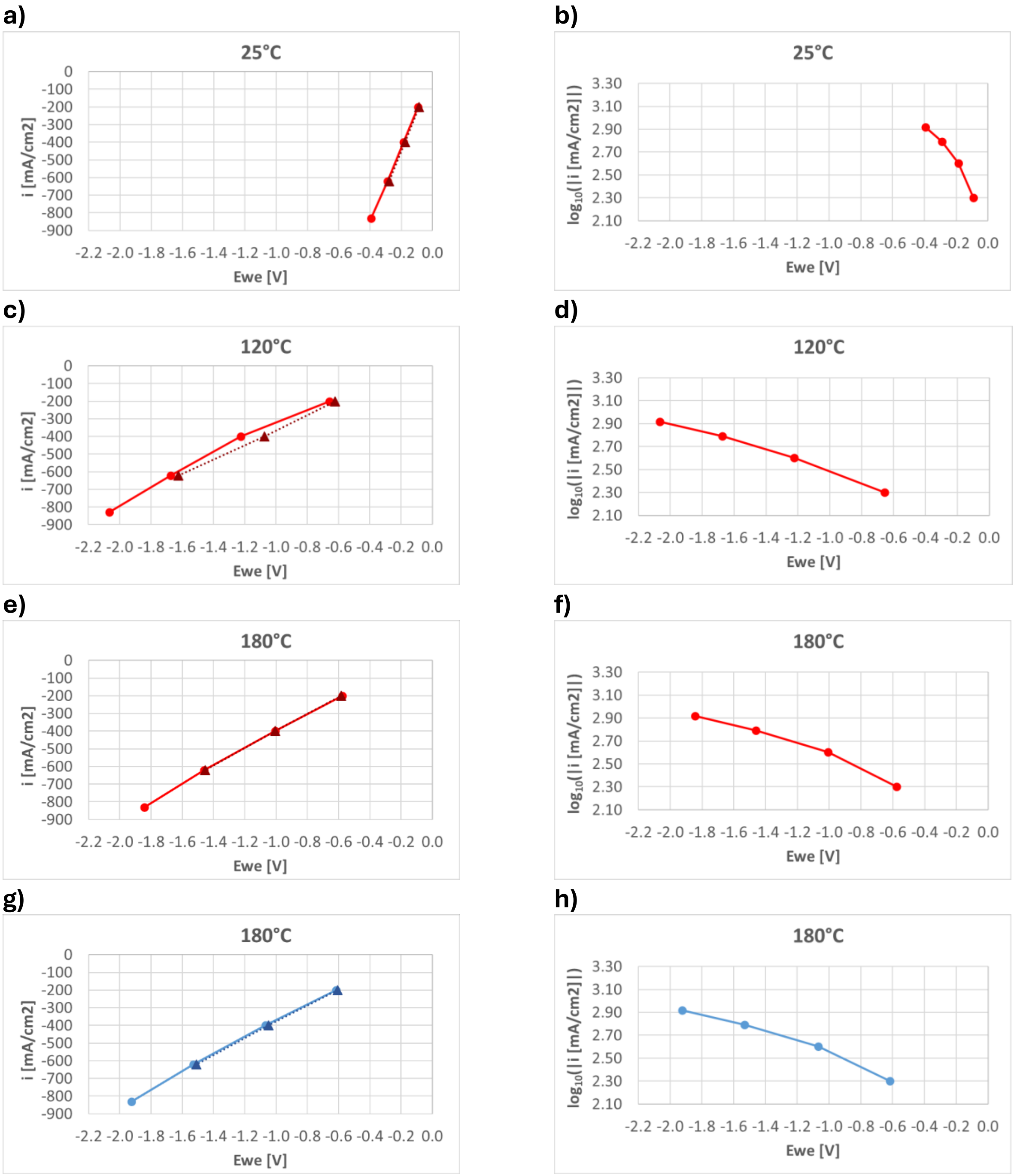

Figure 70 i-V curves (left) and corresponding Tafel plots (right, forward scan only) obtained at 20 bar under varying temperatures: a,b) 25°C; c,d) 120°C; e-h) 180°C. Solid lines with circle symbols indicate forward scans; while dotted lines with triangle symbols indicate backward scans. Red curves: CO2 feed; blue curves: N2 feed.

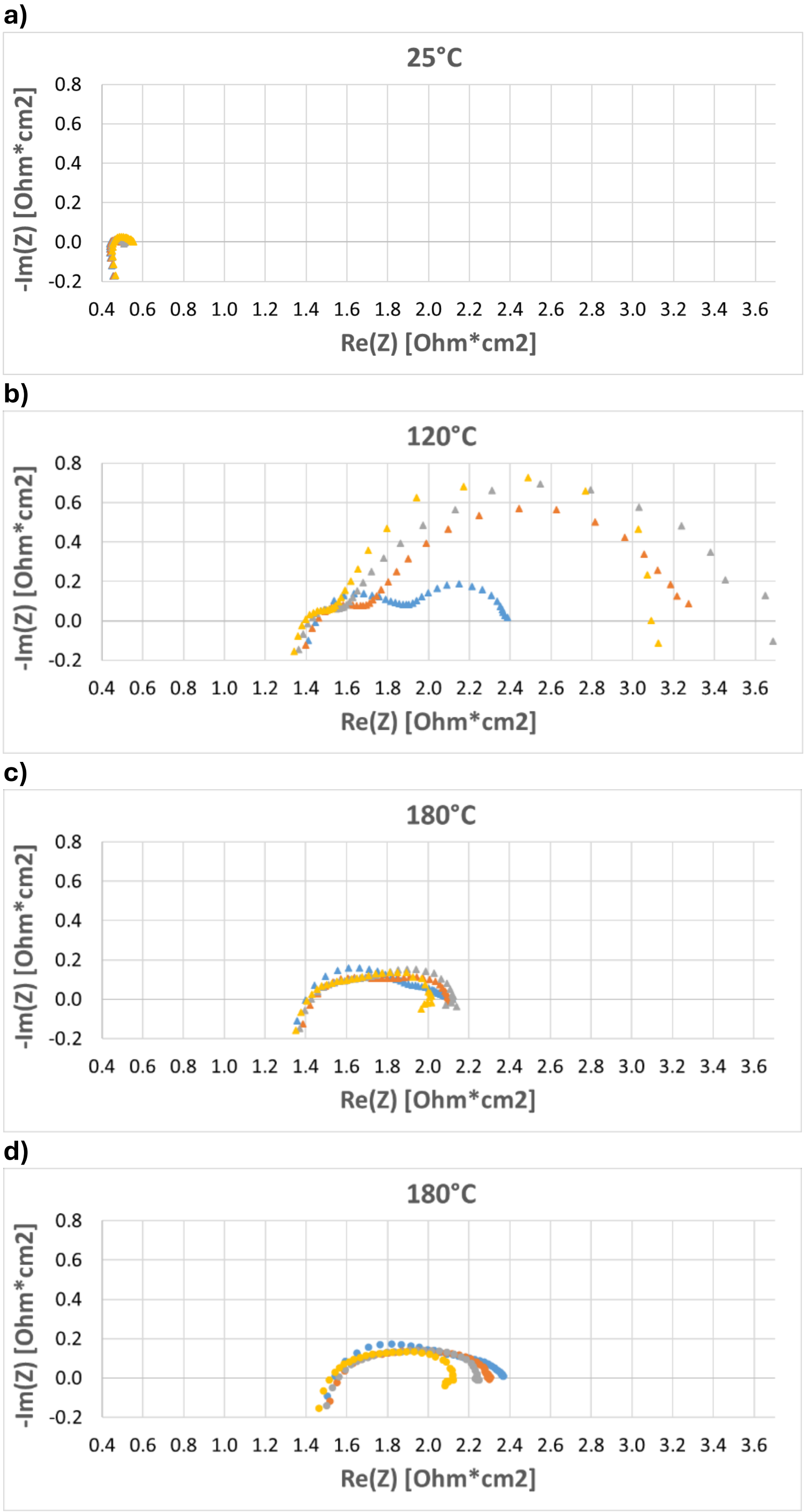

Figure 71 Nyquist plots obtained at 20 bar under varying temperatures: a) 25°C; b) 120°C; c,d) 180°C. Colour legend: blue symbols (-200 mA/cm2), orange (-400 mA/cm2), violet (-600 mA/cm2), grey (-630 mA/cm2), green (-800 mA/cm2), yellow (-830 mA/cm2). Circle symbols indicate N2 feed, triangle symbols indicate CO2 feed.

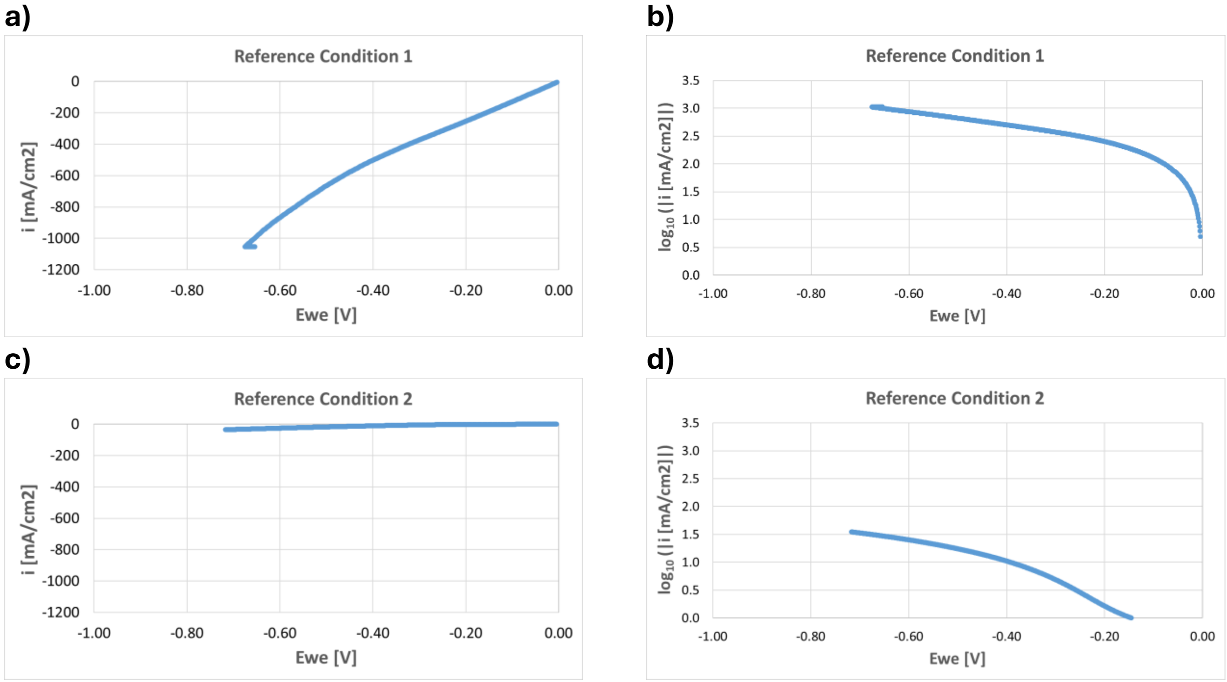

Figure 72 LSV curves (left) and corresponding Tafel plots (right) obtained at 1 bar and 25°C under N2 feed (Reference conditions): a,b) Reference condition 1; c,d) Reference condition 2

4.4. i-R correction results

In this chapter the results of the iR correction made will be presented.

The iR drop was compensated for both the symmetric Pt/Pt Cell (Sample A), tested at 20 bar and 180°C, and the Cu/Pt Cell (Sample B) tested at 20 bar at two temperatures,120 and 180°C. The equivalent circuit used is described by the mode L + R_1 + Q/R_2, shown in **Figure 73**, where L represents the wiring inductance, R_1 the ohmic resistance, Q a constant phase element describing the non-ideal double layer and R_2 the charge transfer resistance.

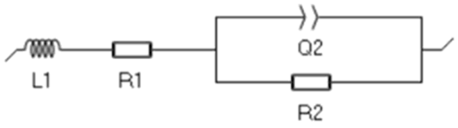

Figure 73 Equivalent circuit used for the iR correction

In **Figure 74** the V-I curves after iR correction are shown. For each data point, the corresponding resistance value obtained from the correction procedure are reported on the graph. A difference can be observed between the curves measured under CO_2 feed and those acquired under N_2 feed. However, the cell voltages reached are very low, with a maximum value of about -0.15V, which is insufficient to significantly drive CO_2 electroreduction.

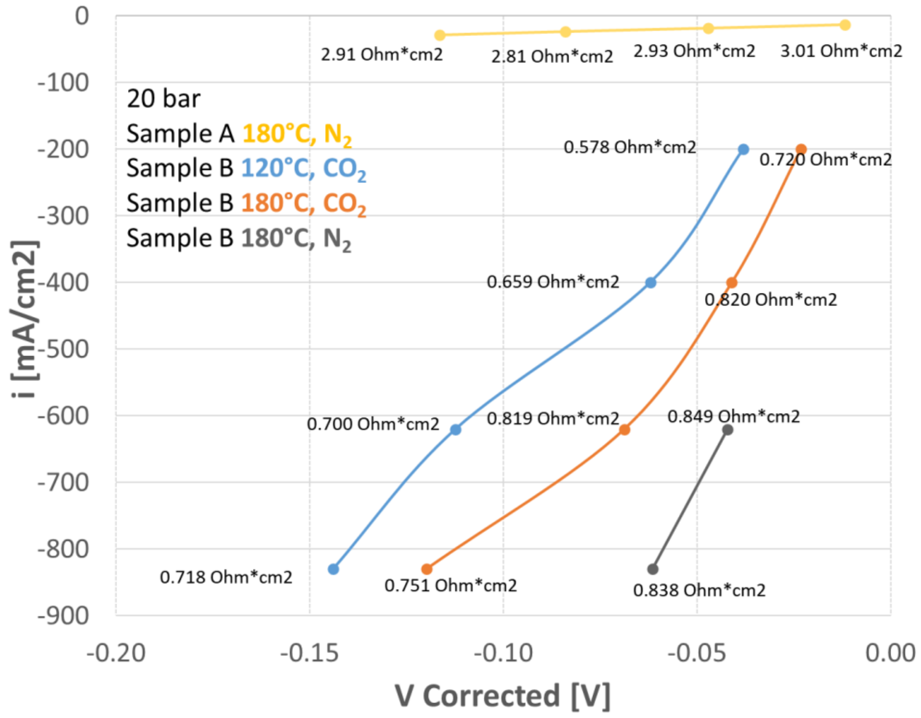

Figure 74 V-i Curves after iR compensation

5. Discussion

In this chapter, the results of the experiments presented in the previous chapter will be discussed.

5.1. Sample A

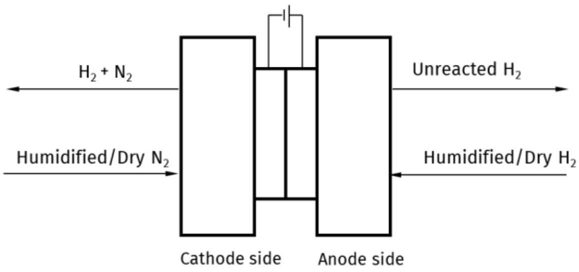

Figure 75 Sample A Cell configuration

Figure 75 shows the cell configuration for the sample A. The cell was supplied with hydrogen at the anode and inert nitrogen at the cathode, both under humidified and dry conditions. At the anode, hydrogen is oxidized to protons and electrons, the protons pass through the PBI membrane and recombine with the electrons at the cathode, forming molecular hydrogen. The purpose of the tests was to investigate the electrochemical behaviour of the membrane and the MEA under different operating conditions.

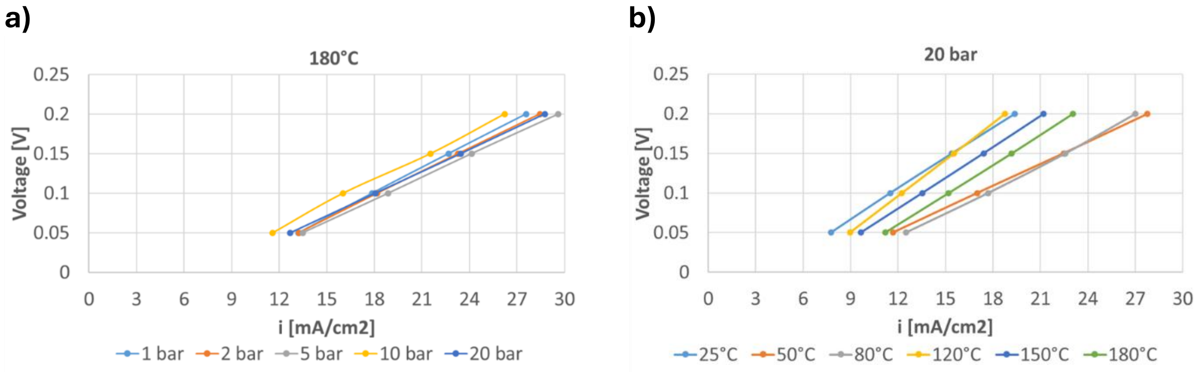

Figure 76 a) V-i Curves obtained at constant temperature (180°C) varying pressure; b) V-i Curves obtained at constant pressure (20 bar) varying temperature

Figure 76 a) was obtained by keeping the cell at a constant temperature of 180°C while increasing the pressure from 1 bar to 20 bar. In contrast **Figure 76 b)** was obtained by fixing the pressure at 20 bar and varying the temperature from 25°C to 180°C. From these two plots, no clear dependence on either temperature or pressure can be observed.

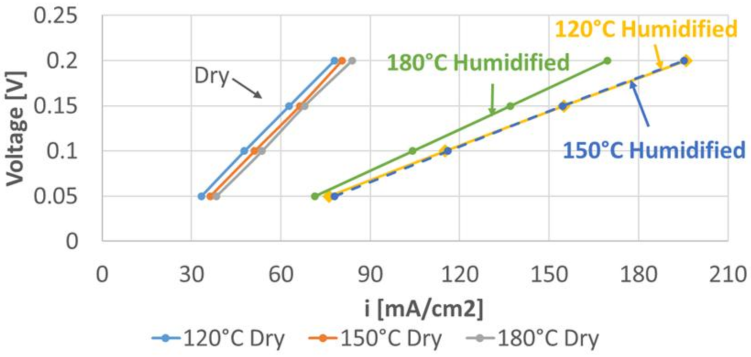

Figure 77 V-i Curves at 1 bar under dry and humidified feed at different temperatures

Figure 77 shows the V-i curves obtained at 1 bar and at different temperatures of 120, 150 and 180°C. The feed gases were tested both in humidified form, by bubbling them through a water reservoir, and in a dry form. Under dry feed conditions, increasing the temperature does not significantly affect the cell performance. With humidified gases, higher performance is observed compared to the dry case. The curves at 120 and 150°C are nearly overlapping, while at 180°C a performance drop is observed. The expected enhancement due to temperature increase is therefore limited by the competing effect of membrane dehydration, which reduces the cell's electrochemical performance.

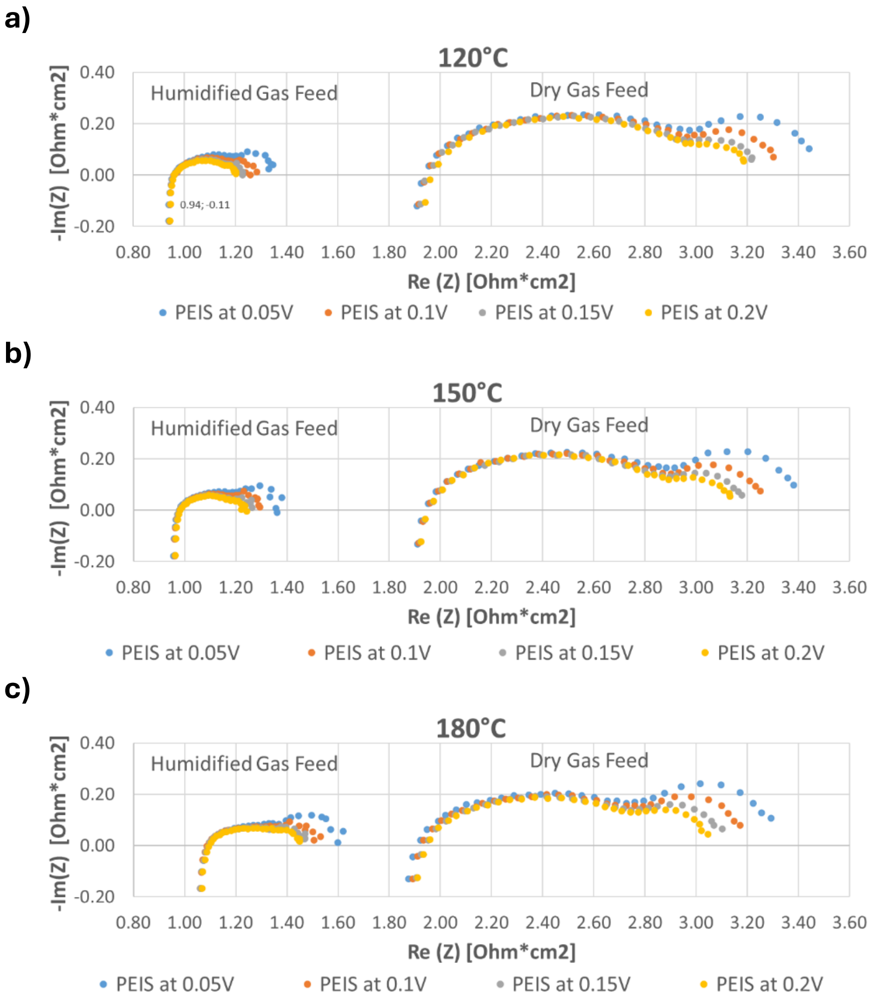

Figure 78 Nyquist plots obtained at 1 bar under dry and humidified feed at different temperature: a) 120°C; b) 150°C; c) 180°C

The behaviour observed in the V-i curves is confirmed by EIS spectra, shown as Nyquist plots at constant voltage in **Figure 78**. For dry gases, no significant differences are observed among the curves at different temperatures. In contrast, for humidified gases, the high frequency intercept values are lower than those obtained with dry feeds, while a slight increase in this intercept values is observed as the temperature increases. These results are consistent with the findings previously discussed for the V-i curves.

a)

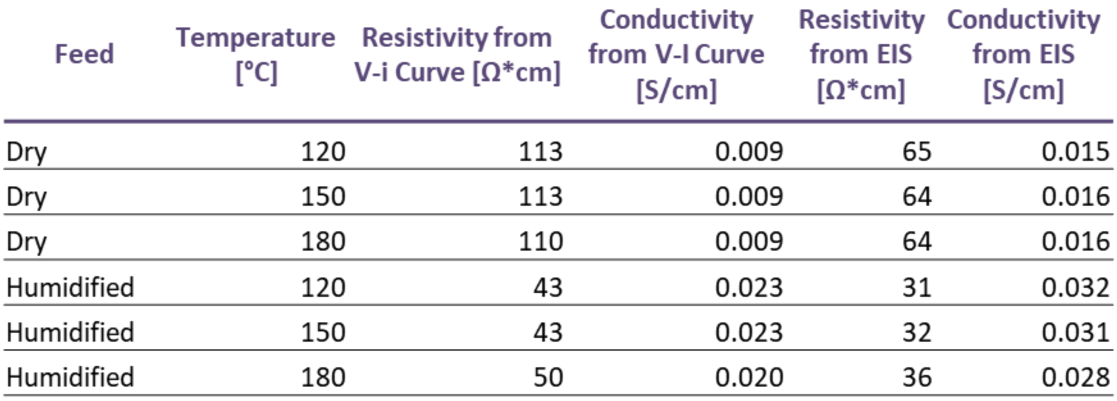

Feed	Temperature [°C]	Resistivity from V-i Curve [Ω*cm]	Conductivity from V-I Curve [S/cm]	Resistivity from EIS [Ω*cm]	Conductivity from EIS [S/cm]
Dry	120	113	0.009	65	0.015
Dry	150	113	0.009	64	0.016
Dry	180	110	0.009	64	0.016
Humidified	120	43	0.023	31	0.032
Humidified	150	43	0.023	32	0.031
Humidified	180	50	0.020	36	0.028

b)

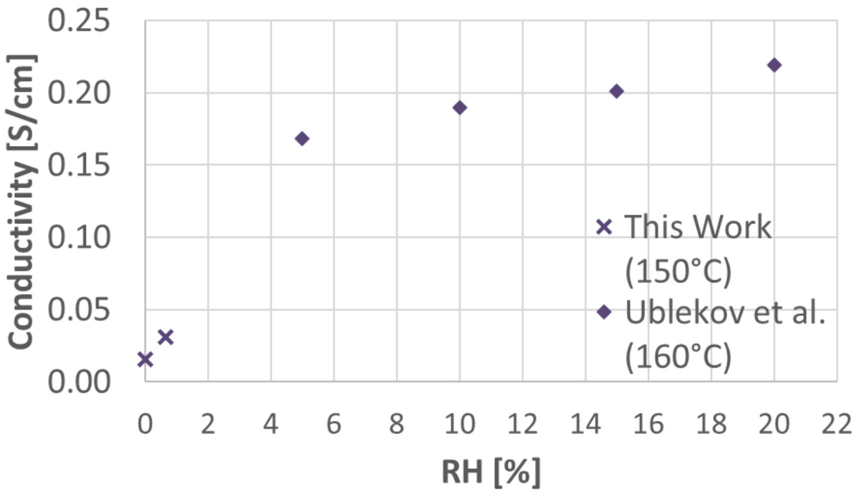

Figure 79 a) Calculated Conductivity; b) Comparison of Conductivity vs. Relative Humidity

From the data of the previous experiments, the resistivities were determined and the corresponding proton conductivities were calculated. The conductivity was obtained either from the slope of the V-i characteristics or, alternatively, by graphically extracting the resistivity from the Nyquist plots and converting it into conductivity. The resulting values are reported in **Figure 79** a). in **Figure 79** b), the conductivity values as function of relative humidity (RH) obtained in this work at 150°C are compared with those at 160°C, reported in [19]. the plot reveals a dependence of conductivity on log (RH). Furthermore, the values measure in this study are significantly lower than the reference proton conductivity of Nafion at 80°C, equal to 0.1S/cm [20].

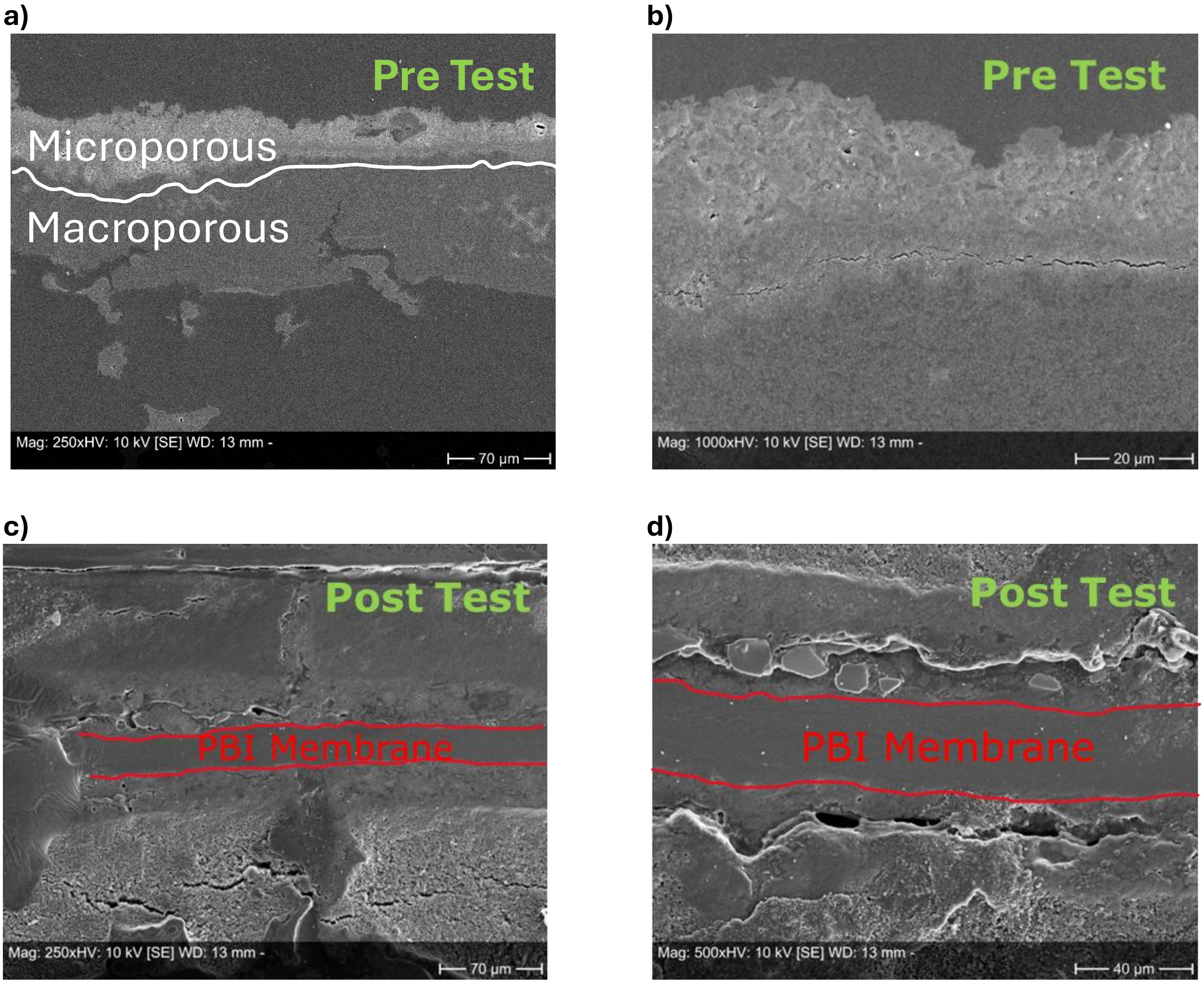

Figure 80 Sample A SEM Analysis: a) pre-test cross-section Mag: 250xHV; b) pre-test cross-section Mag:1000xHV, c) post-test cross-section Mag: 250xHV, d) post-test cross section Mag:500HV

Figure 80 presents SEM cross section images: in a) and b), the electrode is shown before assembly, while in c) and d), the cross sections of the MEA after tests are presented. The images indicate no evident signs of degradation and show a good interfacial contact. Another observation is that the membrane thickness in the assembled MEA, post tetst, is approximately 30 µm, i.e. about one tenth of the value of the value measured for the bare membrane. The reduction in thickness is likely due to the compression induced by the closing of the cell casing.

5.2. Sample B

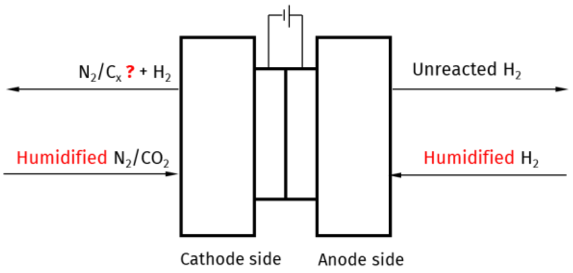

Figure 81 Sample B Cell configuration

The configuration of cell B in shown in **Figure 81**. The cell was fed with N_2 for MEA testing and then also with CO_2 to investigate the possible occurrence of electrochemical Fischer Trosch type reactions. Based on the results obtained with cell A, all further tests were carried out using humidified gases only.

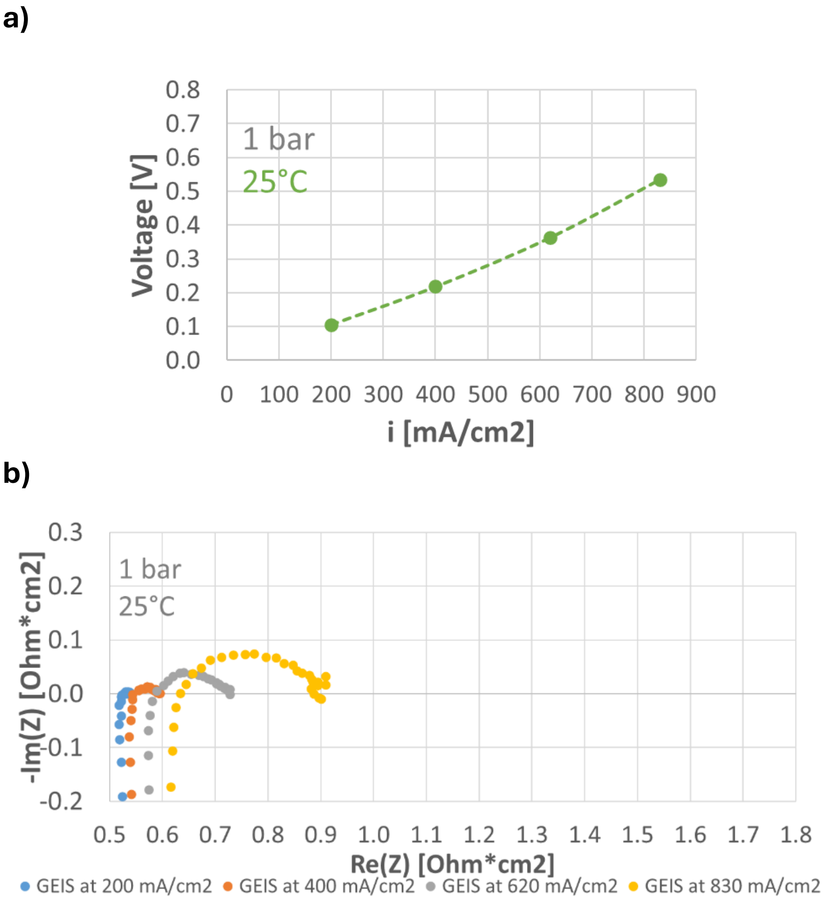

Figure 82 V-i curve a) and Nyquist plots b) obtained at 1 bar and 25°C under N_2 feed.

Figure 82 shows the V-I curve and the Nyquist plot obtained at 1 bar and 25°C, with N_2 supplied to the cathode. The cell exhibits high performance, reaching a current density of 830 mA/cm2 at a voltage of 0.54 V and overall shows a low ohmic resistance.

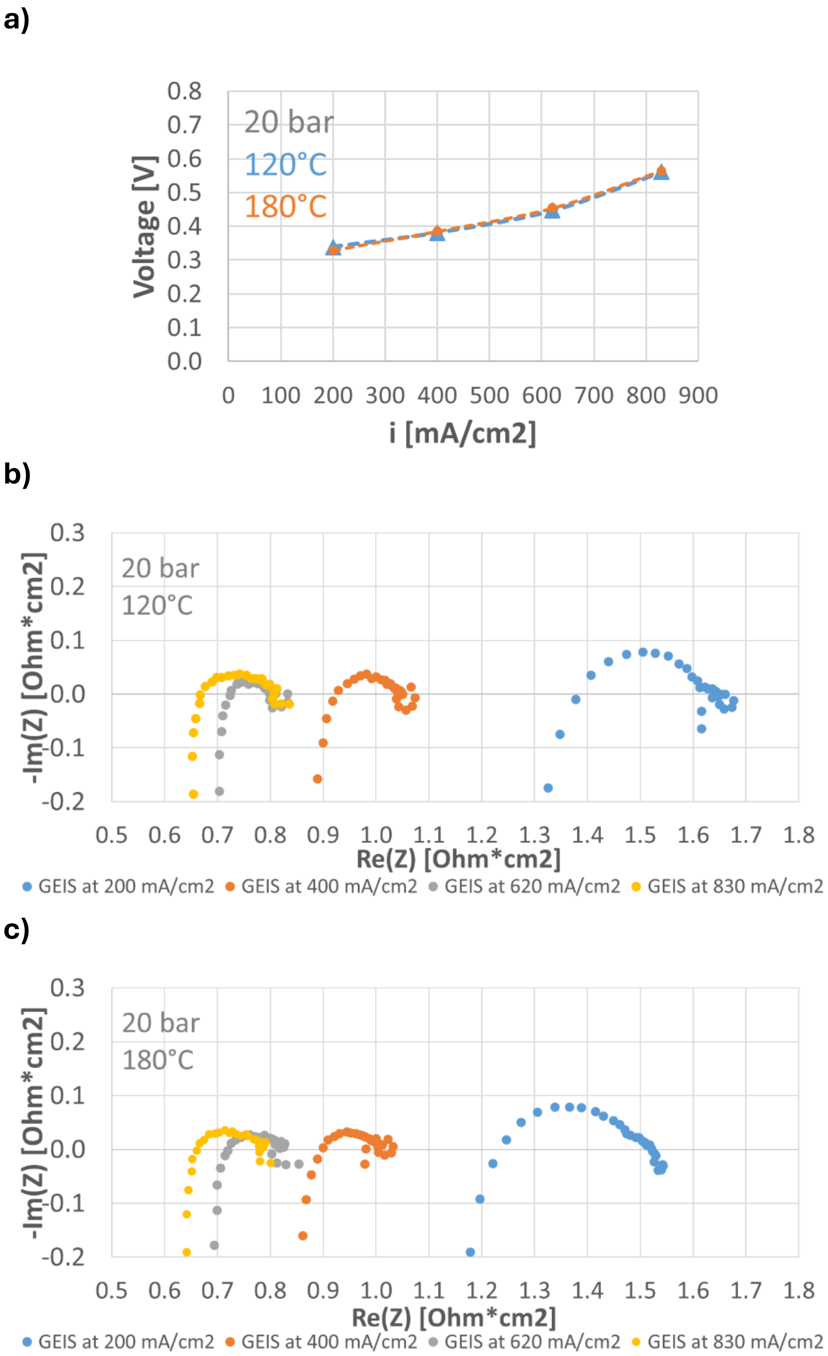

Figure 83 a) V-i curve obtained at 20 bar, 120 and 180°C under N_2 feed; b) Nyquist plot obtained at 20 bar and 120°C under N_2 feed; c) Nyquist plot obtained at 20 bar and 180°C under N_2 feed

Figure 83 a) shows the V-i curves obtained at 20 bar and 120°C (in blue) and at 20 bar and 180°C (in orange). The two curves nearly overlap, suggesting that the temperature has no significant influence. Both curves indicate high performance of the cell. However, at low current densities, a slight performance decrease compared to ambient conditions is observed. The same behaviour spears in the Nyquist plots at 20 bar and 120°C b) and 180°C c), showing a shift toward higher resistance values as the current decreases.

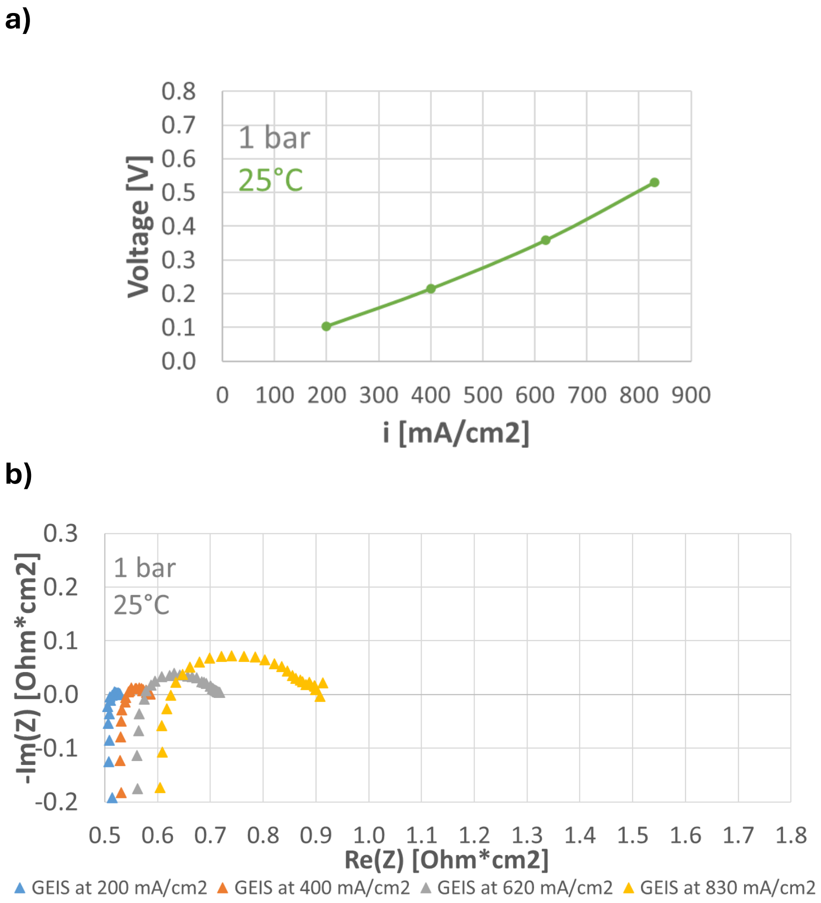

Figure 84 V-i curve a) and Nyquist plots b) obtained at 1 bar and 25°C under CO2 feed.

Figure 84 shows the V-i curve and the corresponding Nyquist plot obtained at 1 bar and 25°C, with CO_2 supplied to the cathode. Under these conditions, the cell exhibit high performance, reaching a current density of 830 mA/cm2 at 0.53 V and displaying a low resistance. Both the V-i curve and the Nyquist plot are very similar to those obtained with N_2 feeding, indicating that replacing N_2 with CO_2 does not significantly affect the electrochemical behaviour of the cell.

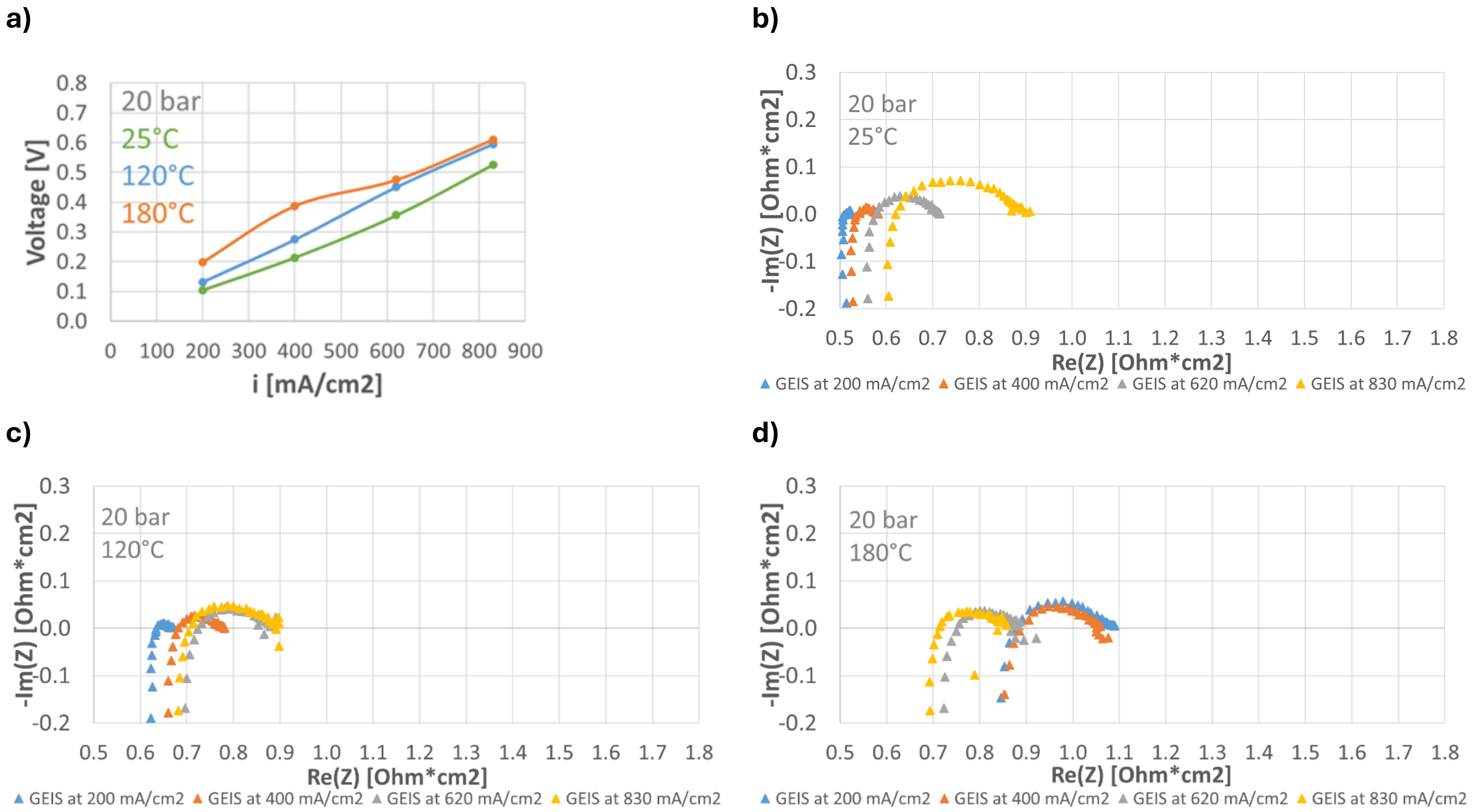

Figure 85 a) V-i curve obtained at 20 bar, 25, 120 and 180°C under N2 feed; b) Nyquist plot obtained at 20 bar and 25°C under CO2 feed; c) Nyquist plot obtained at 20 bar and 120°C under CO2 feed; c) Nyquist plot obtained at 20 bar and 180°C under CO2 feed

The V-i curves at 20 bar and 25°C (in green), 120°C (in blue) and 180°C (in orange) are shown in **Figure 85** a). increasing temperature leads to a lower performance of the cell. In particular, the curves at 120 and 180°C are almost overlapping at high current densities, while at lower currents the performance at 180°C in slightly reduced. This trend is also confirmed by the corresponding Nyquist plots. Therefore, the expected benefit of higher temperature is counterbalanced by insufficient membrane humidification, which limits the overall cell performance.

A qualitative analysis was performed to investigate potential CO_2 conversion using highly sensitive sensors positioned at the cathode outlet. A Honeywell BW CO sensor and PEAKER® hydrogen detector were used. The hydrogen detector, also used for leak control, detected the presence of H_2, thereby confirming hydrogen oxidation at the anode ant recombination at the cathode. Conversely, the CO sensor did not detect any presence of carbon monoxide. Additionally, a silica gel trap was placed on the cathode outlet line to remove water vapour from the gas stream before gas chromatographic analysis. No appreciable colour change was detected in the gel, suggesting a low water content in the outlet gas.

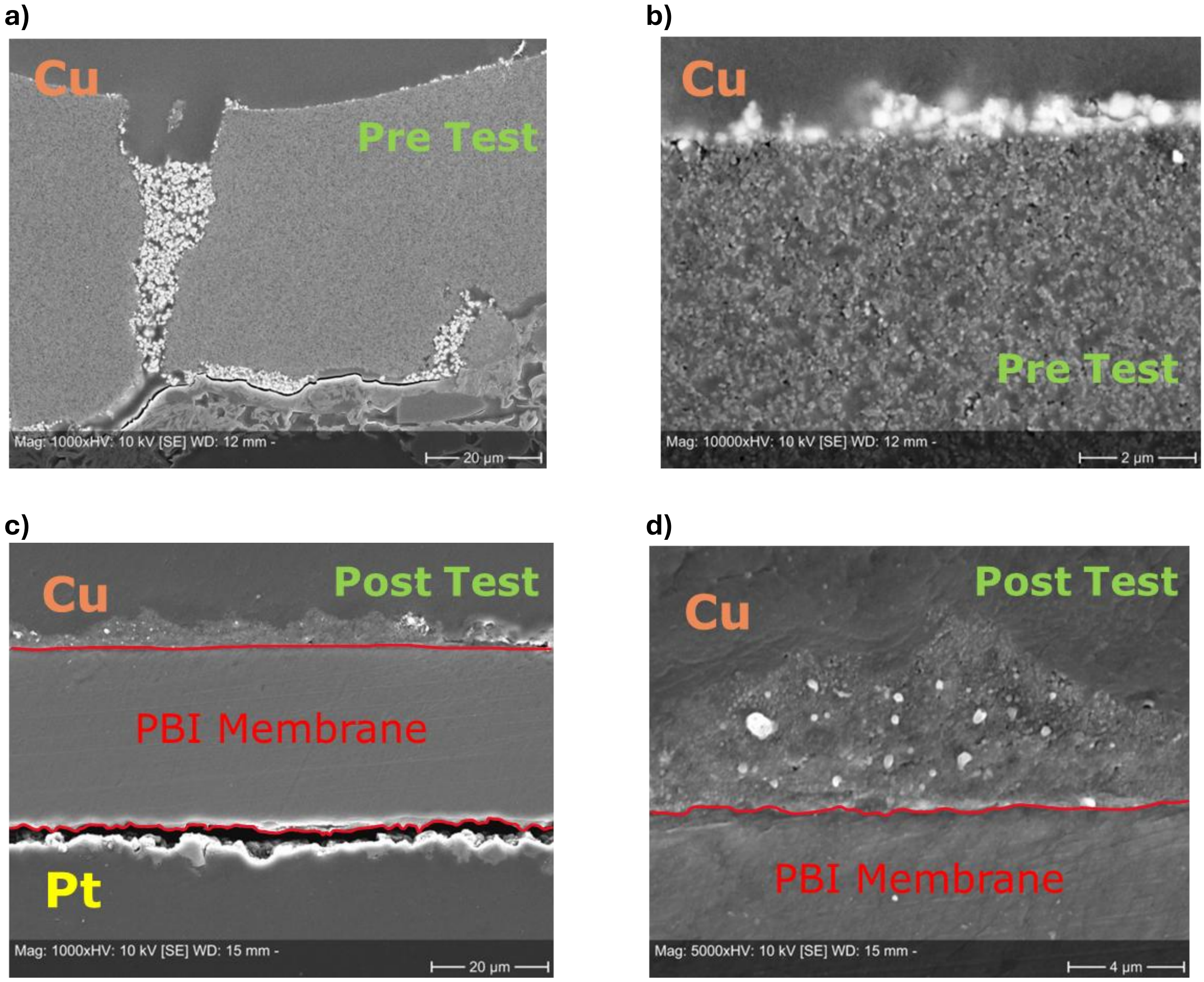

Figure 86 Sample B SEM Analysis: a) pre-test cross-section Mag: 1000HV; b) pre-test cross-section Mag:10000xHV, c) post-test cross-section Mag: 1000xHV, d) post-test cross section Mag:5000HV

Figure 86 shows the SEM images of the cross sections: in a) and b), the electrode is shown before assembly, whereas in c) and d), the MEA cross sections after the tests are presented. The images do not reveal any appreciable signs of degradation and show a good interfacial contact. The apparent detachment visible in **Figure 85** c) is attributed to the cell case opening procedure. Also in this case, like for the Sample B, the membrane thickness post tests is around 30 µm.

5.3. Sample C

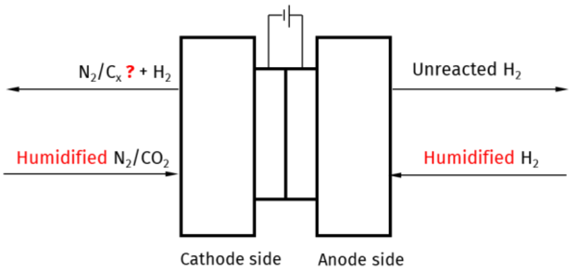

Figure 87 Sample C Cell configuration

Figure 87 shows the configuration of Sample C, which is identical to that used for Sample B, as are the operating conditions of the experiments. The aim was to reproduce the tests carried out with Sample B and the results obtained with Sample C confirmed the observations previously made for Sample B.

6. Conclusions and Future Work

Based on the results obtained in this work, the main conclusions can be summarised as follows. The experimental results demonstrated that Sample B exhibited very high performance among the tested configurations. The membrane performance showed a strong dependence on humidity, highlighting the critical role of water management in maintaining optimal proton conductivity and electrochemical activity. Within the investigated range of operating conditions, no evidence of Fischer-Tropsch type reactions was detected. In addition, the analysis of the overall cell behaviour made it possible to identify the main bottlenecks limiting the system performance, indicating that the electrolyte represented the primary constraint under the investigated conditions, especially under non-optimal humidity levels. Moreover, SEM analysis of the MEA cross sections revealed a significant reduction in membrane thickness in the assembled cell compared with the separate membrane, indicating that the electrolyte layer was significantly compressed by the cell closure. Overall, these findings underline the importance of carefully tailoring electrolyte properties and operating conditions when designing CO_2 electrolysis cells operating at elevated temperatures and pressures for practical applications.

Building on these conclusions, several directions for future work can be identified. First, the MEA (membrane electrode assembly) preparation procedure should be further optimised in order to improve the three phase boundary and thus enhance the overall electrochemical performance. The mechanical design and closing procedure of the cell casing should be further optimised to limit excessive compression of the membrane and preserve a well-defined electrolyte thickness. In addition, repeating the experiments with pure H_2 feeding and different partial pressures of H_2 on the two sides of the cell would allow a more accurate comparison between the measured open circuit voltage and the theoretical Nernst potential. Further tests at different relative humidity values, i.e. varying the humidification levels, would provide deeper insight into the role of water management. Finally, the use of modified gas feed compositions could be explored to achieve more favourable conditions for the desired reaction pathways.

Bibliography

[1] L. Li, X. Li, Y. Sun, and Y. Xie, ‘Rational design of electrocatalytic carbon dioxide reduction for a zero-carbon network’, *Chem. Soc. Rev.*, vol. 51, no. 4, pp. 1234–1252, 2022, doi: 10.1039/D1CS00893E.

[2] X. Li, P. Anderson, H.-R. M. Jhong, M. Paster, J. F. Stubbins, and P. J. A. Kenis, ‘Greenhouse Gas Emissions, Energy Efficiency, and Cost of Synthetic Fuel Production Using Electrochemical CO_2 Conversion and the Fischer–Tropsch Process’, *Energy Fuels*, vol. 30, no. 7, pp. 5980–5989, Jul. 2016, doi: 10.1021/acs.energyfuels.6b00665.

[3] R. G. D. Santos and A. C. Alencar, ‘Biomass-derived syngas production via gasification process and its catalytic conversion into fuels by Fischer Tropsch synthesis: A review’, *Int. J. Hydrog. Energy*, vol. 45, no. 36, pp. 18114–18132, Jul. 2020, doi: 10.1016/j.ijhydene.2019.07.133.

[4] M. Escribà-Gelonch, J. Osorio-Tejada, L. Yu, B. Wanten, A. Bogaerts, and V. Hessel, ‘Techno-economic and life-cycle assessment for syngas production using sustainable plasma-assisted methane reforming technologies’, *Energy Environ. Sci.*, vol. 18, no. 12, pp. 6043–6062, 2025, doi: 10.1039/D4EE05129G.

[5] D. Fan *et al.*, ‘A microchannel reactor-integrated ceramic fuel cell with dual-coupling effect for efficient power and syngas co-generation from methane’, *Appl. Catal. B Environ.*, vol. 297, p. 120443, Nov. 2021, doi: 10.1016/j.apcatb.2021.120443.

[6] C. Panzone, R. Philippe, A. Chappaz, P. Fongarland, and A. Bengaouer, ‘Power-to-Liquid catalytic CO2 valorization into fuels and chemicals: focus on the Fischer-Tropsch route’, *J. CO2 Util.*, vol. 38, pp. 314–347, May 2020, doi: 10.1016/j.jcou.2020.02.009.

[7] G. Busca and G. Garbarino, ‘Industrial Chemistry Module 1: Refinery and Petrochemistry and Green Industrial Organic Chemistry’, 2023.

[8] S. Y. Hwang, G. Yun, B. S. Yeo, and Y. Sohn, ‘Electrochemical Fischer–Tropsch chemistry’, *Chem. Eng. J.*, vol. 520, p. 165806, Sep. 2025, doi: 10.1016/j.cej.2025.165806.

[9] S. El Aggadi *et al.*, ‘Electrochemical Reduction of Carbon Dioxide to Provide Sustainable Solutions for Climate Change’, *ChemBioEng Rev.*, vol. 12, no. 6, p. e70029, Dec. 2025, doi: 10.1002/cben.70029.

[10] X. She, Y. Wang, H. Xu, S. Chi Edman Tsang, and S. Ping Lau, ‘Challenges and Opportunities in Electrocatalytic CO_2 Reduction to Chemicals and Fuels’, *Angew. Chem. Int. Ed.*, vol. 61, no. 49, p. e202211396, Dec. 2022, doi: 10.1002/anie.202211396.

[11] ‘Linear sweep voltammetry’, *Wikipedia*. Nov. 21, 2024. Accessed: Mar. 06, 2026. [Online]. Available: https://en.wikipedia.org/w/index.php?title=Linear_sweep_voltammetry&oldid=1258748088

[12] ‘Cronoamperometria - Enciclopedia’, Treccani. Accessed: Mar. 06, 2026. [Online]. Available: https://www.treccani.it/enciclopedia/cronoamperometria/

[13] ‘Chronopotentiometry (CP)’. Accessed: Mar. 06, 2026. [Online]. Available: https://pineresearch.com/support-article/chronopotentiometry-cp/

[14] ‘EC-Lab software Techniques and Applications manual’.

[15] S. Zhong, P. Sui, P. Holtappels, A. Navarrete, F. Li, and R. Dittmeyer, ‘Robust and efficient electroreduction of CO2 to CO in a modified zero-gap electrochemical cell’, *Chem. Eng. J.*, vol. 509, p. 161119, Apr. 2025, doi: 10.1016/j.cej.2025.161119.

[16] S. Zhong, I. Ait Aissa, G. Huang, P. Holtappels, S. Liu, and R. Dittmeyer, ‘Experimental study of operating parameters in zero-gap CO2 electrolysis’, *Front. Catal.*, vol. 5, p. 1657848, Sep. 2025, doi: 10.3389/fctls.2025.1657848.

[17] S. Zhong, W. Yang, S. Liu, and R. Dittmeyer, ‘Synergistic electroreduction of CO2 to C1-C3 gas products in a pressure-tolerant MEA system’, *Int. J. Hydrog. Energy*, vol. 119, pp. 73–81, Apr. 2025, doi: 10.1016/j.ijhydene.2025.03.234.

[18] S. Zhong, ‘CO2 Reduction Reaction in a Modified Zero-Gap Electrolyzer’, PhD thesis, Karlsruher Instituts für Technologie (KIT), 2025.

[19] F. Ublekov, H. Penchev, V. Georgiev, I. Radev, and V. Sinigersky, ‘Protonated montmorillonite as a highly effective proton-conductivity enhancer in p-PBI membranes for PEM fuel cells’, *Mater. Lett.*, vol. 135, pp. 5–7, Nov. 2014, doi: 10.1016/j.matlet.2014.07.128.

[20] M. A. Barique, E. Tsuchida, A. Ohira, and K. Tashiro, ‘Effect of Elevated Temperatures on the States of Water and Their Correlation with the Proton Conductivity of Nafion’, *ACS Omega*, vol. 3, no. 1, pp. 349–360, Jan. 2018, doi: 10.1021/acsomega.7b01765.